International Scientific-Technical and Production Journal

The Paton WELDING JOURNAL

January 2012 # 1

English translation of the monthly «Avtomaticheskaya Svarka» (Automatic Welding) journal published in Russian since 1948

CONTENTS

EFFICIENCY OF ELECTRODYNAMIC TREATMENT OF ALUMINIUM ALLOY AMg6 AND ITS WELDED JOINTS

L.M. LOBANOV[1], N.A. PASHCHIN[1], A.V. CHERKASHIN[1], O.L. MIKHODUJ[1] and I.P. KONDRATENKO[2]
[1]E.O. Paton Electric Welding Institute, NASU, Kiev, Ukraine
[2]Institute of Electrodynamics, NASU, Kiev, Ukraine

The evaluation of parameters of pulsed current and dynamic pressure at electrodynamic treatment was performed, based on the developed experimental procedure. The influence of charge voltage and capacitance of capacitors on relative effectiveness of electrodynamic treatment was studied. It was established that maximum values of pulsed current and its increment rate are directly dependent on applied charge voltage, while the rate of dynamic pressure increment is the power function of a pulsed current.

The electrodynamic treatment (EDT) based on the combined pulsed effect of electric current and dynamic load on current-conducting materials is a challenging method to control the stressed state of metal structures [1].

Up to now the investigations of mechanisms of the EDT effect on stressed state of aluminium alloys [2], structural steels [3, 4], and also welded joints of these materials were carried out. The peculiarities of changes of micro and macrostructures [5], plastic deformation [6] and residual shape changing [7] of metals and alloys under influence of a pulsed current, initiated at EDT, were studied. The results of investigations, presented in the works [1--7], were obtained using the developed experimental procedure based on tension of flat specimens of «blade» type, their treatment by current pulses with in-process control of drop-

ping the tension force, which was taken as an evaluative characteristic of EDT.

However, no attention was paid to the study of effect of such parameters of EDT as values of pulsed electric current and dynamic force on efficiency of this process.

The aim of this work is investigation of efficiency of eletrodynamic effect during treatment of aluminium alloy AMg6 and its welded joints depending on electric and dynamic parameters of EDT.

To form the pulse of electric current, the pilot-industrial installation was used presented in the work [4]. The supply of a pulsed current to the surface of metal was performed using copper electrode in the way that the specimen being treated is connected to the discharge circuit of the capacitor storage. Here, in the process of passing the discharge current the electric pulsed processes in the current-conducting material being treated are initiated, connected with the mechanism of electric plasticity [1]. Besides, a special design of electrode device transfers impact effect into the material being treated.

The working tool includes a current-conducting striker *1* with a hemispheric edge (Figure 1). The design peculiarities of the tool allow changing the length of electrode stickout *1* by adjusting gears *6, 8* and screw *7* relatively to the surface of welded joint *2* which is the receiver of the electrodynamic effect. The working tool includes also an inductance coil *11*, connected to the discharge circuit of the capacitor storage and defining the duration of a current pulse. The coil is arranged in the working tool above the disc *4* of non-ferromagnetic material.

The interaction of magnetic field of inductance coil and field of induced currents, caused by passing the current pulse along the winding, leads to the appearance of electrodynamic force trying to push out the disc from the coil, here the current-carrying electrode, rigidly connected to a disc, transfers the electrodynamic effect to the surface of material being treated. The superposition of electric plastic and dy-
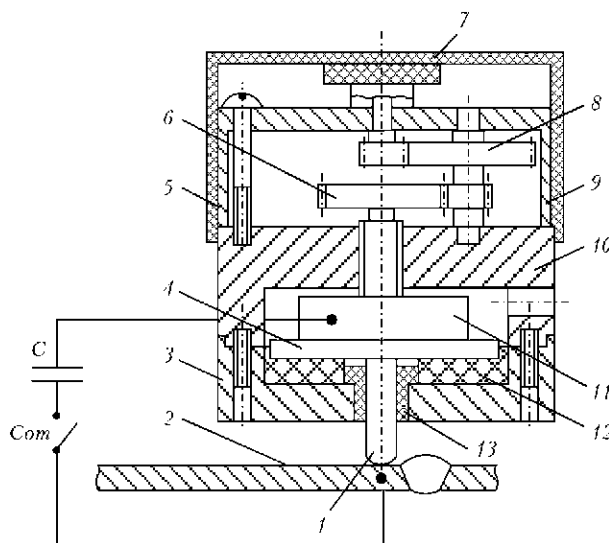

Figure 1. Schematic diagram of working tool for EDT: *C* — battery of capacitors; *Com* — commutator (for designations see the text)

namic processes during passing of the pulsed current through the product being treated determines the intensity of electrodynamic effect.

Working tool body components *3*, *5*, *9*, included into composition of the working tool, provide the required rigidity of the design, and the damping *12* and guiding *13* elements reduce the negative effect of impact action of the disc on the body *10*.

One important peculiarity of EDT should be noted, consisted in difference of character of electrodynamic effect of working tool from characteristic diagrams of a mechanical impact. The rate of increment of dynamic force in our case is determined by leading front of a current pulse and, evidently, can be controlled using hardware.

To evaluate the effect of EDT parameters on the efficiency of the process, the treatment of flat specimens of rectangular section of AMg6 alloy after tension and its welded joints cut out across the weld of plates of $500 \times 500 \times 4$ mm sizes was carried out. Butt welds were performed by the automatic welding using non-consumable electrode in argon in the installation ASTV-2M at the voltage 18 V and current 220 A at the speed of 14 m/h.

The tension of specimens was performed in the rupture machine TsDM-10 with a closed power loop and maximal force of tension 9800 N at the rate of deformation of 0.1 mm/min and temperature of 293 K.

The influence of electric parameters of EDT process such as discharge voltage U and battery capacitance of capacitors C on decrease in resistance of material to deformation $\Delta\sigma$ (difference of values of initial stresses σ_0 and after EDT σ_{EDT}) was studied. For this purpose the specimens of base metal and welded joints of AMg6 alloy were subjected to tension up to preset value of σ_0 and single current discharge was performed with control of stress drop to σ_{EDT}, presetting here the different U and C values.

At the first stage of investigations the $\Delta\sigma$ values at discrete increase of charge voltage U from 200 to 300 and 500 V at constant charge of capacitors $C = 6600$ μF were measured. At the second stage the C value was changed, being discretely increasing from 1400 to 2800 and 6600 μF at invariant $U = 500$ V. The σ_0 values of specimens were preset equal to 55, 130 and 270 MPa. The dependencies of influence of parameters U and C on relative efficiency of EDT $\Delta\sigma/\sigma_0$ are presented in Figure 2. Having analyzed the dependencies $\Delta\sigma/\sigma_0 = f(U)$ at $C = $ const (Figure 2, *a*) and $\Delta\sigma/\sigma_0 = f(C)$ at $U = $ const (Figure 2, *b*) it is seen that parameters U and C are different according to the level of influence on resistance to deformation $\Delta\sigma$ and, as a consequence, on relative efficiency $\Delta\sigma/\sigma_0$ of EDT of AMg6 alloy.

Thus, if to achieve maximal values of efficiency (see Figure 2) the charge voltage U is enough to be increased by 2.5 times, then to achieve the similar
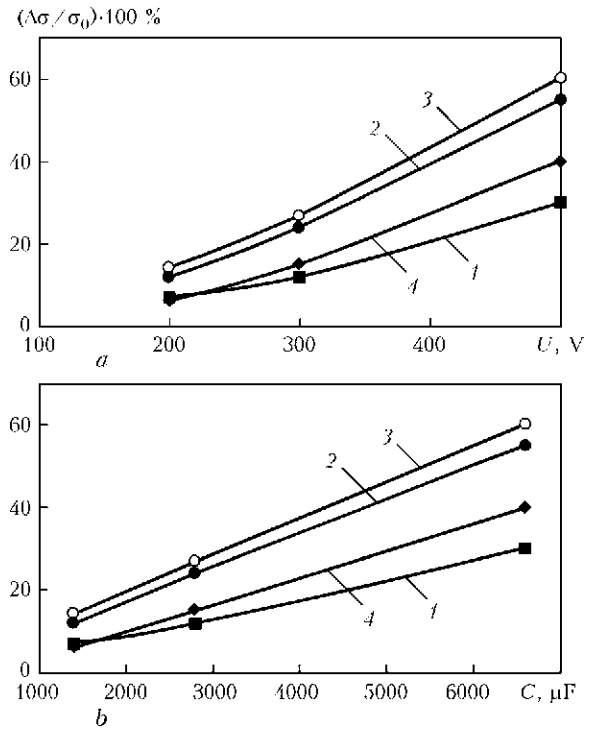
Figure 2. Effect of charge voltage U (*a*) and capacitance of battery of capacitors C (*b*) on relative efficiency of EDT $(\Delta\sigma/\sigma_0) \cdot 100$ % of alloy AMg6 and its welded joints at different values of initial stress: *1* — $\sigma_0 = 55$; *2*, *3* — 130; *4* — 270 MPa; *1*, *2*, *4* — base metal; *3* — welded joint

values of $\Delta\sigma/\sigma_0$ it is necessary to increase the capacitance C by 5 times. Basing on the data of Figure 2, it can be concluded that efficiency of EDT is directly proportional to the capacitance of C at $U = $ const and square of voltages U^2 at $C = $ const, which gives grounds to present it as a function of accumulated energy of the capacitor [8].

The values of efficiency for welded joints are by 5—10 % higher than for base metal, which is explained by the higher sensitivity of weld metal structure to electrodynamic effects [2].

Basing on the dependencies, presented in Figure 2, it can be concluded that increase of $\Delta\sigma$ values at EDT by adjustment of charge voltage U is preferable as compared with the variation of capacitance C. However, the application of capacitors with charge voltage U higher than 500 V is limited, as it is connected with working out of safety rules in operation with high-voltage manual tool. At the same time the increase of the battery capacitance C due to a number of capacitors leads to increase of mass and sizes of equipment for EDT. It causes the necessity of searching for compromising solutions based on use of modern element base and new design schemes of the discharge loop.

The influence of electrodynamic effects at different levels of primary stress σ_0 on relative efficiency EDT $\Delta\sigma/\sigma_0$ determined after single current discharge was evaluated. U values were preset in the range of 200—250 V, and value of σ_0 varied from 55 to 294 MPa, which approximately corresponds to previous experiments. The dependencies $\Delta\sigma/\sigma_0$ on σ_0 at different U

$(\Delta\sigma/\sigma_0)\cdot 100\ \%$
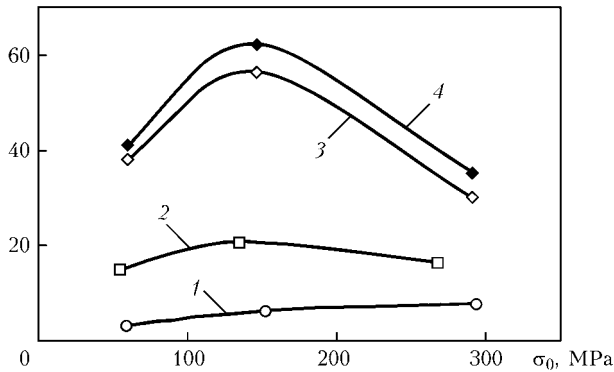
Figure 3. Effect of initial stress σ_0 on relative efficiency $\Delta\sigma/\sigma_0$ at EDT of alloy AMg6 and its welded joints at different values of charge voltage: $1 - U = 200$; $2 - 300$; $3, 4 - 500$ V; $1-3 -$ base metal; $4 -$ welded joint

determined for AMg6 alloy and its welded joints are presented in Figure 3, which shows that maximal efficiency of EDT corresponds to the level of initial stresses close to conditional yield strength of AMg6 alloy, that is confirmed by the data of works [2, 9]. The decrease of $\Delta\sigma/\sigma_0$ values at increase of tensile load higher than relative yield strength can be explained by negative influence of plastic deformation on efficiency of electrodynamic effects, that was earlier noted in the work [9].

The influence of charge voltage U of capacitor battery on parameters of electrodynamic effect of EDT, such as amplitude values of pulsed current I and dynamic load P in the time period t of capacitor discharge, was investigated. The measurements I and P were performed in hardware complex, the appearance and design elements of which are presented in Figure 4. The values of pulsed current I were registered using contactless method (Rogowski loop), which represents a solenoid of toroidal shape, embracing the conductor with current, whose principle of work is based on recording the magnetic field generated by measured current during its passing through the solenoid.

The parameters of dynamic loading P were determined using piezoelectric pressure sensor LKh-604.

The parameters I and P were measured using the following procedure. At the moment of discharge of capacitor battery C (see Figure 4, b) as a result of response of thyristor commutator Com, the pulsed current, passing through the inductance coil 1, flat disc 3, electrode 4, cylindrical specimen 5 subjected to load P, pressure sensor 6, was measured using Rogowski loop 7 and controlled using fast-response digital oscillograph 8.

In this case the mechanical pressure generated by a pulsed magnetic field of inductance coil was transferred through the insulator 2 to the flat disc and electrode, spherical edge of which during indenting into cylindrical specimen transferred impact load to a piezoelectric sensor, whose indications were recorded similarly to current values. Thus, material being treated, whose functions were fulfilled by the cylindrical specimen of low-carbon steel of 9 mm diameter and 6 mm height, was simultaneously affected by dynamic load P of working tool (electrode) and pulsed electric current I, caused by the discharge of capacitor battery.

The amplitude values of parameters I and P were recorded at different levels of charge voltage (Figure 5). During study of distribution of I and P in the time period the assumption was taken, based on the data of works [10, 11], that maximal influence on efficiency of electric pulsed and dynamic effects (to which EDT relates) is exerted by the processes of increment of pulsed current and pressure up to maximum values.
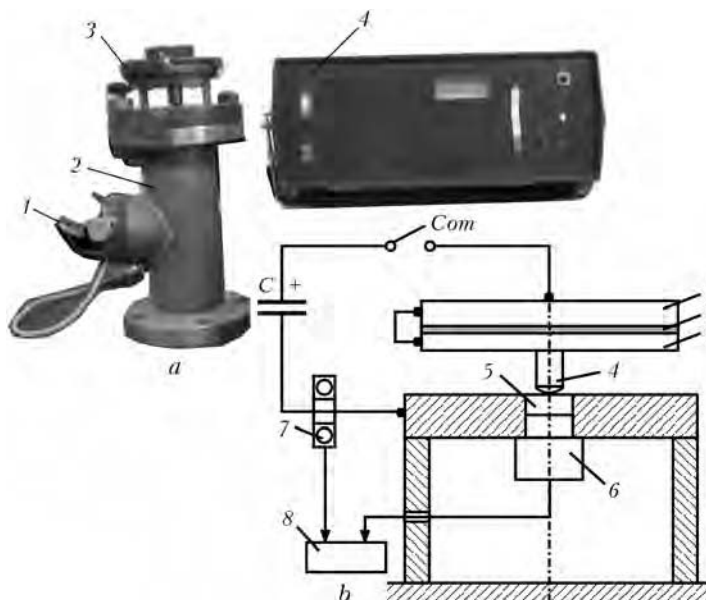

Figure 4. Appearance of hardware complex for measuring amplitude values of pulsed current I and dynamic loading P at EDT (a: $1 -$ Rogowski loop; $2 -$ casing of system for measuring load P; $3 -$ inductance coil with electrode; $4 -$ unit of charge and discharge of capacitors) and its design diagram (b) (for $1-8$ see the text)
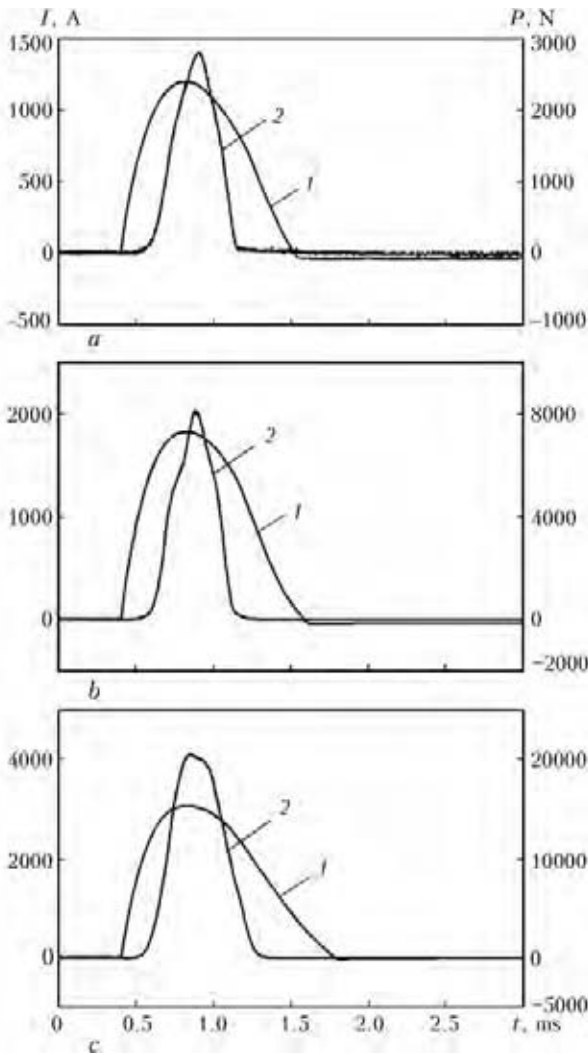
Figure 5. Amplitude values of pulsed current I (1) and dynamic load P (2) at different values of charge voltage: a — $U = 200$ V, $I_{max} = 1195$ A, $P_{max} = 2792$ N; b — $U = 300$ V, $I_{max} = 1838$ A, $P_{max} = 8162$ N; c — $U = 500$ V, $I_{max} = 3080$ A, $P_{max} = 20461$ N

Figure 6. Effect of charge voltage U on pulsed current I, dynamic loading P (a) and rate of their growth v_i and v_p (b)

As is seen from Figure 5, maximal values of pulsed current I_{max} cover the range from 1195 to 3080 A and are in direct dependence on the charge voltage U. This relates also to the rates of current increment up to I_{max} — v_i, which at $U = 200$, 300 and 500 V were, respectively, 3400, 4600 and 8000 A/ms.

The process of growth of dynamic pressure of electrode to the material being treated is running intensively. Thus, the maximal values of amplitude of pressure P_{max} are in the range from 2792 to 20461 N. Here, the time period t of growth of pressure from 0 to P_{max} at increase of values of charge voltage U from 200 to 500 V decreased from 0.375 to 0.340 ms, which determined the increase of rate of v_p of contact interaction of electrode with metal with increase of U. If v_p at $U = 200$ V did not exceed 7500 N/ms, then at increase of voltage up to 300 and 500 V its values were respectively 22000 and 60200 N/ms. Thus, the value of charge voltage U determines such parameters of dynamic pressure as P_{max} and gradient of function of increment P.

It can be seen in comparison of curves of increment of pulsed current and loading (see Figure 5) that the pulse of pressure is shorter and has steeper fronts of increment and drop. In the whole range of U values being investigated the delay of beginning of the process of increment P from increase of I by 0.1 ms occurs, which can be explained by deformation of contact surfaces of electrode and metal being treated. The increment of P begins at pulsed current 600, 800 and 1500 A for voltages, respectively, 200, 300 and 500 V. Thus, the process of contact interaction of electrode with metal begins at values of current approximately corresponding to $0.5I_{max}$.

The dependencies of amplitude values of current I and loading P, and also rates of their increment v_i and v_p on charge voltage U are presented in Figure 6, which shows that with increase of U the increment of I and P (Figure 6, a) as well as v_i and v_p (Figure 6, b) has a linear nature.

CONCLUSIONS

1. The experimental procedure of investigation of effect of electric parameters of EDT, such as charge voltage U and capacitance of capacitors C, on relative efficiency of treatment of AMg6 alloy and its welded joints as a result of electrodynamic effects has been developed.

2. It was established that efficiency of EDT is directly proportional to capacitance C at $U = $ const and square of voltages U^2 at $C = $ const, that corresponds to the expression for accumulated energy of the capacitor.

3. The experimental procedure was developed, on the basis of which the hardware-measuring complex was assembled to investigate the effect of charge voltage at EDT on such parameters as amplitude values of pulsed current I and dynamic loading P.

1. Lobanov, L.M., Pashchin, N.A., Loginov, V.P. et al. (2005) Application of electric pulse treatment of structural elements to extend their service life (Review). *The Paton Welding J.*, **11**, 19−23.
2. Lobanov, L.M., Pashchin, N.A., Loginov, V.P. et al. (2007) Change of the stress-strain state of welded joints of aluminium alloy AMg6 after electrodynamic treatment. *Ibid.*, **6**, 7−14.
3. Lobanov, L.M., Pashchin, N.A., Loginov, V.P. et al. (2007) Effect of electrodynamic treatment on stressed state of welded joints on steel St3. *Ibid.*, **7**, 6−8.
4. Lobanov, L.M., Pashchin, N.A., Skulsky, V.Yu. et al. (2006) Influence of electrodynamic treatment on the stress-strain state of heat-resistant steels. *Ibid.*, **5**, 8−11.
5. Lobanov, L.M., Pashchin, N.A., Loginov, V.P. (2010) Features of structure formation of aluminium alloys AMg5 under the effect of electric current pulses. *Visnyk Ukr. Materialozn. Tovarystva*, **3**, 33−42.
6. Lobanov, L.M., Makhnenko, V.I., Pashchin, N.A. et al. (2007) Features of formation of plastic deformations at electrodynamic treatment of welded joints of St3 steel. *The Paton Welding J.*, **10**, 7−11.
7. Lobanov, L.M., Pashchin, N.A., Loginov, V.P. et al. (2010) Effect of electric pulse treatment on residual change in shape of thin-sheet welded structures (Review). *Ibid.*, **3**, 10−13.
8. Antonov, Yu.A., Ragozin, Yu.I. (2001) Pulse method of residual stress relief. *Fizika i Khimiya Obrab. Materialov*, **3**, 91−95.
9. Lobanov, L.M., Pashchin, N.A., Loginov, V.P. et al. (2011) Influence of repeated loading on the efficiency of electrodynamic treatment of aluminium alloy AMg6 and its welded joints. *The Paton Welding J.*, **4**, 2−5.
10. Stepanov, G.V., Babutsky, A.I., Mameev, I.A. (2004) Nonstationary stress-strain state in long bar induced by high density electric current pulses. *Problemy Prochnosti*, **4**, 60−67.
11. Belova, M.M., Protsenko, S.S., Ivanov, A.V. (1987) Dynamics of deformation of elastic-plastic layer in pulse power generation. *Ibid.*, **12**, 87−91.

RISK OF FAILURE IN THINNING OF MAIN PIPELINE WALL AT THE AREA OF CIRCUMFERENTIAL WELDS IN THE PRESENCE OF BENDING MOMENTS ALONG THE PIPELINE AXIS

V.I. MAKHNENKO, E.A. VELIKOIVANENKO, G.F. ROZYNKA, N.I. PIVTORAK and **O.I. OLEJNIK**
E.O. Paton Electric Welding Institute, NASU, Kiev, Ukraine

The effect of longitudinal bending moment in pipeline with a wall thinning defect of large overall size in circumferential direction on the risk of failure is considered. It is shown that the critical sizes of thinning in circumferential direction can be determined with a certain conservatism on the basis of total nominal stresses induced by bending and internal pressure in pipeline.

Allowable overall size c of defects of thinning along the pipe circumference is much larger than that of s along the generatrix in pipeline loading with internal pressure P that is due to a large extent to higher circumferential normal stresses $\sigma_{\beta\beta}$, as compared with axial ones σ_{zz}, at other things being equal, that is demonstrated visually by the typical diagrams of limiting overall sizes c and s, given in work [1].

However, the thinning with high c values can be rather often observed under loading conditions when alongside with internal pressure P in the zone of thinning the bending moment M_{bend} is acting, caused by soil settling down (for underground pipeline) or wind load at certain air transitions, etc. The nominal stresses at such loading can noticeably change in the zone of a defective area of the pipeline wall.

There is a relationship for points in section $\beta \leq 0$ for nominal longitudinal stresses σ_{zz} in pipeline with internal pressure P and bending moment M_{bend}, acting in longitudinal plane $\beta = 0$, assuming the presence of pure elastic deforming and preserving the shape of pipe transverse sections:

$$\sigma_{zz} = \frac{PR}{2\delta} + \frac{M_{bend} \cos \beta}{\pi R^2 \delta}\left(1 + \frac{\xi}{R}\right), \qquad (1)$$

where R is the internal radius of pipeline; δ is the wall thickness $(-\delta/2 < \xi < \delta/2)$.

Relationship (1) can be presented in the form of

$$\sigma_{zz} = \frac{PR}{2\delta}\,[1 + \kappa(\beta)],$$

where $\kappa(\beta) = \dfrac{2M_{bend} \cos \beta}{\pi R^3 P}\,(1 + \xi/R)$ determines the addition, due to M_{bend}, to nominal stresses σ_{zz}, caused only by pressure in pipeline. If the defect of thinning is located so that $\beta = 0$ is in the middle of the defect length c and $c/2R < 0.1\pi$, then the membrane stresses in this zone prevail for all the β inside the interval

$-0.1\pi < \beta < 0.1\pi \cos\beta \approx 1.0$ and at $\delta/R < 0.1$. Consequently, when determining the critical sizes c_{cr} of defects for these cases it is possible to come from total nominal stresses σ_{zz}, acting in the zone $(-c/2 < \beta < c/2)$ or from the given pressure

$$P_{giv} = P(1 + \kappa)\ldots$$

Thus, on the basis of relationships indicated in work [1], as applied to critical overall sizes of defects of thinning (c_{cr} — along the circumference, s_{cr} — along the generatrix, and $a_{cr} = \delta - \delta_{min}$ in wall depth)

$$c_{cr} = 2R\sqrt{\frac{0.7358 + K_c}{10.511 - 13.838 K_c}}, \qquad (2)$$

where $K_c = \delta_{min}/[\delta]$; $[\delta] = P_{giv}R/[\sigma]$; δ_{min} is the minimum thickness of wall in defect zone; $[\sigma]$ are the allowable stresses for pipe material at the given area. Relationship (2) is valid for K_c within $0.2 < K_c < 0.7596$.

At $K_c < 0.7596$, $c_{cr} \to \infty$, at $K_c < 0.2$, $c_{cr} = 0.694R$. Value of s_{cr} (overall size of defect along the generatrix, negligibly reacting to a bending moment) is determined traditionally by an operating pressure P_{op}, i.e. at $\kappa = 0$

$$s_{cr} = \lambda_{cr}\sqrt{2R[\delta]}\,\frac{1}{1.285}, \qquad (3)$$

$$\lambda_{cr} = 1.299\sqrt{\left(\frac{1.0 - K_s}{0.9 - K_s}\right)^2 - 1.234}, \quad K_s = \frac{\delta_{min}}{P_{op}R}[\sigma].$$

Acceptability of effect of approximation approach of account for bending moment on critical sizes c_{cr} of defect of thinning was studied in this work on the basis of analysis of three-dimensional stressed state in the zone of defect of thinning for pipe steel with yield strength $\sigma_y = 480$ MPa, tensile strength $\sigma_t = 564$ MPa, modulus of elasticity $E = 2\cdot10^5$ MPa, Poisson's factor $\nu = 0.3$.

Figure 1 shows a pipeline element, cut out by coordinate planes $\beta = 0$, $z = 0$, $\beta = \beta_*$ and $z = z_*$, with external defect of wall thinning of an ellipsoid type, whose planes of symmetry coincide with planes $z = 0$ and $\beta = 0$. In plane $\beta = \beta_*$ the stresses $\sigma_{\beta\beta} = PR/\delta$ and $\sigma_{\beta z} = \sigma_{\beta r} = 0$ are acting, in plane $z = z_* - \sigma_{zz} = P_{giv}\dfrac{R\cos\beta}{2\delta}$ and $\sigma_{rz} = \sigma_{\beta z} = 0$, while in planes $\beta = 0$ and $z = 0$ the symmetry conditions are valid: the conditions of free surface are on internal surface $r = R$, $\sigma_{rr} = -P$ and $\sigma_{r\beta} = \sigma_{rz} = 0$, on the external surface $- r = R + \delta(z, \beta)$.

All the examined area was divided into separate finite elements (Figure 2), formed by orthogonal surfaces of a cylindrical system of coordinates, i.e. $r = $ const, $\beta = $ const, $z = $ const. Eight node points, obtained by crossing these surfaces, determine the calculation volume $\Delta V_{m, n, k}$ of each of finite elements,
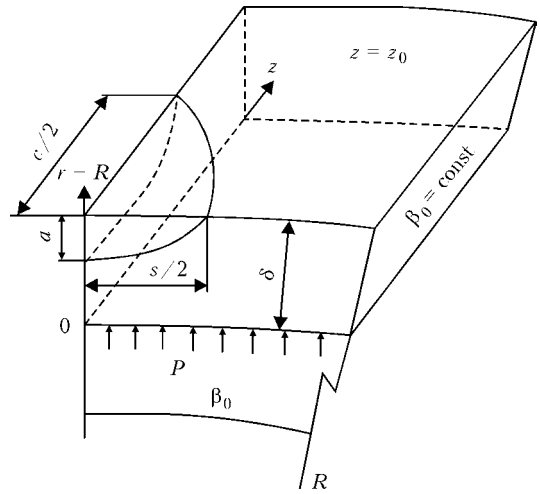
Figure 1. Region of pipeline $2R \times \delta$ in the zone of defect of thinning $c \times s \times a$, confined by surfaces $z = 0$, $z = z_*$, $\beta = 0$, $\beta = \beta_*$, $r = R$ and $r = R + \delta(z, \beta)$

for which the appropriate components of tensor of increment of deformations $\Delta\varepsilon_{ij}$ in the system of coordinate $i, j = r, z, \beta$ are expressed through components of vector of increments of displacements in the following way for the model of a finite element:

$$\Delta\varepsilon_{rr} = \frac{\Delta U_{m, n, k} - \Delta U_{m-1, n, k}}{r_{m, n, k} - r_{m-1, n, k}},$$

$$\Delta\varepsilon_{\beta\beta} = \frac{\Delta U_{m, n, k}}{r_{m, n, k}} + \frac{\Delta V_{m, n, k} - \Delta V_{m, n-1, k}}{(r\beta)_{m, n, k} - (r\beta)_{m, n-1, k}},$$

$$\Delta\varepsilon_{zz} = \frac{\Delta W_{m, n, k} - \Delta W_{m, n, k-1}}{z_{m, n, k} - z_{m, n, k-1}},$$

$$\Delta\varepsilon_{r\beta} = \frac{1}{2}\Big[r_{m, n, k}\frac{(\Delta V/r)_{m, n, k} - (\Delta V/r)_{m-1, n, k}}{r_{m, n, k} - r_{m-1, n, k}} + \qquad (4)$$
$$+ \frac{\Delta U_{m, n, k} - \Delta U_{m, n-1, k}}{(r\beta)_{m, n, k} - (r\beta)_{m, n-1, k}}\Big],$$

$$\Delta\varepsilon_{z\beta} = \frac{1}{2}\left[\frac{\Delta V_{m, n, k} - \Delta V_{m, n, k-1}}{z_{m, n, k} - z_{m, n, k-1}} + \frac{\Delta W_{m, n, k} - \Delta W_{m, n-1, k}}{(r\beta)_{m, n, k} - (r\beta)_{m, n-1, k}}\right],$$

$$\Delta\varepsilon_{rz} = \frac{1}{2}\left[\frac{\Delta U_{m, n, k} - \Delta U_{m, n, k-1}}{z_{m, n, k} - z_{m, n, k-1}} + \frac{\Delta W_{m, n, k} - \Delta W_{m-1, n, k}}{r_{m, n, k} - r_{m-1, n, k}}\right].$$
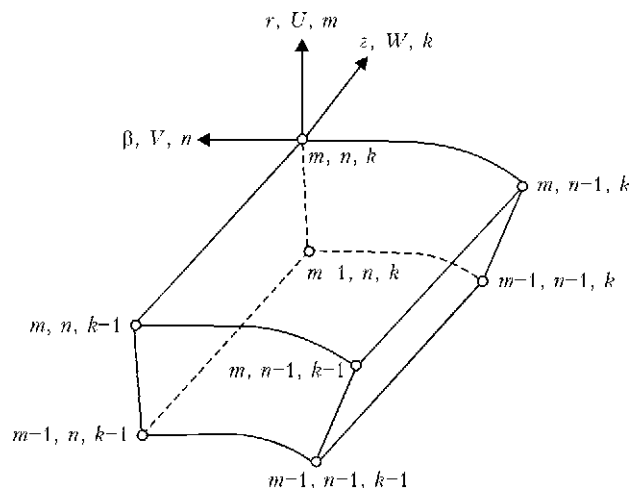
Figure 2. Scheme of finite element in system of coordinates β, z, r with appropriate displacements U, V, W and numeration of nodes m, n, k

The link of components of tensor $\Delta\varepsilon_{ij}$ with components of stress tensor σ_{ij} is realized on the basis of theory of elastic-plastic yielding of Prandtl−Reiss, associated with a yielding condition of Mises, i.e. the following relations given in work [2] are valid:

$$\Delta\varepsilon_{ij} = [\psi(\sigma_{ij} - \delta_{ij}\sigma) + \delta_{ij}K\sigma] - b_{ij} \quad (i, j = z, r\beta),$$

where ψ is the function of material state in finite element m, n, k; δ_{ij} is the unit tensor (Kronecker symbol); $\sigma = \dfrac{1}{3}(\sigma_{rr} + \sigma_{zz} + \sigma_{\beta\beta})$; $K = \dfrac{1 - 2\nu}{E}$; b_{ij} is the known function of stresses obtained at the previous step of observing the elastic-plastic deformations (denoted by index*):

$$b_{ij} = \left[\frac{\sigma_{ij} - \delta_{ij}\sigma}{2G} + \delta_{ij}K\sigma\right]^*.$$

Function of state ψ is determined at each step of observation coming from the condition of yielding, i.e.

$$\psi = \frac{1}{2G}, \text{ if } f = \sigma_{eq}^2 - \sigma_y^2 < 0, \tag{5}$$

$$\psi > \frac{1}{2G}, \text{ if } f = 0 \text{ and } \Delta f > 0,$$

where $\sigma_{eq} = -\sqrt{\dfrac{1}{2}(\sigma_{ij} - \delta_{ij}\sigma)(\sigma_{ij} - \delta_{ij}\sigma)}$; σ_y is the yield strength of material with account for work hardening, obtained at the previous step of observation; condition $f > 0$ is inadmissible.

Increments of components of tensor of plastic deformations at each step of observation are determined by the following relationships:

$$\Delta\varepsilon_{ij}^p = \left(\psi - \frac{1}{2G}\right)(\sigma_{ij} - \delta_{ij}\sigma) \quad (i, j = r, z, \beta).$$

Significant non-linearity, contained in conditions (5), is realized by iteration. An appropriate algorithm of iteration process is offered in work [2] and tested well enough in practice [3].

Components of stress tensor for each finite element (m, n, k) are connected with appropriate components
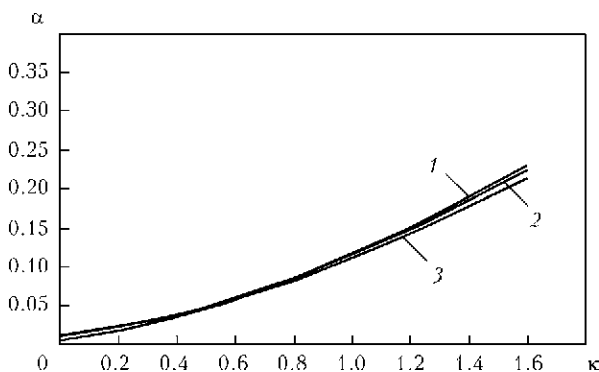

Figure 3. Results of calculation of failure probability depending on κ values at B_z from the Table at different a of 10 (*1*), 12 (*2*) and 14 (*3*) mm at $D = 1420$ mm, $\delta = 18$ mm, $P = 7.5$ MPa and $A = 522$ MPa)

in neighboring volumes or at the boundary surfaces by equilibrium equations.

Resolving system of algebraic equations relative to three components of vector of increments of displacements in each node (m, n, k) is formed at each step of observation and iteration by ψ as a result of minimizing of functional

$$E = -\frac{1}{2}\iiint\limits_Q (\sigma_{ij} + Y_{ij})\Delta\varepsilon_{ij}rdrd\beta dz + \int\limits_\Gamma q_i\Delta U_i$$

by unknown increments of displacements

$$\Delta U_i = \begin{vmatrix} \Delta U \\ \Delta V \\ \Delta W \end{vmatrix},$$

where Q is the volume of examining area with boundary Γ, in which the components of power load q_i ($i = r$, β, z) are preset:

$$Y_{ij} = \frac{1}{\psi}\left(\frac{\sigma_{ij} - \delta_{ij}\sigma}{2G}\right)^* + \delta_{ij}\frac{(K\sigma)^*}{K} \quad (i, j = r, \beta, z).$$

At a very small step of observation, when the linear relations are valid (4), the given algorithm allows accounting for the large deformations by means of displacement of nodes U, V, W (by specifying coordinates of nodes r, β, z in expression (4)). Here, the change in volumes of finite elements, indicated in coefficients of resolving equations, occurs only due to elastic deformations, i.e. it is negligible up to failure of integrity and can be neglected.

After receiving the data on kinetics of stress-strain state in the zone of thinning with the growth of P and M_{bend}, it is important to solve the problem concerning the model of integrity failure, as the traditional approach, based on maximum stresses in one separate point (element), is much conservative, in particular with account for a real shape of surface in the zone of a corrosion thinning.

The Weibull probabilistic approach, based on fault probability α at least in one point of «hot section» S_j in the zone of thinning, is worthy of attention, i.e.

$$\alpha = 1 - \exp\left\{-\int\limits_{S_j}\left[\left(\frac{\sigma_{jj} - A}{B_j}\right)^\eta\right]\right\}\frac{dS_j}{h_0^2} \quad (\sigma_{jj} > A).$$

Here, σ_{jj} (normal stresses in section with a normal j) and A, B, η (parameters of Weibull distribution) are determined on the basis of processing the appropriate experimental data.

It is possible to assume $\eta = 4.0$, $A = \dfrac{\sigma_t + \sigma_y}{2}$. The h_0 value is the geometric characteristic of a finite element in the zone of defect of thinning, at which the further decrease in sizes of the finite element does not influence the σ_{jj} value, B is determined on the basis of experimental critical sizes s_{cr} at $j = \beta$ or c_{cr} at $j = z$ (relationships (2), (3) at assumption that $\alpha =$

Results of calculation of parameter B_j and appropriate α_j at $P_{op} = 7.5$ MPa

a, mm	B_z, MPa	c_{cr}, mm ($\alpha = 0.05$)	α	B_β, MPa	s_{cr}, mm ($\alpha = 0.05$)	α_β
10	4980	840	0.00514	970	126	0.0099
12	5270	650	0.011	840	90	0.0066
14	4995	530	0.0112	525	66	0.0029

Figure 4. Results of calculation of effect of bending moment at c_{cr} from the Table for different a of 10 (*1*), 12 (*2*) and 14 (*3*) mm at $D = 1420$ mm, $\delta = 18$ mm, $P = 7.5$ MPa, $A = 522$ MPa and $B_z = 5080$ MPa

= 0.05, and the test pressure in pipe $P_{test} = 1.2P_{op}$ for $j = \beta$ and $P_{test} = 1.47P_{op}$ for $j = z$ and $w = 0$.

In accordance with these recommendations the values of B_j are determined for the examining pipe at $h_0 = 2$ mm, $A = 522$ MPa and different depths a of the defect.

It is seen from these data that increase in depth of the defect in the ranges of $10 \leq a \leq 14$ mm decreases the critical values of c_{cr} from 840 to 530 mm. However, in this case the B_z value is changed in relatively narrow ranges, such as 4980−5270 MPa, but not monotonously.

It is seen from Figure 3 that the curves of effect κ are arranged well enough on one curve at $P_{op}(1 + \kappa) = 1.47$ MPa; $\alpha = 0.05$, i.e. the bending here adds mainly the membrane stresses in section $z = 0$. The use of average B_z value for different a, as shown in Figure 4. without changing the quality pattern, gives quantitatively somewhat other results. It is characteristic that the presence of bending moment has a low influence on the risk of failure due to longitudinal size s of wall thinning.

The risk of failure α_β for $a = 14$ mm, $s = s_{cr} = 66$ mm, $P_{op} = 7.5$ MPa at different κ values is the following:

κ	0	0.2	0.4	0.6	0.8	1.0
α_β	0.0029	0.0033	0.0040	0.0034	0.0026	0.0018

CONCLUSIONS

1. It is shown that in evaluation of critical sizes s_{cr} and c_{cr} of defects of thinning of main pipeline wall in the presence of longitudinal bending moments, caused by soil settling, wind load, etc., it is possible to apply the recommendations of work [1] for s_{cr}, i.e. relationship (3), as the longitudinal bending moment has a low effect on s_{cr}.

2. For the circumferential overall size c_{cr} of defects of thinning, rather typical of the zone of site circumferential welds, the presence of bending moment can increase greatly the risk of failure. In this case the values of c_{cr} at known values of bending moment M_{bend} and internal pressure P can be evaluated by the relationships given in work [1], i.e. by expression (2) using the given pressure P_{giv}.

1. (2000) *Fitness-for-service*: American Petroleum Institute Recommended Practice 579. 1st ed.
2. Makhnenko, V.I. (1976) *Computational methods of investigation of welding stress and strain kinetics*. Kiev: Naukova Dumka.
3. *MRK-KhR−2000*: Procedure for determination of residual life of WWER nuclear reactor body during service. Moscow; St.-Petersburg.

INVESTIGATIONS ON LASER BEAM WELDING OF HIGH-MANGANESE AUSTENITIC AND AUSTENITIC-FERRITIC STAINLESS STEELS

V. QUIROZ, A. GUMENYUK and **M. RETHMEIER**
BAM Federal Institute for Materials Research and Testing, Berlin, Germany

4.4 kW Nd:YAG laser and 5 kW CO_2 laser were applied to welding 1.5 mm stainless steel sheets in CW mode. Manganese austenitic and lean duplex steels were selected as test materials and for comparison with standard austenitic and duplex steels. The influence of main laser welding parameters on process stability and resulting weld quality, as well as the effects of weld edge preparation on the weld appearance and quality levels, were investigated. The welded joints obtained were subjected to radiographic tests for detection of internal imperfections, tensile and potentiodynamic tests were performed to evaluate the mechanical and corrosion properties. The results provide an insight into the advantages and limitations of the laser beam welding process for joining high-manganese alloyed stainless steels. Conditions for the production of defect-free and corrosion-resistant welds having good mechanical properties could be determined.

Instabilities in the nickel price as a consequence of the high demand for stainless steels and, for instance, current forecasts of supply shortages in feedstock [1] are driving the introduction of more cost effective alternatives. The partial substitution of less expensive manganese and small amounts of nitrogen for nickel in austenitic and duplex stainless steels has been reported to be a viable option [2–6]. The role of nitrogen is crucial, as it helps to stabilize the austenite phase and further results in increased strength and work hardening [7] without affecting the ductility properties of the material [8]. That is favourable for weight reduction and better energy absorption in crash [9].

Corrosion, microstructure and mechanical properties of various CrMnNi-steels have already been extensively investigated [3, 6, 10–13]. However, weldability is still an insufficiently explored aspect. In this respect, the laser welding method offers several advantages in comparison with other processes as high welding speed and low heat input, which reduces effectively component distortion and metallurgical damage. Laser weldability is closely related to some spe-

cific process characteristics. The keyhole and, consequently, process stability can, for example, intensively be affected by the laser type and parameters [14]. This directly influences the weld quality, as spatter, underfilling, humping and porosity may arise in dependence of the keyhole behaviour. Furthermore, the high resulting cooling rate can alter the weld metal phase balance, when welding duplex stainless steels, as the austenite formation, which is primarily controlled by the diffusion of nitrogen, is diminished [15].

In this study, laser welding experiments applying two different laser sources was carried out with the objective of analysing the influences of corresponding process specificities on weldability of the austenitic and austenitic-ferritic CrMnNi-steel, in comparison with standard CrNi-steel grades. The obtained weld quality was examined in terms of weld appearance, internal imperfections, microstructure, as well as resulting corrosion and mechanical properties.

Experimental. For the investigations, the austenitic CrMnNi 1.4376 and lean duplex 1.4162 steels were selected as test materials. The standard austenitic 1.4301 and duplex 1.4362 steels were chosen for comparison. Chemical composition of the materials investigated is given in Table 1. All sheets had thickness of 1.5 mm.

Table 1. Chemical composition of the investigated materials, wt.%

	C	Cr	Ni	Mn	Si	P	S	Cu	Nb	Mo	N
1.4376	0.03	18.03	5.09	6.55	0.42	0.023	0.005	0.23	0.01	0.10	0.15
1.4301	0.04	18.82	8.79	1.36	0.38	0.027	0.004	0.45	0.01	0.19	0.05
1.4162	0.04	22.42	1.83	3.84	0.34	0.028	0.004	0.43	0.01	0.11	0.14
1.4362	0.03	22.86	4.33	1.40	0.002	0.023	0.002	0.52	0.01	0.13	0.12
Fe — balance.											

Table 2. Laser characteristics

	CO_2 laser	Nd:YAG laser
Wavelength, μm	10.6	1.064
Laser beam delivery	Mirror	600 μm fibre
BPP, mm·mrad	17 (TEM_{20})	24
Focal distance, mm	200	200
Focus diameter, μm	~400	~600

Table 3. Laser welding parameters investigated

	Butt welding			Overlap welding		
	P_L, kW	v_w, m/min	F, mm	P_L, kW	v_w, m/min	F, mm
CO_2	2.4	3	0	2.4	2.5	0
	3.6	4		3.6	3.0	
	5.0	6		5.0	6.0; 7.0	
Nd:YAG	2.0	3	0	2.0	2.0	0; −3
				3.0	3.0	
				4.0	4.0; 5.0	

Welding was performed with 4.4 kW Nd:YAG and 5 kW CO_2 laser. Data on their characteristics are listed in Table 2.

Experiments were conducted in butt and overlap joint configurations. The effects of the weld edge preparation by using laser cutting or shear cut edges on weld quality were investigated for butt joints. Shielding gas for Nd:YAG laser welding was argon. For welding experiments with the CO_2 laser, a mixture of helium and argon (50/50) was necessary to suppress plasma. The shielding gas was applied coaxially. In addition, experiments were carried out with a trail gas nozzle. In case of the duplex steels, nitrogen was applied as shielding gas in order to examine its influence on the austenite reformation in weld metal. Pure argon was used as forming gas for butt welding. Other investigated welding variables were the shielding gas flow rate, focal point position F, laser power P_L and welding speed v_w (Table 3).

Radiographic non-destructive testing was used for evaluation of the weld internal imperfections. Cross sections of the welds were produced using conventional techniques to analyse the resulting microstructure. The obtained austenite fraction in the duplex steel weld metal was assessed by image analysis. The Vickers microhardness was determined at a load of 0.5 kg, and the weld tensile properties were determined for 4 transverse specimens.

Potentiodynamic experiments in salt solution (pH 4.5) were carried out at the room temperature to investigate pitting corrosion of all base materials, as well as of the produced butt and overlap joints. A standard hydrogen electrode (SHE) was used as reference one. The critical pitting (E_{cr}) and repassivation (E_{rep}) potentials were determined for pickled and non-pickled samples from dynamic cyclic anodic polarization curves. E_{cr} and E_{rep} were obtained from the points, where, respectively, the current density continuously exceeds 0.01 mA·cm^{-2}, and where the current density again goes near zero.

Results and discussion. *Process stability and weld quality.* Spatter formation proved to be related with several process variables. It was found, for example, that spatter was much more pronounced by

using the Nd:YAG laser (Figure 1). This may be linked to the missing stabilizing effect of plasma, which is given in case of the CO_2 laser, at least in the keyhole depth.

High manganese content in the steel grade also had negative effect on the process stability. Vaporization of this volatile element enhanced melt expelling from the weld pool [16]. Another factor affecting the process stability was the focal point position (see Figure 1). By choosing the focus point in the negative range, spattering was considerably reduced. In addition, spattering was more severe in the overlap joints in comparison with butt ones. High shielding gas flow rates also supported spatter formation by causing instabilities on the weld pool behaviour. A stable spatter-free process could be achieved with flow rate up to about 20 l/min.

Oxidation of the weld surface and heat tint formation was influenced by the shielding gas type and supply. By CO_2 laser welding the use of a bypass led to a better weld surface quality. Complete oxidation prevention was successfully achieved for both laser welding processes with the additional trail gas nozzle.

The weld geometry was found to be strongly dependent on the joint edge quality. Shear cut joint preparations provided an irregular sheet edge geometry which resulted into gap sizes far exceeding the desired zero gap. Figure 2, *a* shows, for example, irregular weld shape with top bead depression and root concavity for this case. On the other hand, weld edge preparation by laser cutting led to a satisfactory weld geometry (Figure 2, *b*). A further advantage concerns the possibility to integrate laser welding and cutting, which may bring advantages in industrial processing.

Radiographic examinations detected no cracks for either CO_2- or Nd:YAG-welds. Pore formation was found to be dependent on the laser process, penetration mode, material and welding speed. Intense porosity only occurred at partial penetration in the overlap joints and was considerably more severe for Nd:YAG
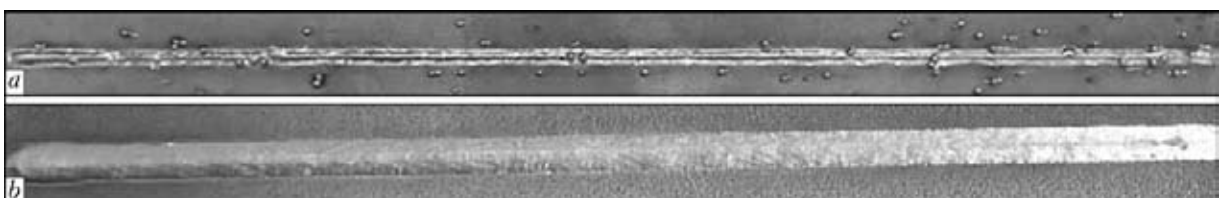

Figure 1. Spattering in the 150 mm weld zone in welding with Nd:YAG laser at v_w = 4 m/min, F = 0 (*a*) and −3 (*b*) mm
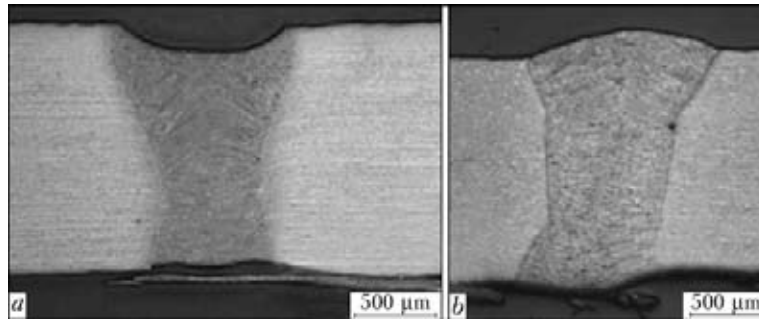
Figure 2. Butt weld with shear (*a*) and laser (*b*) cut edges

Table 4. Cr/Ni equivalents and solidification mode for all studied materials according to H&S and Hull diagrams

Material	H&S			Hull			Solidification
	Cr_{eq}	Ni_{eq}	Cr_{eq}/Ni_{eq}	Cr_{eq}	Ni_{eq}	Cr_{eq}/Ni_{eq}	
1.4376	18.82	10.14	1.86	18.35	9.40	1.95	FA
1.4162	23.10	6.32	3.66	22.72	6.00	3.79	F
1.4301	19.67	11.25	1.75	19.23	11.04	1.74	FA
1.4362	23.06	7.65	3.02	23.02	7.66	3.01	F

laser welding. It only arose at the lowest investigated welding speeds in the standard CrNi-steels (1.4301 and 1.4362). This may be explained in the keyhole behaviour. At low welding speeds, unstable melt flow leads to swelling of the keyhole, causing bubbles to generate from the keyhole tip in an unstable molten pool. In contrast, at high welding speeds the better keyhole stability can be reached [14].

Microstructure. Both studied austenitic steels underwent a primary ferrite solidification. This was determined from Cr/Ni equivalents (Table 4) and confirmed in microstructural examinations. The Hammer and Svenson (H&S) and Hull diagrams provided a tolerable correlation between the composition and the solidification mode, taking into account the special austenitizing effect of manganese.

Rapid cooling resulting from laser welding led to dendritic structure with retained delta-ferrite (Figure 3). The cooling rate also influenced the amount of primary ferrite. At high rates, transformation of reduced amount of delta-ferrite to austenite was occurred.

Duplex stainless steels owe their specific properties to the balanced two-phase microstructure consisting of ferrite and austenite of approximately equal pro-

portions. The weld metal solidified in a ferritic mode, as predicted by H&S Cr/Ni equivalents.

By application of 100 % N_2, a maximal austenite content of about 20 % was obtained. In comparison with the specimens welded only in argon or argon/helium atmosphere, the austenite content values considerably increased (Figure 4).

No significant differences were found between the nitrogen absorption in Nd:YAG- or CO_2-laser welding under the conditions investigated.

Figure 4 also reveals that the lean duplex steel 1.4162 has a lower capacity for austenite reformation, which can be explained in the poorer austenitizing properties of manganese, compared to nickel.

In general, the effect of nitrogen on austenite formation is limited, because its absorption is hindered by the small weld pool surface and the higher partial pressure of metal vapour in the keyhole [17]. In the micrographs of both duplex steels 1.4362 and 1.4162 (see Figure 4) welded in 100 % N_2 atmosphere mainly allotriomorphic grain boundary austenite, but also small amounts of intergranular austenite precipitates can be observed.

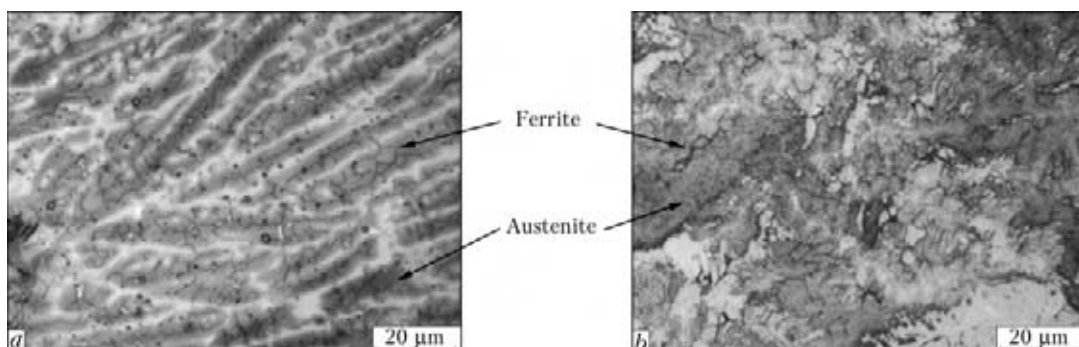Figure 5 shows the Vickers microhardness measurements in the centre of the weld cross sections. These

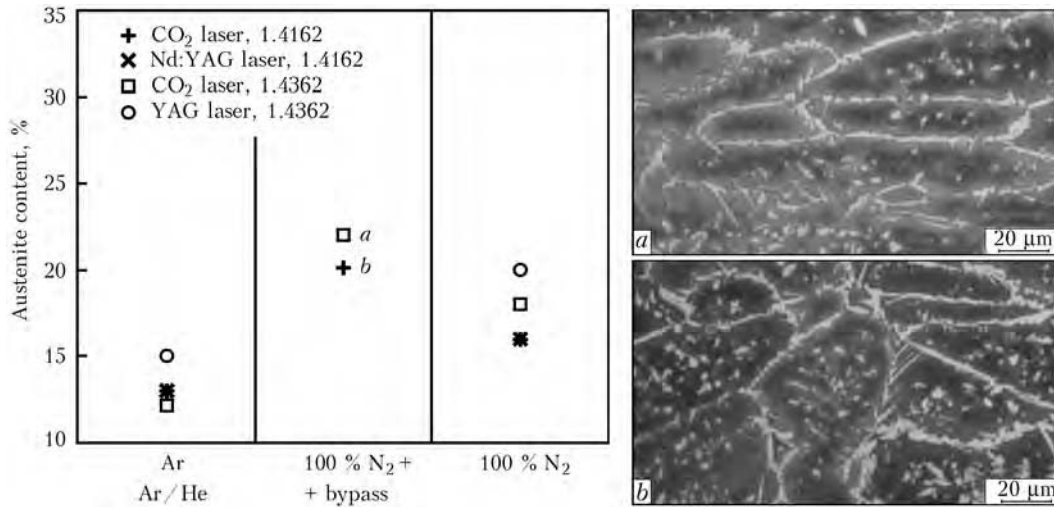Figure 3. Steel 1.4301 (*a*) and 1.4376 (*b*) weld microstructure

Figure 4. Austenite content in duplex steel welds obtained in CO_2- and Nd:YAG laser welding with and without nitrogen addition, and their microstructure (for explanation see the text)

reveal an increase of hardness in the weld metal for both duplex steels welded with 100 % N_2. The higher ferrite content and effect of nitrogen led to an increment of the hardness in this area. In the HAZ and in the bulk material similar lower values are obtained.

Regarding the austenitic steels, only a slight increase can be observed from the base material to HAZ and weld. Hardness of austenitic stainless steel 1.4376 is higher in comparison with standard CrNi-steel which results from the higher nitrogen content.

Mechanical properties. The mechanical properties of the investigated materials are mainly characterized by the corresponding microstructure. Austenitic stainless steels owe high work hardening properties and can achieve elongations of 50 %. The austenitic high-manganese alloyed steel possesses not only a high strength due to the higher nitrogen content, but also a good formability. Duplex steels have better properties than the austenitic ones due to the combination of strength and ductility provided by the ferrite and austenite phases, respectively. However, the enhanced amount of ferrite in the weld metal, in consequence of the high cooling rates, is expected to influence the mechanical properties.

The results of tensile tests of 4 welded samples per investigated material transversally to the welding direction show that the strength of the welded joints is close to that of the base material (Table 5).

Table 5. Tensile strength of base metal and welded samples, MPa

Steel	1.4376	1.4301	1.4162*	1.4362*
Base metal	750	650	750	770
Sample 1	740	665	750	760
Sample 2	755	655	750	765
Sample 3	700**	655	750	550**
Sample 4	750	655	750	760*
*Welded in 100 % N_2 atmosphere. **Fractured along the fusion line.				

Failure occurred predominantly in the base material. Only single sample of steel 1.4376 and 1.4362 was fractured along the fusion line, which led to a reduction of the measured tensile strength.

Corrosion properties. The results of potentiodynamic tests revealed the austenitic stainless steel 1.4301 to exhibit the higher E_{cr} and E_{rep} potentials in comparison with the manganese-alloyed steel 1.4376, indicating a superior pitting resistance (Figure 6). According to the obtained E_{cr} values, the austenitic steel 1.4301 is approximately equivalent to the lean duplex steel 1.4162, and CrNi-duplex steel 1.4362 had the highest E_{cr} values.

Since the chromium content for both austenitic and also for both duplex stainless steels is similar (see Table 1), it appears that nickel has decisive influence on the corrosion properties of the materials. In study [11] it could be demonstrated that nickel is enriched in the surface during active dissolution, which does not apply to manganese. This is supposed to support the passive film formation, as in this way the dissolution rate decreases. The influence of manganese on corrosion resistance is also related to the increased amount of inclusions, e.g. manganese and chromium oxides that act as preferential sites of pitting [6]. The pitting corrosion behaviour of butt as
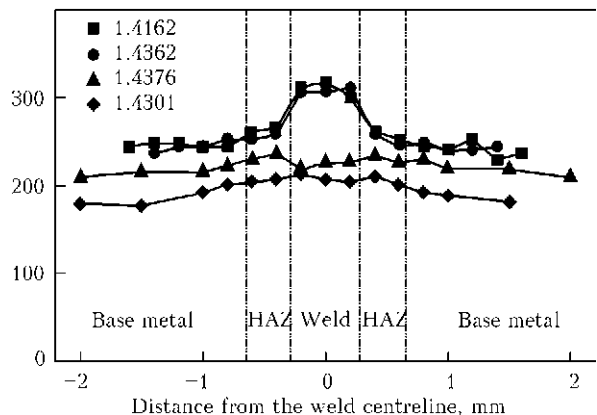

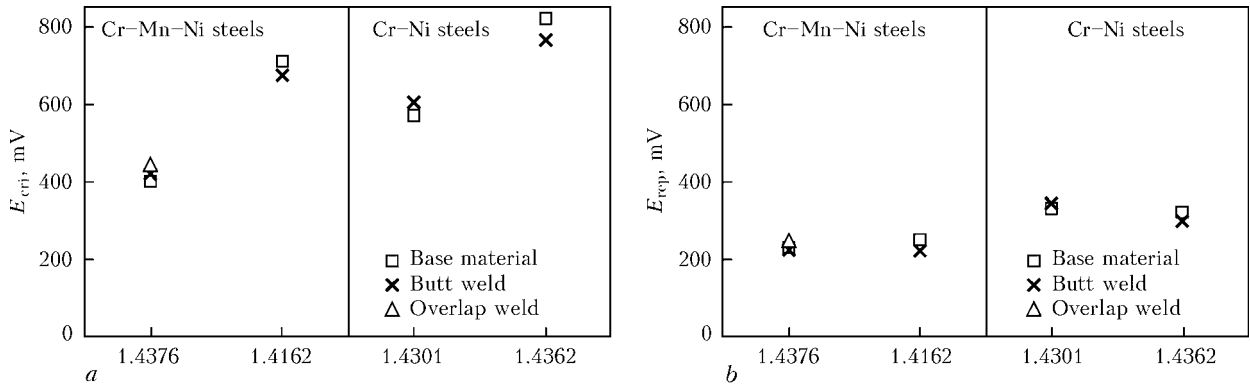**Figure 5.** Hardness measurements in the middle of weld metal on all materials investigated

Figure 6. Critical pitting E_{cr} (*a*) and repassivation E_{rep} (*b*) potentials obtained from anodic current density/potential curves for all investigated previously pickled materials

well as overlap welds and base materials is comparable in all cases (see Figure 6). This indicates that a good weld quality can be obtained under the investigated conditions.

CONCLUSIONS

CO_2- and Nd:YAG laser welding of austenitic and austenitic-ferritic manganese-alloyed stainless steels was proven to be suitable for the production of high quality butt and overlap welded joints. Welds on all the investigated materials showed strength, hardness and corrosion performance that is consistent with or close to that of the base metal. Though following aspects need to be considered:

• manganese-alloyed steels are, in comparison with standard CrNi-steels, more prone to cause process instabilities that led to spatter formation;

• porosity tends to arise by incomplete penetration in the overlap joint and is highly influenced by the welding speed. Though, it was possible to avoid weld imperfections by adequate parameter settings;

• temper colours on the weld surface can be prevented by using a trail gas nozzle behind the weld;

• regarding the weld edge preparation, laser cutting is more effective than shear cutting as it allows the gap size reduction and weld homogeneity;

• the use of nitrogen as shielding gas during laser welding of duplex steels improves austenite reformation. Maximal austenite fraction in the weld of 20 % could be obtained. Although the austenite proportion is not so large, a good weld quality can be achieved;

• concerning the corrosion properties, the lean duplex steel 1.4162 was found to be comparable with the conventional steel 1.4301. The austenitic manganese-alloyed steel 1.4376 exhibited the lowest corrosion resistance, and standard duplex steel 1.4362 — the highest.

1. Hunt, B. (2010) *Nickel in perspective.* Wood Mackenzie.
2. Charles, J. (2007) The new 200-series: An alternative answer to Ni surcharge? Risks and opportunities? *La Revue de Metallurgie*, June, 308—317.
3. Kim, K., Kim, Y, Lee, Y. et al. (2004) Application study of an automotive structural part with Ni-alloyed high strength austenitic stainless steel: Paper 2001-01-0884. In: *Proc. of SAE World Congress*, 2004.
4. Klueh, R.L., Maziasz, P.J., Lee, E.H. (1988) Manganese as an austenite stabilizer in Fe—Cr—Mn—C-steels. *Materials Sci. and Eng. A*, 102(1), 115—124.
5. Singhal, L.K. (2006) Stainless steels recent developments and outlook: Demand, capacity and product development. In: *Joint India/OECD/IISI Workshop*, Vol. 15, 21.
6. Toor, I., Hyun, P.J., Kwon, H.S. (2008) Development of high Mn—N duplex stainless steel for automobile structural components. *Corrosion Sci.*, 50(2), 404—410.
7. Zuev, L.B., Dubovik, N.A., Pak, V.E. (1997) Nature of hardening of high-nitrogen steels based on iron-chronium-manganese austenite. *Stal*, 27(10), 71—75.
8. Myslowicki, S. (2007) *Das Auscheidungs- und Korrosionsverhalten eines stickstofflegierten, austenitischen Chrom-Nickel-Stahls mit abgesenkten Nickelgehalt.* Aachen: Shaker.
9. Ratte, E., Leonhardt, S., Bleck, W. et al. (2006) Energy absorption behaviour of austenitic and duplex stainless steels in a crash box geometry. *Steel Res. Int.*, 77(9/10), 692—697.
10. Honeycombe, J., Gooch, T.G. (1972) Effect of manganese on cracking and corrosion behavior of fully austenitic stainless steel weld metals. *Metal Construction and British Welding J.*, 4(12), 456—460.
11. Falkenberg, F., Johansson, E., Larsson, J. (2007) Properties of various low-nickel stainless steels in comparison to AlSl 304. In: *Proc. of Stainless Steel World Conf. & Expo 2007* (Maastricht, the Netherlands), 355—371.
12. Tzaneva, B.R., Fachikov, L.B., Raicheff, R.G. (2006) Pitting corrosion of Cr—Mn—N steel in sulphuric acid media. *J. Appl. Electrochemistry*, 36(3), 347—353.
13. Zardiackas, L.D., Williamson, S., Roach, M. et al. (2003) Comparison of anodic polarization and galvanic corrosion of a low-nickel stainless steel to 316LS and 22Cr—13Ni—5Mn stainless steels. In: *Stainless steels for medical and surgical applications*, 107—118.
14. Katayama, S. (2009) Fundamentals of fiber laser welding. In: *Proc. of Int. Colloquium on High Power Laser Welding* (Berlin).
15. Amigo, V., Bonach, E.V., Teruel, L. et al. (2006) Mechanical properties of duplex stainless steel laser joints. *Welding Int.*, 20(5), 361—366.
16. Brooks, J.A. (1975) Weldability of high N, high Mn austenitic stainless steel. *Welding Res. Suppl.*, 189—195.
17. Dong, W., Kokawa, H., Sato, Y. et al. (2003) Nitrogen absorption by iron and stainless steels during CO_2 laser welding. *Metall. and Mater. Transact. B*, Febr., 75—82.

INCREASING WEAR RESISTANCE OF TITANIUM BY ARGON ARC OVERLAYING

V.P. PRILUTSKY[1], **S.B. RUKHANSKY**[1], **S.V. AKHONIN**[1], **N.F. GADZYRA**[2] and **N.K. DAVIDCHUK**[2]
[1]E.O. Paton Electric Welding Institute, NASU, Kiev, Ukraine
[2]I.M. Frantsevich Institute of Problems of Materials Science, NASU, Kiev, Ukraine

Results of the comprehensive investigations aimed at development of a fundamentally new overlaying consumable for deposition of wear-resistant layers on the surface of titanium alloys, i.e. titanium flux-cored filler wire, are given. The process was developed for overlaying by using the argon arc controlled by the external transverse alternating magnetic field. It is shown that the deposited metal provides a 10 times increase in tribotechnical surface properties of titanium VT1-1.

Titanium alloys are finding an increasingly wider application in power engineering, motor car construction, aerospace engineering, aircraft engineering and other industries. However, independently of the type and system of alloying, titanium alloys are susceptible to contact seizure in friction and, consequently, to considerable wear and mechanical damage of contact surfaces. Susceptibility to frictional seizure is an important drawback of titanium alloys, which makes it difficult and in a number of cases impossible to use them in friction units of machines and mechanisms. Tribotechnical properties of parts of titanium alloys can be improved by using the same friction surface treatment technologies as those used for other metals: thermochemical treatment, electroplating, spraying, laser and electric-spark surface alloying, etc. However, the efficiency of these technologies for titanium alloys is low, as a rule, and does not meet the necessary requirements. For instance, thickness of a layer in thermochemical treatment does not exceed 100 μm, electroplated coatings fail rapidly, thickness of the plasma-deposited layer is not in excess of 0.35 μm, and depth of the molten zone in laser and electric-spark surface alloying is no more than 120 μm. Essential drawbacks of such coatings are a limited thickness of the deposited layer and its cracking. The most promising process for this purpose is overlaying by the arc method using the specially developed composite materials and alloys that contain carbides [1].

The authors of study [2] developed a titanium-base wear-resistant overlaying consumable that is dispersion-strengthened by carbides. The alloy suggested provides high tribotechnical properties of the deposited surface in overlaying on titanium parts. However, low deformability of this alloy does not allow making a consumable from it in the form of a filler wire. The absence of such materials hampers considerably development of a reliable overlaying process, which

could make it possible to change surface properties of the titanium parts by the argon-arc method in the automatic mode.

The purpose of this study was to develop the fundamentally new type of an overlaying consumable for titanium, which would provide a deposited layer on the surface of the titanium parts with the required level of tribotechnical properties, as well as to elaborate the process for depositing it by using the argon arc.

The new overlaying consumable was developed on a base of titanium flux-cored wire, which consists of a sheath of commercial titanium of the VT1-00 grade with a core located inside it [3]. The core contains a composite powder produced as a result of interaction between nanosized non-stoichiometric silicon carbide in the form of its carbon solid solution and titanium.

Synthesis of the solid solution of carbon in silicon carbide is provided in the dispersed silicon−thermally expanded graphite (TEG) system, this leading to development of self-propagating high-temperature synthesis (SHS) of non-stoichiometric silicon carbide with a decreased value of the lattice parameter [4]. A distinctive feature of the suggested process is that owing to structural peculiarities of TEG its mechanical mixing with dispersed silicon results in formation of conglomerates of particles with a honeycomb-like structure. This structural state of the charge allowed the SHS method to be modified by initiating it in microvolumes and intensifying the gas-transport reactions. Performance of certain operations on preparation of TEG and temperature treatment of the charge creates conditions for development of «glow» SHS of silicon carbide. Such non-equilibrium synthesis conditions provide a characteristic structural state formed as a result of violation of stoichiometry, this leading to formation of a nano-composite structure of the particles, similar to that of the solid solution of carbon in silicon carbide [4].

Examinations of structure of these particles characterised by a decreased value of the lattice parameter show that the «glow» SHS process provides formation
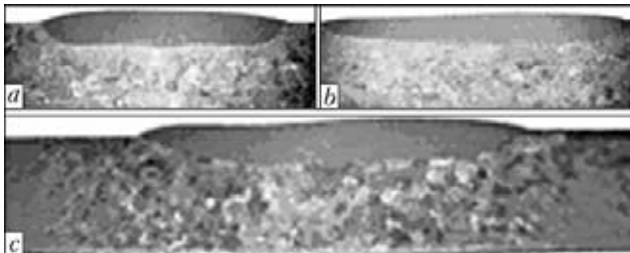
Figure 1. Effect of values of magnetic induction on width of deposited layers: a — B = 6.2 (S1); b — 7 (S2); c — 7.5 mT (S3)

of the states that are caused by the planar carbon defects present in a structure. The concentration of these defects is not in excess of 1 at.%, this leading to a formula content of silicon carbide equal to $Si_{0.993}C_{1.007}$ [5].

The exothermic reaction occurring in a mixture of the synthesised silicon carbide powder (solid solution of carbon in silicon carbide) and electrolysis titanium powder leads to formation of new phases, such as titanium carbonitride and silicide (TiC_xN_y and Ti_xSi_y). Variations in weight proportions of the charge components allows achieving different formula states of titanium carbonitride and silicide, which is a result of non-equilibrium of the process and exothermicity of the reaction between silicon carbide and titanium. The proportion of the components established by optimising the charge composition is 25SiC−75Ti. This resulted in formation of the finely dispersed composite powder containing titanium carbonitride $TiC_{0.4}N_{0.6}$ and titanium silicide Ti_5Si_3 intended for use as a flux-cored wire core.

The flux component containing fluorides of alkaliearth metals was added to the charge of the core to prevent porosity in overlaying and increase density of the deposited metal.

Noteworthy is the expediency of performing overlaying by the argon arc method, which is the most extensively used and versatile method for automatic welding of titanium. The main difference of the overlaying process from the welding one is that in overlaying it is necessary to ensure the minimal depth of penetration of the base metal. This requirement is difficult to meet by using the free-burning argon arc, as it causes uncontrollable deep penetration of the base metal at the centre of the arc column. As a result, the deposited metal mixes with the base one, thus leading to anisotropy of properties of the deposited
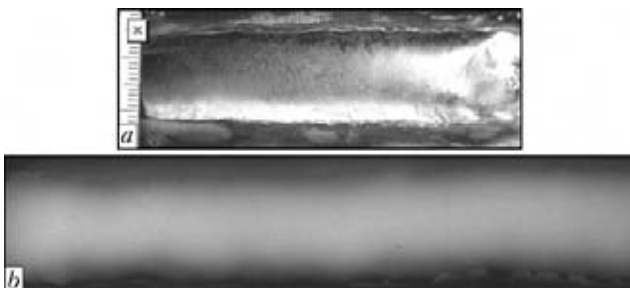

Figure 2. Appearance (*a*) and X-ray photograph (*b*) of deposited layer
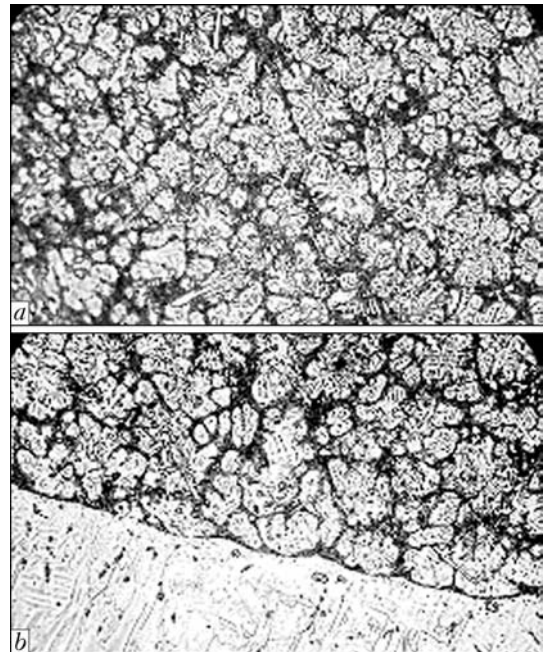
Figure 3. Microstructure (×200) of central part of deposited metal layer (*a*) and fusion zone (*b*)

layer both through the height and along the length. Moreover, changing the width of the deposited layer by this method in one pass is a real problem.

The external transverse magnetic field that allows controlling the process of formation of the deposited layer was used to regulate the width of this layer and, at the same time, decrease the depth of penetration of the base metal [6].

The investigations conducted resulted in the development of the process for manufacture of the 3 mm diameter flux-cored filler wire, as well as in the determination of the main parameters of the magnetic field providing the deposited layer with the required properties in one pass. For instance, a change of 6.2–7.5 MT in the value of magnetic induction B at frequency f = 4 Hz provides the deposited layer up to 20 mm wide at a penetration depth of no more than 2 mm (Figure 1).

The deposited metal layer features a satisfactory formation (Figure 2, *a*) and is free of pores (Figure 2, *b*). Microstructural examinations of the deposited metal layers revealed the presence of a uniform dendritic structure (Figure 3). Characteristic structural peculiarities observed in the central part of the deposited metal persist also in the immediate proximity to the fusion zone, this being indicative of stability of functional properties in the entire volume of the deposited metal layer.

Examinations of phase composition of the deposited metal layer by X-ray diffraction analysis showed that it consists of three phases: α-Ti, hypostoichiometric titanium carbide TiC_x ($x \approx 0.5$), in which part of the carbon atoms are replaced by the nitrogen atoms, and a high-temperature phase of titanium silicide Ti_5Si_3 (Figure 4).

Figure 4. Typical X-ray pattern of metal of the layer deposited on the VT1-1 substrate

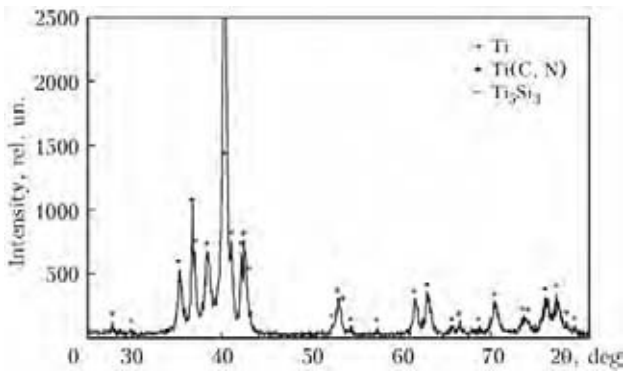Evaluation of properties of the deposited metal layers showed that the values of microhardness ($HV0.2$) amount to 14−15 GPa, and those of hardness ($HV30$) − to 9.0−9.5 GPa.

Tribological tests were carried out on the deposited metal specimens (S1, S2, S3) made under different process conditions (see Figure 1). To compare, tribological properties of the VT1-1 substrate were investigated as well. Wear resistance was evaluated from the loss of weight of a specimen on a friction path of 1 km. The test results are presented in Figure 5.

Comparison of the intensity of wear (weight loss) of the deposited specimens with that of the substrate specimen showed that the deposited specimens are superior by almost an order of magnitude to the substrate in wear resistance under the 2 and 4 kg loads. Under a load of 6 kg the value of wear resistance of the deposited specimens decreases, but compared to that of the substrate it is 2 to 6 times higher. Wear of the mating body (steel 45, $HRC = 45−48$) decreases under the 2 and 4 kg loads from 5 to 7 times, whereas under the 6 kg load it decreases by a factor of 2.6 to 2.8.

Therefore, the investigations conducted proved the possibility of a 10 times increase in tribotechnical
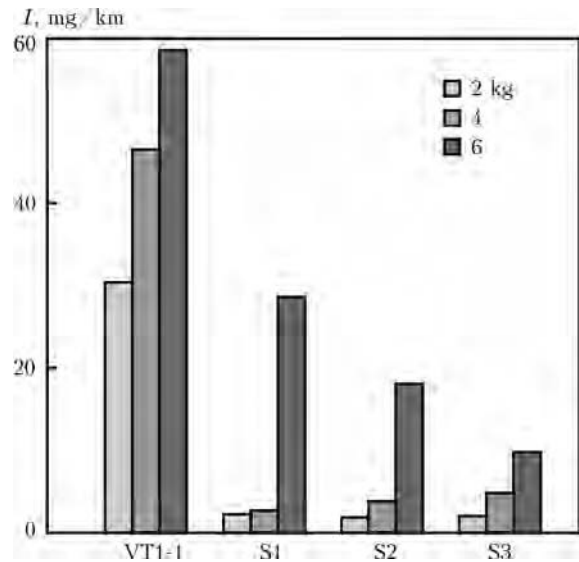
Figure 5. Intensity I of wear of specimens versus load

properties of surfaces of the plates of titanium alloy VT1-1.

1. Vanzhula, T.V., Zamkov, V.N., Prilutsky, V.P. (2003) Improvement of wear resistance of parts of titanium alloys (Review). *The Paton Welding J.*, **8**, 30−34.
2. Takahashi, W., Okada, M., Shida, Y. et al. (1993) Wear resistant titanium alloys. *J. Jap. Soc. Heat Treat.*, 33(**5**), 283−288.
3. Gurevich, S.M., Zamkov, V.N., Prilutsky, V.P. et al. *Flux-cored wire*. Pat. 3883713 USA. Int. Cl. B 23k 35/22. Publ. 13.05.1975.
4. Gadzyra, N.F., Gnesin, G.G. (2003) Technological aspects of synthesis of nanoparticles of solid solution of carbon in silicon carbide and nanocomposite powders on its base. Nanocrystalline materials. In: *Transact. of I.N. Frantsevich IPM. Series Physico-Chemical Principles of Powder Materials*. Kiev, 64−75.
5. Gadzyra, N.F., Gnesin, G.G., Mikhajlik, A.A. (2005) Segregation phenomena in non-equilibrium solid solution powders with an excess of the carbon atoms replacing the silicon atoms in SiC structure. *Sverkhtv. Materialy*, **5**, 56−64.
6. Paton, B.E., Zamkov, V.N., Prilutsky, V.P. (1996) Narrow-groove welding proves its worth on thick titanium. *Welding J.*, **5**, 37−41.

COMBINED DIFFUSION PROCESS OF JOINING BIMETAL ELEMENTS OF HEAT EXCHANGE SYSTEM

Yu.A. KHOKHLOVA, V.E. FEDORCHUK and **M.A. KHOKHLOV**

E.O. Paton Electric Welding Institute, NASU, Kiev, Ukraine

A possibility of joining stainless steel to aluminium at lower temperatures owing to deposition on steel of a sprayed layer of commercial aluminium and molten gallium at different exposure times has been experimentally established. Optimization of microstructure and properties of a region of diffusion zone is achieved by application of a short-time heating with passing of low-voltage current.

Special processes of joining dissimilar materials of the type of metal−nonmetal, metal−semiconductor and metal−metal in different combinations are often used in development and manufacturing of samples of sophisticated equipment. Here, in a number of cases the technology should provide a reliable joint at temperatures not exceeding 250 °C, as heating can lead to irreversible structural changes and lowering (loss) of service properties of materials as a whole. In addition, high requirements are made of the joints as to mechanical properties, vacuum tightness, electrical conductivity, etc.

The purpose of this work was finding a low-temperature process of joining stainless steel and aluminium alloy. Solution of this problem will allow producing bimetal assemblies for heat exchanger systems of aerospace microelectronics (Figure 1). The assembled item is 12Kh18N9T steel tube with outer diameter of 25 mm in a flange of AMg5 aluminium alloy of 100 mm length.

A promising technology for producing bimetal joints at up to 250 °C temperatures, in our opinion, is the diffusion process with gallium application [1]. Gallium melts at the temperature of about 30 °C, readily wets and dissolves most of the metals and solidifies with
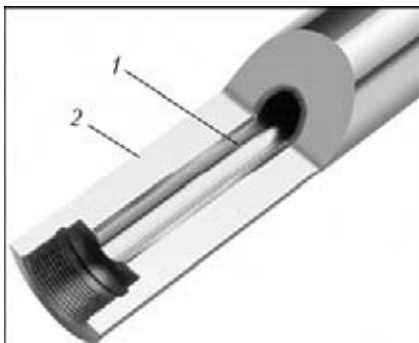

Figure 1. Bimetal block of heat exchange system: *1* — stainless steel; *2* — aluminium

volume increase that allows applying it as activator of adhesion of the surfaces being joined with subsequent volume diffusion. Activation consists of a mechanochemical process, including fragmentation, delamination and dissolution of oxide films, wetting of juvenile surfaces, as well as inter- and intragranular diffusion. Mechanochemical activation leads to increase of the solubility of difficult-to-dissolve materials, acceleration of chemical reactions, increase of catalytic and improvement of physicotechnical properties, and lowering of material surface activation temperature in the solid-phase process of their joining [2].

In order to form a strong steel-aluminium joint and prevent its embrittlement, a layer of commercial aluminium AD1 was sprayed on the steel tube surface (Figure 2). The process of spraying is performed by microplasma method, i.e. heating, dispersion and transfer of condensed particles of spraying material with formation of 200 μm layer on the substrate. MPN-004 system was applied for spraying, which allows aluminium to be deposited at substrate temperature of up to 150 °C. Formation of metal coatings with fixing of hard metal particles, characterized by high kinetic energy, on the substrate surface, occurs at high-speed impact (Figure 2, *b*) that provides high adhesion properties.

The bimetal assembly materials have as close as possible values of the coefficient of linear temperature expansion, thus providing an equivalent joint without part distortion (Table 1). As to the coefficient of heat conductivity, the materials for the heat exchange system are selected so that the radiator from AMg5 alloy ensures heat removal from the steel core through an interlayer of intermediate metal (gallium).

Gallium layer of 0.05−0.15 mm thickness was applied on the surfaces being joined by the method of mechanical rubbing, parts were joined by the mated surfaces, and diffusion hardening of the gallium interlayer was performed at assembly heating in the vacuum furnace or by passing current up to 140 and 250 °C. An advantage of second heating is its short duration, and heat evolution chiefly in the zone of contact of surfaces being joined. As a result, reactive diffusion initiates faster, heat evolution into the ma-
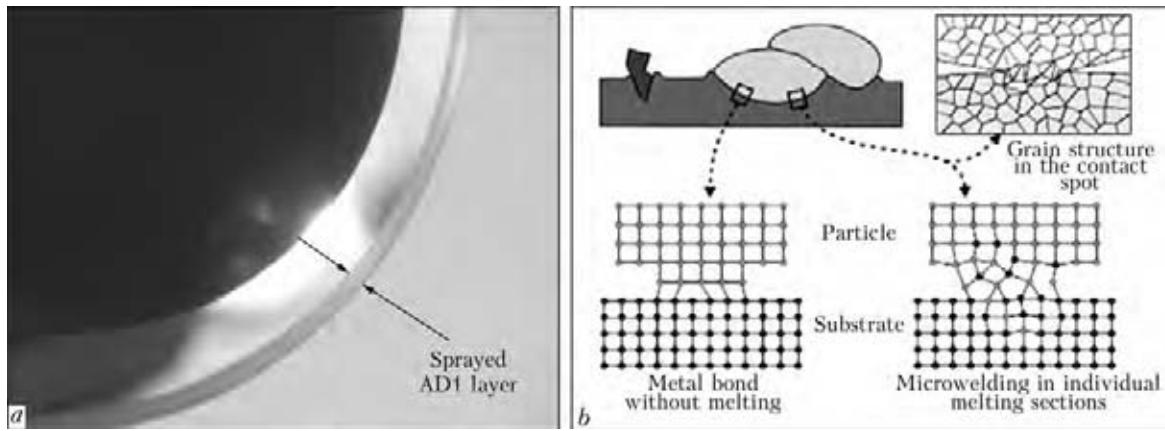
Figure 2. Fragment of stainless tube with sprayed layer of aluminium AD1 (*a*) and schematic of metal coating formation (*b*)

Table 1. Physical properties of joined materials

Material	Specific heat capacity, J/(kg·K), at 100 °C	Coefficient of linear thermal expansion·10^6, K^{-1}, at 100 °C	Heat conductivity coefficient, W/(m·K)	Young's modulus, GPa	Melting temperature, °C
AMg5 aluminium alloy	922	24.7	126	71	625
AD1 commercial aluminium	945	24	226	71	660
12Kh18N9T stainless steel	469	17	16	189	1300
Commercial gallium	–	–	28.1	10–45	30.15

terial is reduced, and diffusion layer depth decreases, that is favourable for the joint microstructure and mechanical properties. A condition for formation of a sound joint is tight fitting of the parts and removal of gallium flash from the end faces. Gallium fillets filling the item end face gaps at solidification with volume increase, may lead to formation of extended cracks in the aluminium flange bulk. Temperature was controlled during heating with a thermocouple and thermal imager Fluke Ti25.

Analysis of the structure and distribution of chemical elements showed that gallium diffusion occurs in the direction of AMg5 alloy, whereas no chemical presence of gallium was found in steel (Figure 3). A multistage process of formation of metastable phases from the main alloying elements of AMg5 alloy and gallium proceeds with formation of a hard intermetallic layer and increase of its melting temperature [3]. Analysis of binary diagrams of equilibrium state showed that the temperature of transition into the

liquid state of intermetallics of Ga–Mg and Ga–Zn systems is equal to more than 285 °C, and from 254 up to 1000 °C for Cu–Ga system.

Liquid gallium diffused along the aluminium grains (Figure 4) to the depth of up to 3 mm. This resulted in formation of a layer of solid solution and intermetallic phases in the gap and adjacent aluminium volume. Transmission electron microscopy examination of the fine structure of AD1/AMg5 joint zone through a gallium interlayer revealed the following. AD1 structure is characterized by a comparatively equilibrium state that is indicated by formation of an equiaxed substructure uniformly distributed through the entire volume of metal, adjacent to the joint plane, as well as formation of perfect (contracted) boundaries and subboundaries (Figure 5, *a*).

Structure in the joint zone (from AMg5 side) is characterized by appearance of structural-phase formations (interlayers), having a clear orientation along the line of gallium deposition with about 0.81–
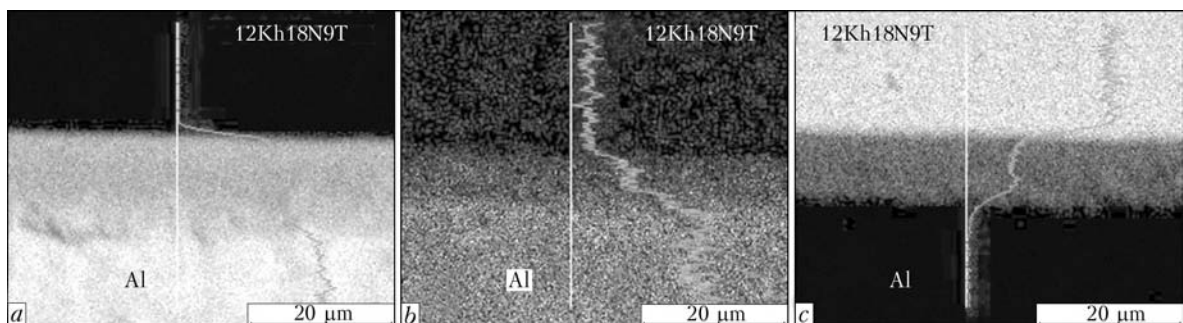

Figure 3. Maps of distribution of aluminium (*a*), gallium (*b*) and iron (*c*) across the section of stainless steel and aluminium joints (SEM)
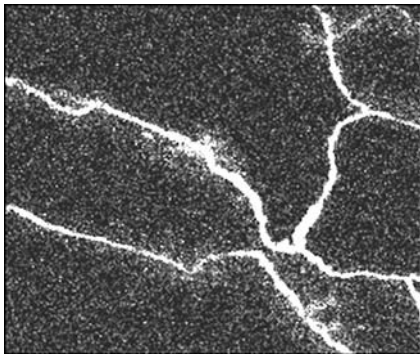
Figure 4. Maps of gallium distribution in the volume of AMg5 alloy as a result of reactive diffusion (×1000) (SEM)

1.10 μm interlayer thickness, and different phase compositions. A certain part of the interlayers consists of practically clean gallium. Gallium sections of the interlayers have an either columnar substructure with growth direction normal to the line of gallium deposition (Figure 5, *b*), or a comparatively equiaxed structure of Ga-phases (Figure 5, *c*) with intergranular precipitates of Ga_2Mg-phases. The gallium-containing regions of such interlayers are characterized by an equilibrium structural state.

It should be noted that phase composition of the interlayers becomes more complicated at shifting from the line of gallium deposition towards AMg5. At removal for up to 300 μm distance from the joint plane, formation of the structural-phase state is observed, which is characterized by an increase of volume fraction of dispersed phase precipitates ($h \times l \sim 0.03 \times 0.06$ μm; 0.06×0.1 μm; 0.03×0.37 μm; $d \sim 0.03-0.10$ μm) of Ga_2Mg, Ga_2Zn, Al_6CuMg_4, Al_2CuMg, Cu_9Ga_4 composition. Here, in addition to densely and uniformly distributed dispersed phases of various stoichiometric composition, also phase formations of a special type are observed in the diffusion zone: these are more massive ($h \times l \sim 0.65 \times 1.70$ μm; $0.73 \times$

$\times 1.07$ μm; 0.75×2.35 μm) extended «strip-type» phases of a complex composition, forming in the direction parallel to the fusion line (Figure 5, *d*).

Structure of this type of phase formations is quite clearly visible on TEM images, and its composition corresponds to Ga_2Mg with dispersed Ga_2Zn; Cu_9Ga_4 of sizes $d \sim 0.017-0.030$ μm. In addition, it is particularly characteristic that «strip-type» phase precipitates are surrounded by fringes around their contour, consisting of dense clusters of highly dispersed phases of various composition: Ga_2Mg; Ga_2Zn; Cu_9Ga_4, etc. Thus, it can be stated that the diffusion layer growth occurs with volume increase due to rotation of AMg5 grains at growth of newly-formed phases.

Such a graded distribution of phases, their definite clear orientation further promote non-uniformity of dislocation density distribution, and, therefore, formation of stress raisers in the respective zones of the studied joint. At nanoindentation testing [4, 5] of the influence of gallium reactive diffusion on the properties of AMg5 alloy, an anomalous adsorption lowering of strength and metal softening (Rebinder effect) were found [6]. Figure 6 shows the difference in dimensions of Berkovich indenter imprints in the central and grain-boundary region of the structure of AMg5 alloy sample at heating up to 250 °C in the vacuum furnace for 1 h.

Stabilization of aluminium mechanical properties occurs at final solidification of solid-liquid phases with gallium. Solidification duration corresponds to the time of new phases growing for the thickness of deposited gallium interlayer [7]. Determination of the moment of microstructure stabilization at minimum width of the diffusion zone and achievement of satisfactory mechanical properties, depending on heating time, were simulated experimentally and by molecular dynamics method at temperatures of 50, 140 and
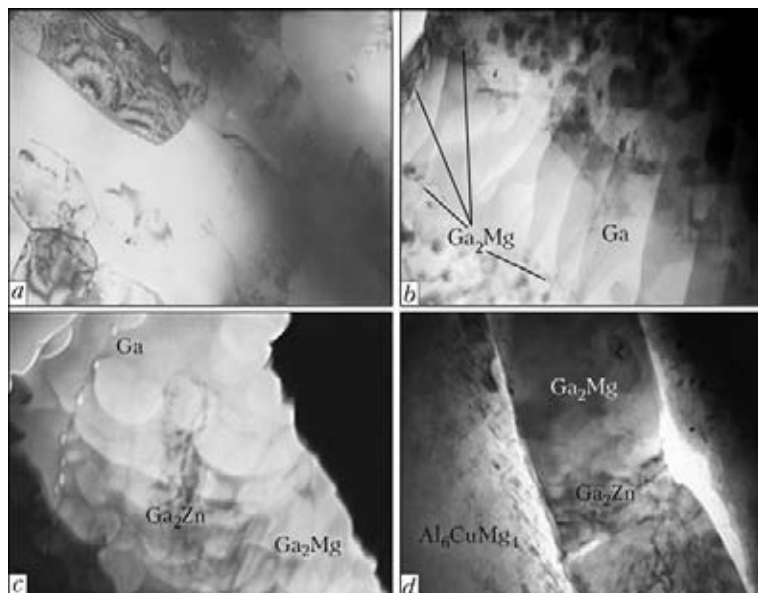
Figure 5. AD1 microstructure (*a* — ×15,000), laminated rounded and columnar fragments of gallium (*b*, *c*) and phases (*d*) in the intergranular space of AMg5 alloy (×50,000) (TEM)

Table 2. Dependence of diffusion layer width on exposure time and diffusion coefficient at heating up to 140 °C

Temperature, °C	Diffusion layer width, cm	Time during which diffusion advanced to specified depth, s	Diffusion coefficient·10^{-7}, cm^2/s
50 (furnace)	0.13	36000	2.35
140 (same)	0.15	36000	3.13
140 (same)	0.30	86400	5.20
140 (current)	0.01	60	4.76
140 (same)	0.02	120	33.30
250 (same)	0.05	210	104
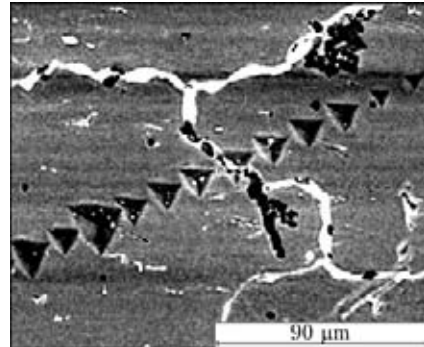
Figure 6. Microstructure of AMg5 alloy with indentor imprints (SEM)

250 °C. It is known that the mechanism of gallium diffusion in aluminium is mainly related to the ratio of atomic radii: closeness of dimensions of gallium and aluminium atoms promotes gallium diffusion through aluminium vacancies. Therefore, modelling of the dynamics of aluminium atomic lattice change was conducted by the vacancy mechanism. A limited quantity of atoms was considered in the model (5325), which was, however, sufficient for the experiment to have physical sense. 3D models of the crystalline lattice were assigned according to aluminium lattice period. Modelling results are atom coordinates in each step. Difference of coordinates was used to determine atom displacement. Of all atom displacements those without jumping (atom oscillation around the node) are not taken into account. Displacements, leading to jumps, were used to calculate the diffusion coefficient. Activation energy was determined by Arrhenius graph in $\ln D (1/T)$ coordinates by tangent of angle.
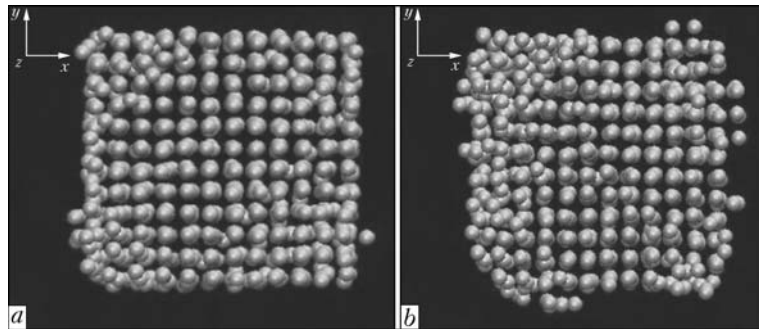
Figure 7. Dynamics of variation of aluminium crystalline lattice with temperature rise (volume modelling by molecular dynamics method): $a - T = 140$; $b - 250$ °C
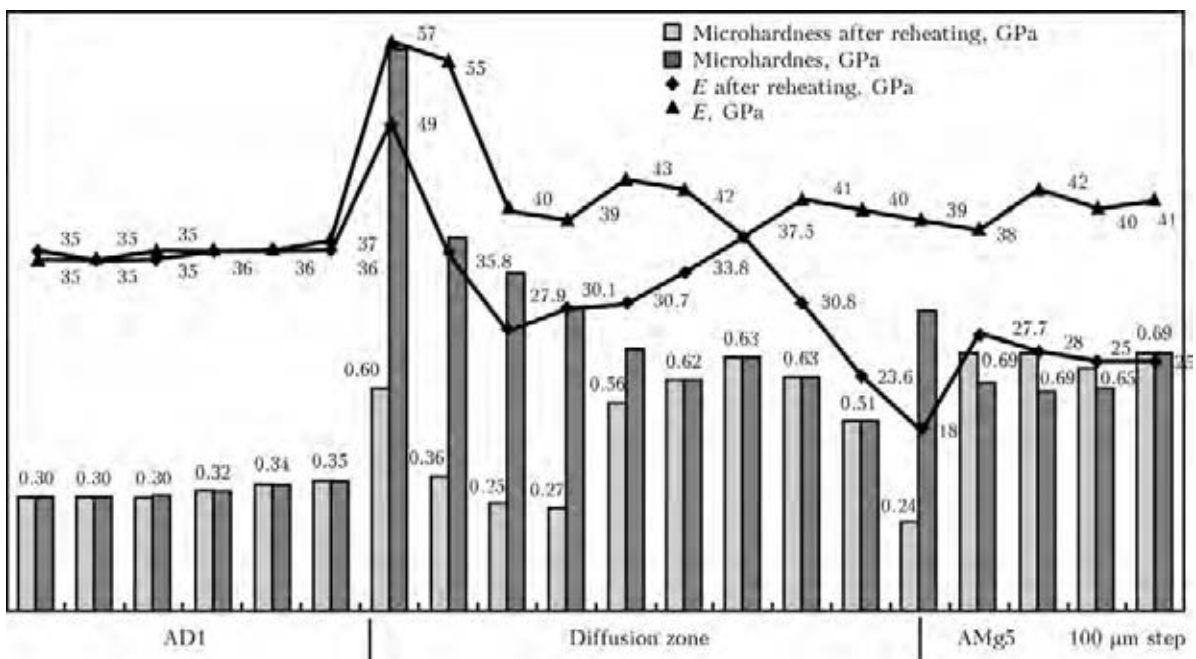
Figure 8. Diagram of Meyer hardness distribution and Young's modulus E in diffusion joint on the boundary of AD1 with AMg5 at heating by current up to 140 °C and after reheating up to 280 °C
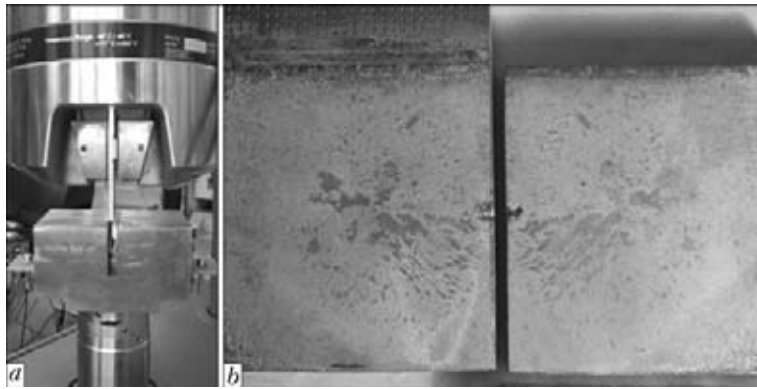
Figure 9. Shear strength tests in tensile testing servohydraulic machine MTS (*a*) of flat overlap sample of AMg5−Ga−AD1 diffusion joint (*a*) and sample fractograph after testing (*b*)

Increase of the number of atom jumps, contributing to diffusion, is due to greater activity of atoms with temperature rise [8] (Figure 7, *a*) and rises from 28 (at 50 °C) up to 4346 (at 250 °C). Diffusion coefficients are equal to, m^2/s: $2.86\cdot10^{-10}$ for 50 °C, $7.56\cdot10^{-10}$ for 140 °C and $4.74\cdot10^{-9}$ for 250 °C. Activation energy is equal to 0.62 eV.

Experimental modelling of the dependence of diffusion layer growth on temperature-time exposure of AD1−Ga−AMg5 samples confirmed the general tendency (Table 2): with increase of temperature and time of heat treatment gallium rheological properties are enhanced and an extended diffusion zone forms.

Furtheron, repeated heat treatment of all the samples in the furnace up to 280 °C for 10 h was conducted to determine process optimum temperature and time, at which the diffusion layer structure will preserve its properties. It is established that in samples processed at temperature of 140 °C by passing current no significant change of either diffusion layer microstructure, or its mechanical properties is observed (Figure 8).

At shear strength testing (Figure 9, *a*) to GOST 6996−66 (material thickness a = 6 mm, gauge length l = 125 mm, grip h = 60 mm, overlap b = 40 mm) breaking load F was equal to 4710 N, shear stress was 2.94 MPa, respectively, that is much higher than the minimum value required by the specification (0.2 MPa). One can see in the fractograph of fracture plane (Figure 9, *b*) that at joint assembly complete wetting and adhesion of the surfaces being joined occurred with minimum edge effect. According to the specification the summary area of joint defects is less than 10 %.

Maximum breaking force G of «anti-shear» at diffusion overlap area of 15×15 mm^2 was equal to 400 N. Tearing force (maximum breaking force per a unit of overlap surface) was $\tau \approx 1.7$ MPa.

Shear strength of circular samples was equal to 9−11 MPa.

It should be noted that application of polymer-based metal adhesives mixed with metal powders for assembly of heat exchange systems of microelectronics insulation is not rational, as the heat conductivity coefficient in such materials is many times lower than in metals (0.02−0.6 W/(m·K)).

Shear fracture force of aluminium alloy joints, MPa

Al−Al (adhesive joint, liquid metal Fe1 WURH [9])	2.4
Al−Al (adhesive joint), polymer adhesive ABRO [10]	5.9
AMg5−AD1 (required by specification)	0.2
AMg5−Ga−AD1 (welding by passing current at 140 °C)	2.94

Retrofitting of the technology of solid-phase joining of steel-aluminium assembly through an interlayer of eutectic gallium resulted in various variants of assembly of heat exchange system component (Figure 10) with a high value of shear fracture force.

In conclusion it should be noted that a possibility of joining stainless steel to aluminium at 140 °C temperature using a sprayed layer of commercial aluminium and gallium interlayer was established experimentally. The most favourable microstructure and properties of the diffusion zone are observed at application of heating by low-voltage passing current. Strong permanent joints of bulk configuration were produced without surface melting or distortion of
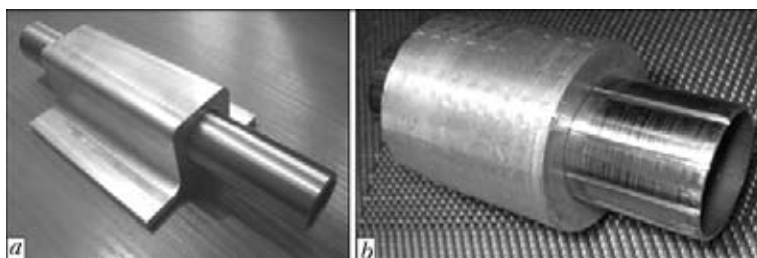

Figure 10. Model samples of steel−aluminium diffusion joint made at 140 °C temperature over a conical surface (*a*) and with longitudinal slots (*b*)

parts. This process of joining the bimetal assembly is recommended for joining over closed, mated or cylindrical surfaces, using the effect of thermal shrinkage and reduction.

1. Ishchenko, A.Ya., Khokhlova, Yu.A., Fedorchuk, V.E. et al. (2010) *Technological features of producing joints of commercial aluminium with AMg5 alloy at activation of surfaces being joined by molten gallium*: Transact. Nikolaev: NUK, 68–74.
2. Avvakumov, E.G. (2009) *Fundamentals of mechanical activation, mechanosynthesis and mechanochemical technologies*: Integration projects. Novosibirsk: Nauka.
3. Khokhlova, Yu.A., Fedorchuk, V.E., Khokhlov M.A. (2011) Peculiarities of intergranular mass transfer of gallium in aluminium alloy during solid phase activation of surfaces being joined. *The Paton Welding J.*, **3**, 13–15.
4. Ishchenko, A.Ya., Khokhlova, Yu.A. (2009) Evaluation of mechanical properties of microstructural constituents of welded joints. *Ibid.*, **1**, 34–37.
5. Khokhlova, Yu.A., Khokhlov, M.A. (2009) Nanoscale effect in diffusion joints with gallium. In: *Abstr. of Int. Conf. on Welding and Related Processes*. Nikolaev: NUK, 111.
6. Likhtman, V.I., Shchukin, E.D., Rebinder, P.A. (1962) Physico-chemical mechanics of metals. In: *Adsorption phenomena in processes of deformation and fracture of metal*. Moscow: AN SSSR.
7. Tikhomirova, O.I., Pikunov, M.V. (1969) Influence of shape and size of second component particles on properties of gallium solders. *Poroshk. Metallurgiya*, 82(**12**), 51–56.
8. Poletaev, G.M., Starostenkov, M.D. (2010) Contributions of different mechanisms of self-diffusion to fcc metals in equilibrium conditions. *Fizika Tv. Tela*, 52, Issue 6, 1075–1082.
9. *www*.svarka-lib.com/node/298/print/64.html
10. *www*.autodela.ru/main/top/test/svar

INFLUENCE OF VIBRATION OF PARTS ON STRUCTURE AND PROPERTIES OF METAL IN SURFACING

Ch.V. PULKA[1], **O.N. SHABLY**[1], **V.S. SENCHISHIN**[1], **M.V. SHARYK**[1] and **G.N. GORDAN**[2]
[1]Ternopol Ivan Pulyuj National Technical University, Ternopol, Ukraine
[2]E.O. Paton Electric Welding Institute, NASU, Kiev, Ukraine

Presented are the investigation results of structure and properties of metal deposited by induction method with superposition of vibrations in a period of melting of a surfacing consumable. It is shown that the superposition of vibrations leads to improvement of wear resistance of the deposited metal due to refinement of its structure.

An induction surfacing using powders from high-carbon chromium alloy PG-S1 (sormite 1) is widely used for manufacture of operating elements of agricultural machines: plough shares, blades of top cutters, chisels of cultivators etc. At that a deposited metal has a coarse-grain structure with inclusions of coarse chromium carbide [1, 2].

A new technology of induction surfacing using vibrations [3–6] was proposed for refinement of structure and improvement of properties of the deposited metal. It lies in the fact that a part is subjected to vertical and horizontal vibration at the moment when a powder charge is in a molten state. At that, direction of oscillation application (Figure 1) as well as their frequency and amplitude have a great importance.

Investigations of structure, microhardness of structural constituents and wear resistance of the metal deposited by induction method with and without vibration superposition were performed for evaluation of the efficiency of developed technology. The flat samples from steel St3, i.e. sample 1 without vibration, 2 and 3 with vertical and horizontal vibrations, correspondingly, were deposited for performance of the investigations by induction method using a charge containing PG-S1 alloy powder. Surfacing was carried out on a high-frequency generator of VChG 6-60/0.44

type at constant specific power W and time of deposition t (Figure 1, *b*). The modes were similar for all three variant of surfacing, i.e. circuit voltage 5.4 kV; anode voltage 10 kV; circuit current of lamp 1.2 A; anode current of lamp 2 A; deposition time 35 s; oscillation amplitude 0.2 mm at 50 Hz frequency.

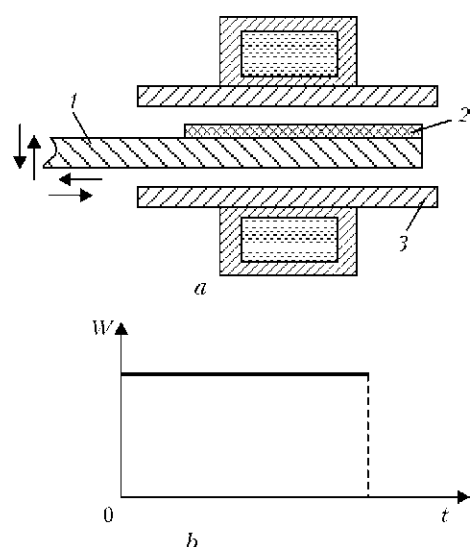**Figure 1.** Surfacing scheme (*a*: *1* — part being deposited; *2* — powder-like charge; *3* — inductor; arrows show direction of vibration application — vertical or horizontal), and specific power W of generator in the process of surfacing (*b*)
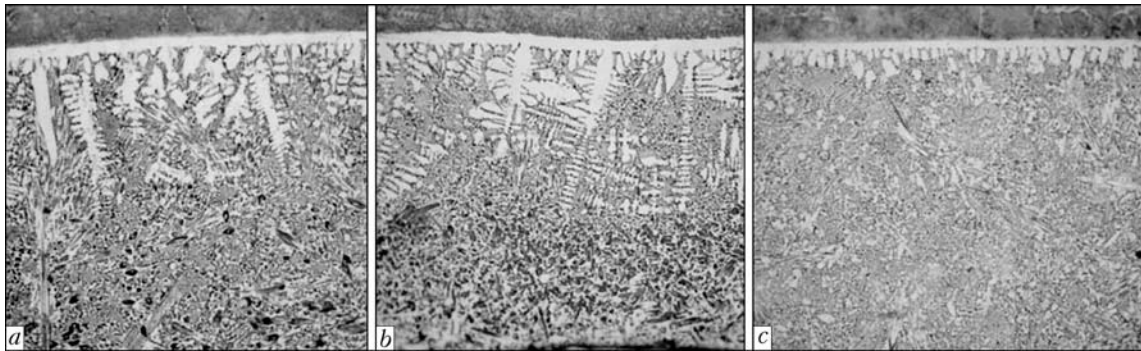
Figure 2. Microstructure (×200) of the deposited metal of samples 1–3 (a–c)

Samples for investigation of structure and wear resistance of the deposited metal were cut out from the deposited blanks.

Etching of the samples for performance of metallographic investigations was made by stages. Structure of the deposited metal was determined by electroplating technique in 20 % solution of chromic acid (20 V voltage and time of etching 10 s) through a chemical etching in 4 % solution of nitric acid.

Microstructure of the base metal consists of ferrite and pearlite and microstructure of the deposited metal in all investigated samples is made of primary carbides (complex carbides of $(Fe, Cr)_7C_3$ and $(Fe, Cr)_3C$

Figure 3. Distribution of carbon and chromium on thickness of the deposited metal in samples 1–3 (a–c)

type) in a form of coarse plates of «pencil» type, having hexagonal cut with well-defined interface to matrix, of carbide eutectics and matrix austenite structure.

The excess carbides, as a rule, are situated in a form of separate plate precipitates in the central part along the width and thickness of the deposited bead. Rectangular and hexagonal precipitates are the carbides of different dispersion. Part of them is the excess plate carbides being sufficiently uniform distributed in the matrix. Microhardness of the carbides varied in the ranges HV0.5-11710–12830 MPa.

Common for all variant of the deposited metal is:

• presence in the deposited layer of hypoeutectic zone adjoining to a joining line which is characterized by formation of the dendrites of solid solution (alloyed austenite) with axes of the first and second order, as well as the carbide eutectics crystallized in an interdendritic space. Microhardness of austenite for samples 1 and 2 made HV0.5-4120–4410 MPa and that for sample 3 was HV0.5-4800–5090 MPa. Besides, a structural inhomogeniety represented by the fact that the hypoeutectic dendrite zone had non-uniform distribution was found along the joining line from the sormite side;

• formation of boundary white strip of the solid solution (alloyed austenite) of variable width 10–20 μm between the deposited and base metals with microhardness HV0.5-3030–3410 MPa for sample 1, and HV0.5-3410–3810, HV0.5-3860 MPa for samples 2 and 3, correspondingly;

• existence of a diffusion zone from the base metal side near the joining line representing itself fine plate pearlite and ferrite along the grain boundaries sometimes with orientation on Widmanstatten structure with microhardness HV0.5-2440 MPa appeared as a result of carbon diffusion from the sormite into the base metal.

Microhardness of the structural constituents for three samples is given in the Table.

Differences in the structure of three variants of the deposited metal should be noted. Notable refinement of the carbide constituent is caused by horizontal vibration. The carbides, having hexagonal shape with 10–12 μm mean length of the side, without vibration (Figure 2, a) are refined up to 7–10 μm at vertical
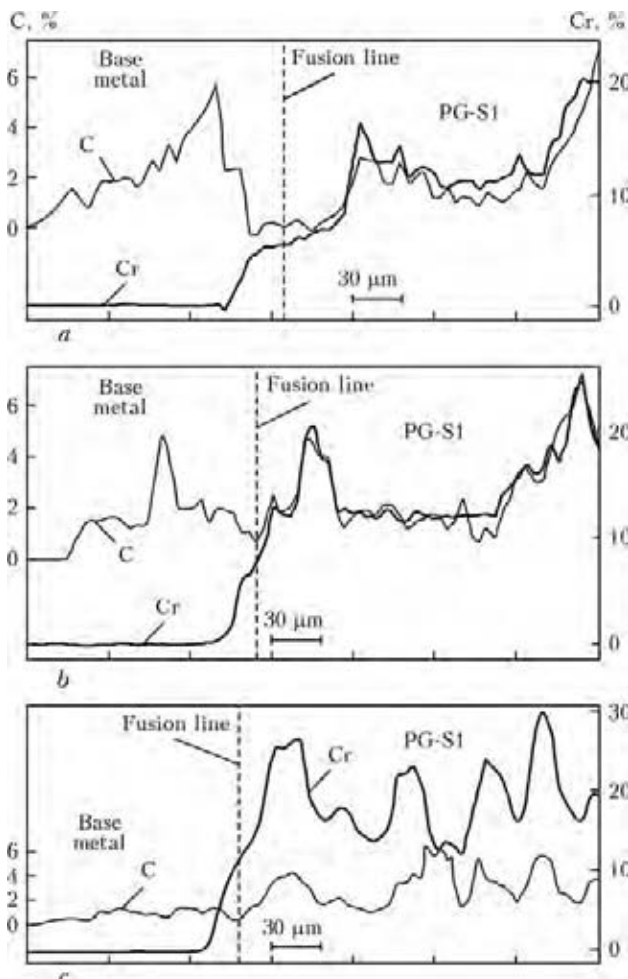
Microhardness of structural constituents of the deposited metal of PG-S1 type, MPa

Sample No.	Chromium carbide	Matrix	White strip
1	11710−12830	4120−4410	3030−3410
2	11710−12830	4120−4410−4800	3410−3810
3	11710−12830	4800−5090	3860

Figure 4. Relative wear resistance (*1*) and hardness of the deposited metal (*2*) of samples 1−3

vibration (Figure 2, *b*) and 3.5−7 μm at horizontal one (Figure 2, *c*).

The maximum depth of the eutectic zone is in samples 1 and 2 (see Figure 2, *a*, *b*) and in sample 3 (Figure 2, *c*) − the minimum one. Zone of austenite dendrites takes the smallest percent along the length of deposit in sample 3 in comparison with samples 1 and 2. The joining line from sormite side at horizontal vibration mainly represents itself the white strip with formation of almost equiaxial austenite grains (see Figure 2, *c*).

Micro X-ray spectrum analysis on the Cameca microanalyzer CAMEBAX SX-50 (Figure 3) was carried out for investigation of distribution of the elements (chromium, carbon) at transfer from the base metal to the deposited one. The analysis for all cases was performed approximately in a center of the deposited layer normal to fusion line at depth up to 350 μm from the fusion boundaries. It is determined that carbon is bounded in the carbides of $(Fe, Cr)_7C_3$ and $(Fe, Cr)_3C$ type in metal of the investigated samples and notable redistribution of carbon near the fusion line was not observed.

Measurements of hardness of the deposited metal on the LECO hardness meter at 0.5 and 3 N loading (Figure 4) showed that sample 3 has the highest hardness. Laboratory tests on wear resistance of the deposited metal of samples 1−3 on machine NK-M [7] were also performed. Test conditions were the following: abrasive − quartz sand with particle size 0.2−0.4 mm; friction path 415 m; pressure 0.466 MPa;

standard sample − annealed steel 45. Figure 4 shows that sample 1 has the lowest wear resistance (2.2) and samples 2 and 3 − the highest (3.1 and 3.4, respectively). Surfacing on scheme accepted for sample 3 provides the highest wear resistance that is explained by favorable structure of the deposited metal and formation mainly of $(Fe, Cr)_7C_3$ carbides and certified by the results of micro X-ray spectrum analysis.

1. Tkachev, V.N., Fishtejn, B.M., Kazintsev, N.V. et al. (1970) *Induction surfacing of hard alloys*. Moscow: Mashinostroenie.
2. Pulka, Ch.V. (2003) Hardfacing the working components of tillage and harvesting agricultural machinery (Review). *The Paton Welding J.*, **8**, 35−40.
3. Shably, O.M., Pulka, Ch.V., Senchishin, V.S. et al. *Method for surfacing of thin plane steel parts*. Pat. on useful model 54204 UA. Int. Cl. B23K 13/00. Publ. 25.10.2010.
4. Pulka, Ch.V., Senchishin, V.S. *Device for surfacing of thin shaped disks*. Pat. on useful model 59994 UA. Int. Cl. B23K 13/00. Publ. 10.06.2011.
5. Pulka, Ch.V., Senchishin, V.S. *Method of surfacing of parts*. Pat. on useful model 64371 UA. Int. Cl. B23K 13/00. Publ. 10.11.2011.
6. Shably, O.M., Pulka, Ch.V., Senchishin, V.S. (2011) Vibroinduction surfacing of thin plane parts. In: *Abstr. of 10th Int. Symp. of Ukr. Mechanical Engineers* (Lviv, 25−27 May, 2011), 289−290.
7. Yuzvenko, Yu.A., Gavrish, V.A., Marienko, V.A. (1979) Laboratory machines for assessment of wear resistance of deposited metal. In: *Theoretical and technological principles of surfacing. Properties and tests of deposited metal*. Kiev: PWI.

MANUFACTURE OF STAINLESS STEEL–ALUMINUM TRANSITION PIECES BY VACUUM PRESSURE WELDING METHOD

G.K. KHARCHENKO[1], **Yu.V. FALCHENKO**[1], **V.E. FEDORCHUK**[1], **S.G. GRIGORENKO**[1] and **M.M. RUDENKO**[2]

[1]E.O. Paton Electric Welding Institute, NASU, Kiev, Ukraine
[2]Chernigov State Technical University, Chernigov, Ukraine

Technology of vacuum pressure welding of bimetal tubular transition pieces from 10Kh18N10T stainless steel with AD1 aluminum was developed. It is established that modifying the steel blank surface using holes promoted localizing of plastic deformation in the butt joint and producing welded joints with the strength not lower than that of aluminum.

Keywords: vacuum pressure welding, bimetal joint, aluminum AD1, steel 10Kh18N10T, transition piece, microstructure

Possibility of formation of the safe tube joints from dissimilar metals is a key issue in series of current structures, for example, energy devices.

Joining of the tubes from aluminum alloys with tubes from steel using transition pieces is widely used in the assembly structures where they have the high requirements on working capacity. The tubes from stainless steel and aluminum alloys being joined with the help of inserts and transition pieces are used in the vessels for storage and transportation of cryogenic products.

Significant difference in the values of melting temperature of steel (around 1539 °C) and aluminum (660 °C), differences in the coefficients of linear expansion, i.e. $23.5 \cdot 10^{-6}$ for aluminum and $11.9 \cdot 10^{-6}$ for iron at room temperature, $31.1 \cdot 10^{-6}$ and $14.3 \cdot 10^{-6}$ $1/°C$, respectively, at 500 °C, and presence of a refractory oxide film Al_2O_3 on the surface of aluminum promote a complexity of obtaining of aluminum to steel welded joints.

The aim of the present paper lied in development of a technological process of vacuum pressure welding of bimetal steel–aluminum tubular transition pieces with the strength on the level of that of aluminum.

The cylinder samples and flat samples from steel 10Kh18N10T ($50 \times 20 \times 2$ mm) and aluminum AD1 ($50 \times 20 \times 4$ mm) were used for studying the influence of surface treatment on formation of the welded joints. Surface of the stainless steel samples was grinded or grinded and polished before welding and samples from aluminum were scraped. Welding of the samples was carried out in a free state in vacuum at 500 °C temperature, 8 MPa pressure and rate of heating around 5 °C/min. Deformation of the joint made, approximately, 25 %. Temperature and pressure of the process of welding were selected based on operation recommendations [1, 2].

Formation of the brittle intermetallic compounds in a butt joint promotes the main difficulties in diffusion vacuum welding of stainless steel with aluminum. There is virtually no influence of the intermetallics on mechanical characteristics of the joint on elementary stage of development, when they do not form a solid layer in a contact. Presence of a solid intermetallic layer in the contact reduces ductility and strength of the joint. This is a result of high brittleness of new phase as well as internal stresses appearing due to volumetric changes [3]. Welding of the metals forming intermetallics requires minimization of the third stage of the process of diffusion welding, i.e. stage of volumetric interaction determined by diffusion processes, in accordance with the recommendations of work [3]. Therefore, welding time made 1 min.

The joints after welding were cut on strips of 50×9 mm size by erosive cutting machine. Bend testing of the joints was carried out. Analysis of the obtained results indicates that the samples, steel surface of which was grinded, have bigger bending angle. Bending angle of such joints makes 120°. However, cracking along edges of the joint should be noted in both cases.

Application of the soft perforated inserts allows plastic deformation being localized on an interface of welded parts [4, 5]. 1.3–1.5 times increase of cracking resistance of the parts can be achieved in welding of cerment joints with modifying ceramic coating [6] by making of «reinforcing holes» in it. Therefore, «blind» holes were drilled in the surface of steel plate for eliminating cracking of the joints.

The holes in the surface of steel plate were 2.5 mm in diameter, approximately 1.2 mm of depth and made with 10×10 mm pitch. Obtained joints were also bend tested. Bending angle made 180°, and no cracking of the joint was observed at that.

The metallographic investigations of bimetallic joints (Figure 1) were carried out. Separate areas with intermetallic layer (Figure 1, *a*) were found in a joining zone of samples with holes. The intemetallics took
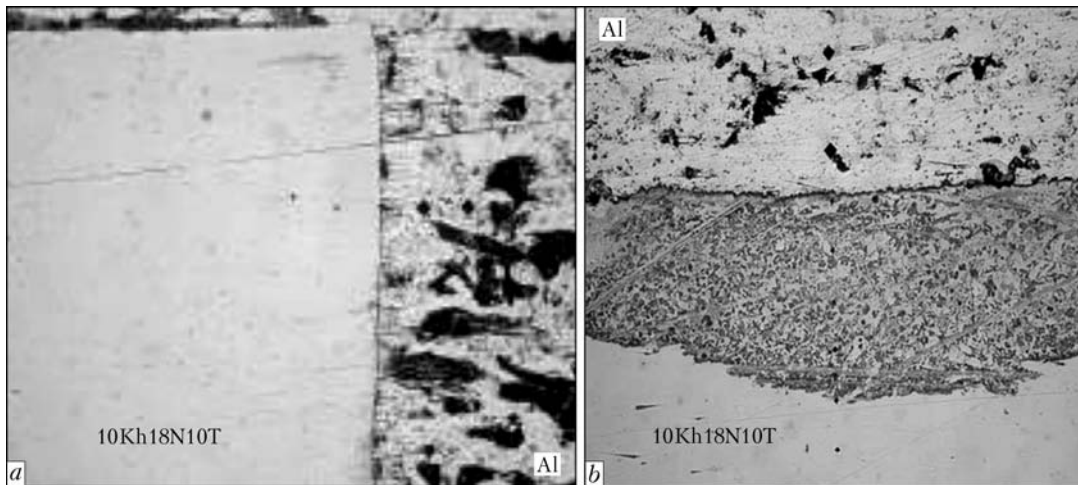
Figure 1. Microstructure (×100) of joining zone of the samples from 10Kh18N10T steel and aluminum AD1 with (*a*) and without (*b*) holes on the surface of steel blank

50−70 % of area of joining zone (Figure 1, *b*) in the sample without holes. It should be noted that both samples were simultaneously welded.

Increase of plastic deformation rate results in 2−3 times reduction of thickness of the intermetallic layer [7]. Strains acting in the contact at the initial time of welding significantly exceed the yield strength and, as a result, elasto-plastic deformation of the microflanges is actively developed. The rate of deformation reduces 2−3 times in several seconds after loading application, and the process transfers in a transitional creep stage [8].

It can be assumed that difference in the thicknesses of formed intermetallic layer of the samples with holes and without them is caused by different rates of plastic deformation in the near-contact layers of aluminum relative to the surface of stainless steel. The rate of plastic deformation of aluminum in the first case was higher than in the second one.

The authors obtained no positive results after experiments on welding of tubular blanks on air. Obtained joints destroyed in cutting.

Tubular blanks from stainless steel 10Kh18N10T and aluminum AD1 were welded in P-115 unit vacuum chamber. Outer diameter of steel tube made 25 mm, internal one was 20 mm, height made 30 mm, and that of aluminum tube was 41.5 and 23.6 mm, correspondingly, at 30 mm height.

A demountable unit designed for alignement and fixing of the tubular blanks before welding was manufactured for the experiment performance. Figure 2 shows scheme of the unit and its general appearance. Support washer *1* was inserted inside the unit and aluminum blank *2* was position on it. Steel blank *3* was in tight contact with the aluminum one and was centered from above by guide washer *4*. Fixing of tubular blanks and alignment bushes was carried out using two steel rims *5*, to which ears *6* with holes were welded. The holes (Figure 3) were drilled in the

Figure 2. Scheme of unit for obtaining of bimetal tubes (*a*), and ready-assembled appearance (for designations see the text)
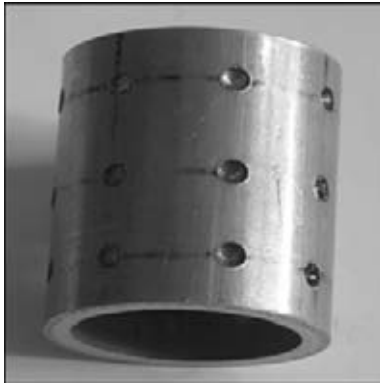
Figure 3. Appearance of steel blank

Figure 4. Macrosection of welded joint: A — places of the holes filled with aluminum

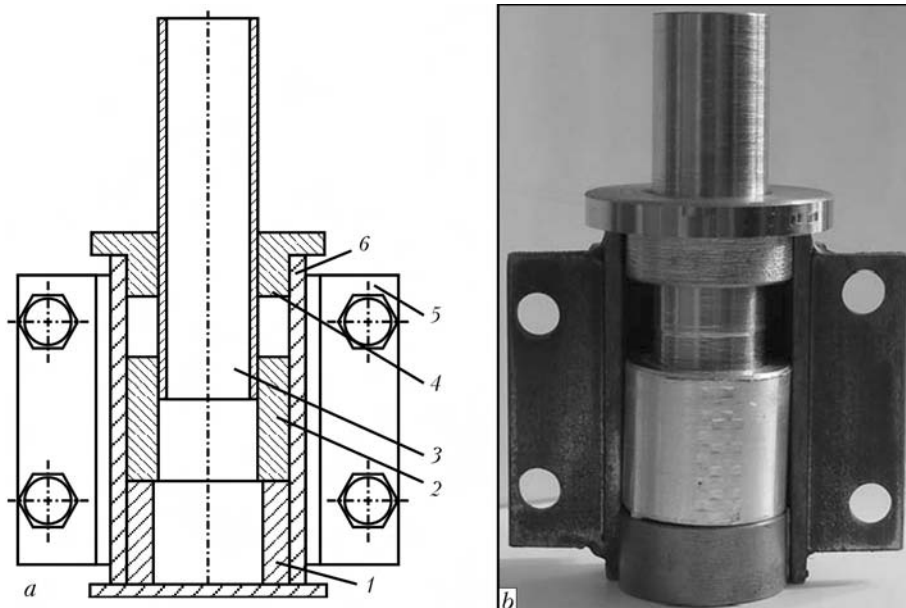surface of steel tube in accordance with the procedure elaborated on the samples. A conicity was developed at the end of steel tube for alignment with aluminum one. The surfaces to be welded were degreased with acetone immediately before welding.

Obtained bimetal joint after welding was cut on cylinder blanks of 5 mm thickness using erosive cutting machine. Figure 4 shows macrosections of 10Kh18N10T−AD1 welded joint. As can be seen from the Figure, complete filling of the holes with aluminum extruded as a result of plastic deformation of the near-contact volumes of metal takes place in the process of welding. Mechanical tests showed that the failure of welded joints takes place along aluminum.

CONCLUSIONS

1. Technology for vacuum pressure welding of bimetal 10Kh18N10T−AD1 tubular joints was developed.

2. Modifying the surface of more strength steel blank using holes allows increasing the rate of plastic deformation of near-contact layers of aluminum that provides obtaining of the welded joints with minimum thickness of intermetallic layer.

1. Bachin, V.A., Kvasnitsky, V.F., Kotelnikov, D.I. et al. (1991) *Theory, technology and equipment of diffusion welding*. Moscow: Mashinostroenie.
2. (1981) *Diffusion welding of materials*: Refer. book. Ed. by N.F. Kazakov. Moscow: Mashinostroenie.
3. Kopylov, Yu.N., Kazakov, N.F., Grishin, I.S. et al. (1973) About formation of joints in vacuum diffusion welding. In: *Proc. of 7th All-Union Sci.-Techn. Conf. on Vacuum Diffusion Bonding of Metals, Alloys and Nonmetallic Materials* (Moscow, May 1973), 12−25.
4. Musin, R.A., Lyamin, Ya.V. (1991) Intensification of plastic deformation of inserts in diffusion welding. *Avtomatich. Svarka*, **8**, 26−29.
5. Musin, R.A., Lyamin, Ya.V. (1994) Deformability of perforated inserts in diffusion welding. *Svarochn. Proizvodstvo*, **6**, 24−26.
6. Lyamin, Ya.V. (1998) *Development of methods for intensification of diffusion welding process and increase in strength of cermet joints*: Syn. of Thesis for Cand. of Techn. Sci. Degree. Perm.
7. Ternovsky, A.P., Karakozov, E.S., Zimidchenko, S.S. (1983) Specifics of formation of dissimilar metal joints in diffusion welding by scheme of forced deformation. *Avtomatich. Svarka*, **3**, 31−34.
8. Konyushkov, G.V., Kopylov, Yu.N. (1974) *Diffusion welding in electronics*. Moscow: Energiya.

TENDENCIES IN DEVELOPMENT OF CONTROL OF METAL TRANSFER PROCESSES IN SHIELDING GASES (Review)

A.M. ZHERNOSEKOV

E.O. Paton Electric Welding Institute, NASU, Kiev, Ukraine

Trends in development of modern arc power sources and gas-shielded consumable electrode welding technologies are analyzed. Different types of electrode metal transfer and the possibility of controlling them by varying the welding current parameters are considered. A high potential of the controllable gas-shielded pulsed-arc welding process is substantiated.

Gas-shielded consumable electrode welding takes a leading position among arc processes in the industry of Western Europe, USA and Japan [1, 2]. However, new functional capabilities of welding equipment, including arc power sources, which are opened up due to development of power electronics, do not always promote appearance of qualitatively new welding technologies. Developers often advertise welding equipment implementing various control algorithms, but ensuring just one type of electrode metal transfer, as entirely new technologies.

In this work the author has analyzed the tendencies in development of control of metal transfer in shielding gases and consumable electrode welding technologies, and has shown the role of pulsed-arc process with controllable transfer of electrode metal.

Many characteristics of gas-shielded welding process depend on the type of electrode metal transfer, which has an essential influence on various technological characteristics of the welding arc, for instance, heat balance, its spatial stability, intensity of running of metallurgical reactions in the welding zone, burning and spattering losses, as well as penetration depth, parameters and shape of welds [3].

There exist several types of electrode metal transfer in shielding gases [4], the main of which are fine-drop or globular transfer with short-circuiting (SC) of the arc gap; fine-drop or globular transfer without arc gap SC and spray process, and rotating spray process is also found. Metal vapour transfer is present to varying degrees in all the gas-shielded consumable electrode welding processes. However, mixed metal transfer types are often found, due to variation of welding process parameters. Control of metal transfer by the principle of «one pulse per drop» should be treated separately.

Type of metal transfer, as well as forces acting on electrode metal in the arc, are quite comprehensively described in works [4, 5]. Each type of metal transfer is characterized both by advantages and disadvantages. Therefore, transfer type determines many technological characteristics of the process of gas-shielded consumable electrode welding, for instance, welded thickness range.

Each type of electrode metal transfer has its own range of values of welding currents and arc voltages (Figure 1). For consumable electrode pulsed-arc welding (CEPAW) the most effective range of average welding currents is from 60 up to 300 A, that of arc voltages — from 16 to 32 V.

Metal transfer type depends on many welding process parameters. The main parameters in terms of process control are composition of electrode wire and shielding atmosphere; value, polarity, density and shape of welding current; applicability of various mechanisms of welding wire feed. There exist various disturbing impacts that should be taken into account in welding equipment design, as they can change metal transfer type. For instance, at CEPAW reduction of mains voltage or electrode extension may lead to a change of transfer from fine-drop without SC to transfer with SC [6]. Condition of wire surface also can influence the change of electrode metal transfer type. Gas-shielded welding, as a rule, is performed at direct
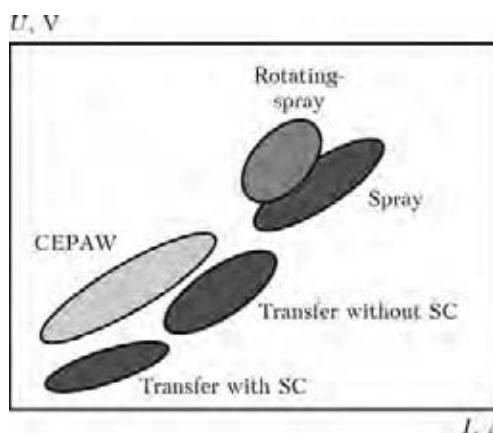

Figure 1. Range of welding currents and arc voltages at various types of metal transfer
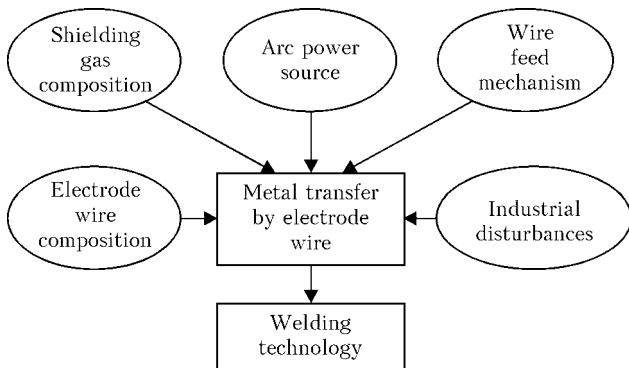
Figure 2. Schematic of the main welding process parameters acting on electrode metal transfer

current. Presence of magnetic blow in the welding process changes the arc length and shape that in its turn, influences drop formation and detachment. Figure 2 shows the schematic of the main components of the welding process, affecting electrode metal transfer.

Compositions of shielding gas mixture and welding wires are varied to improve the quality of weld metal, acting primarily on the metal surface tension forces and degree of welding arc constriction [7–9]. Here fine-drop metal transfer is achieved at lower values of welding current.

Welding wire feed mechanisms also allow effective control of drop detachment process, particularly in welding with SC [10, 11]. Welding arc power sources have a special role in achieving the required type of electrode metal transfer. Variation of welding current shape allows effectively controlling the processes of drop formation, time of its staying in the arc and many other parameters.

Optimization of parameters in Figure 2, influencing metal transfer in consumable electrode welding, depends on specific technology goals. As a rule, first one parameter is optimized, and then, allowing for control effectiveness — the next one. For instance, in CEPAW of steels in gas mixtures, first gas mixture composition was optimized.

Modern pipeline transportation requires high values of working pressure of energy carrier pumping and application of high-strength pipe steels X80 and X100. Consumable electrode welding of such steels necessitated development of new shielding mixtures, for instance Ar + 12 % CO_2 + 5 % He, allowing good fusion with side walls at multipass automatic welding [9]. Then the shape of welding current pulses is optimized, and systems of automatic stabilization of process parameters are developed.

Many techniques are used to control the process of consumable electrode welding with arc gap SC [12]. Figure 3 shows the main companies, manufacturing equipment which implements the processes of welding with SC.

Advantages associated with application of SC metal transfer are described in different ways by welding equipment manufacturers. Surface Tension Transfer (STT) process of Lincoln Electric, uses a fast inverter power source for operation, which allows controlling welding current shape [13, 14]. An improved Waveform Control Technology is applied in the arc power source, which provides considerable advantages compared to traditional MIG with SC welding. This process is predominantly designed for welding root welds, as well as lowering spatter, particularly in pure CO_2.

Cold Metal Transfer (CMT) process of Fronius is realized through wire feed reversal [15, 16]. The advantages include slight spatter, also when pure CO_2 is used, possibility of welding over a larger gap due to reduced heat input and brazing, as well as welding metal with different thermophysical properties, for instance steel to aluminium [16].

EWM implements Cold Arc process, designed for welding with SC, which allows joining steel sheets from 0.3 to 1.5–2.0 mm thick, as well as zinc-plated sheets, reliably control welding of root welds in difficult-of-access places, performing welding of magnesium alloys, welding of steel–aluminium, steel–magnesium and aluminium–magnesium joints.

Fast Root technology of Kemppi also realizes the process with SC by numerical control of welding current and arc voltage. Fast Root was mainly developed for welding root welds, but it can also be used for thin metal welding [10].

SELMA-ITS developed a welding process with forced SC (FSC) of the arc gap [10, 13], allowing spatter to be reduced in pure CO_2.

Japanese specialists are also working on the process of arc welding with SC. Work on control of welding current pulse shape SP-MAG (superimposition of currents) is of interest [17]. Advantages of the method include low metal spatter, arcing stability, as well as possibility of heat input control. Developed Metal Transfer Stabilization (MTS) control system prevents formation of large drops and reduces spatter.

Thus, manufacturers produce under various trade marks electric welding equipment realizing the process of welding with SC with the above advantages. It is applied in various industries — car, transportation engineering, food and chemical industry, sheet metal forming.
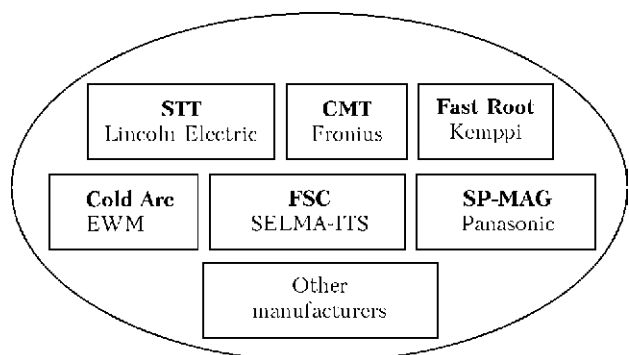

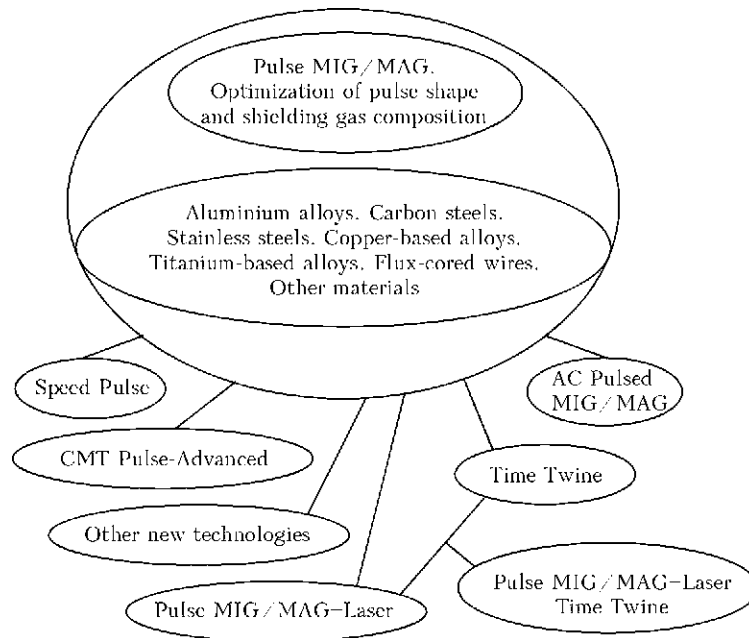**Figure 3.** Manufacturers of equipment for gas-shielded welding with SC

Figure 4. Schematic of CEPAW process development

Technologies implementing the processes of welding with spray and rotating spray transfer of electrode metal are improved. EWM, Germany, introduced integral-inverter MIG 5000 HIGH-SPEED system, realizing high-speed welding by a rotating arc [18].

As a rule, processes of welding with longer electrode extension and transition to rotating-spray arc found limited technological application. German researchers applied continuous wires of 1.2 mm diameter, Ar + 4 % O_2 shielding gas, extension was 25–35 mm, and welding speed was up to 30 m/h. Obtained results of investigation of rotating arc welding process lead to the conclusion of availability of a possible alternative to submerged-arc welding [18].

Controlled pulsed-arc transfer has a special place among the various types of electrode metal transfer [19]. It is applied not only for welding dissimilar materials, but also for realization of new intermediate types of metal transfer, as well as combined hybrid welding technologies. Figure 4 shows the diagram of development of CEPAW applications.

Intensive development is found in the direction associated with regulation of the shape of welding current pulse for CEPAW process. This direction emerged at PWI as far back as in 1980s [20, 21]. Also highly important are the thermophysical properties of the materials being welded, that is reflected, for instance, in construction of systems for automatic stabilization of CEPAW process [22].

Work by Japanese experts in the field of controlling the welding current shape for CEPAW is of scientific interest [23]. In the case of aluminium-magnesium alloys at square-wave shape of welding current pulses, drop detachment leads to fine spatter. Therefore, a pulse shape is proposed which allows elimination of spatter sticking to the item and improvement of weld appearance (Figure 5, *a*).

Shielding gas with 20–25 % CO_2 is used for carbon steel. In the shop at large mechanical engineering plants, which have centralized feeding of gas mixture, variations of mixture composition can be up to several percent. This destabilizes drop transfer of metal acting by «one drop per pulse» principle. Therefore, Japanese specialists form two-step pulses (Figure 5, *b*). Thus, drop transfer of metal is achieved even at up to 30 % CO_2 content in the mixture, and formation of very fine spatter which appears after detachment of the main drop, is suppressed. In addition to spattering reduction, also saving of shielding gas (argon) is achieved.

At CEPAW of stainless steel, which has higher surface tension, Ar + CO_2 mixture with high argon content and O_2 addition is applied. However, synchronous metal transfer through the arc is often disturbed. Therefore, pulse shape was developed, which slows down the process of drop detachment as it grows (Figure 5, *c*).

Method with superposition of low-frequency pulses for grain refinement and lowering of sensitivity to solidification cracking is of interest. PWI also performed such welding current modulation. So, in CEPAW of butt joints on AMg6 alloy, low-frequency modulation in the pause enabled elimination of burns-through and disturbance of weld formation because of fit-up inaccuracies [24].

Pulsed-arc welding was further developed in new technologies. Pulsed arc power sources were introduced, which implement the upgraded Speed Pulse process [25]. The proposed approach enables detachment of several electrode metal drops per pulse, and involving part of the spray process in low-current region. Thus, pulsed arc becomes more effective — penetration depth is increased and welding speed rises.
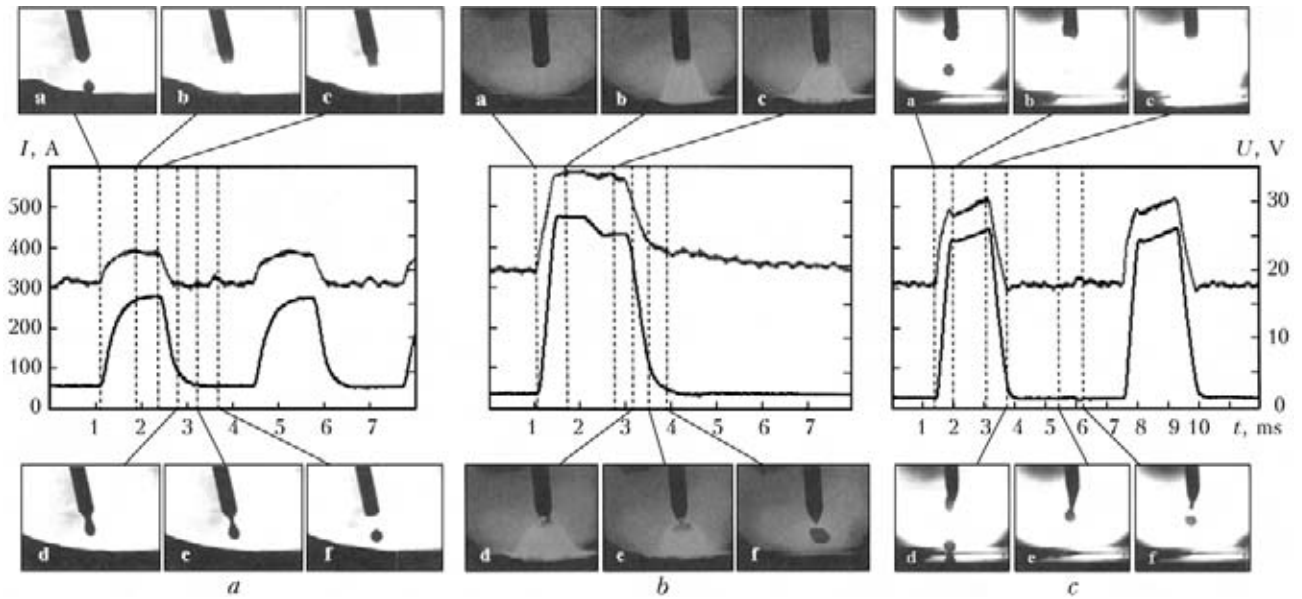
Figure 5. Welding current shapes and nature of electrode metal transfer at CEPAW of aluminium-magnesium alloys (*a*), carbon (*b*) and stainless (*c*) steels [23]
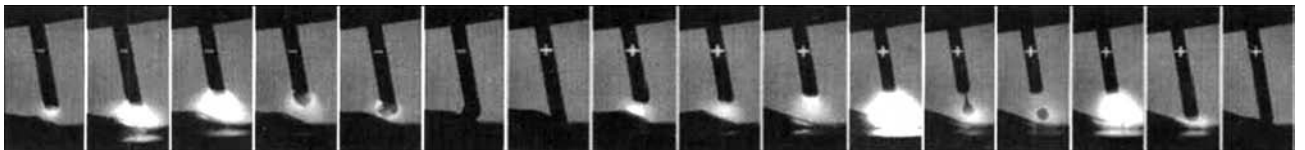
Figure 6. CMT Pulse-Advanced process [26]

The new process was well-established in carbon steel welding [25].

Fronius proposed CMT Advanced and CMT Pulse-Advanced processes [26]. Compared to the already known technology of cold metal transfer, CMT Advanced ensures low heat input. New technology enables filling wider gaps as a result of variation of heat input cycles. Figure 6 shows a cinegram of CMT Pulse-Advanced process. Drop detachment occurs at the moments of SC and action of reverse polarity pulses (as in «classical» pulsed-arc welding). Thus, two types of electrode metal transfer — with SC and fine-drop pulsed-arc without SC — are combined.

«Classical» CEPAW is performed at single-polarity direct current. Hence, the issue of magnetic blow remains urgent. A direction, related to CEPAW, is developing, where the base arc current changes its polarity (Figure 7) [27, 28]. Thus, heat input is decreased. The advantages of AC Pulsed MIG process are low weld pool temperature (welding thin-walled items), better drop detachment, and prevention of magnetic blow.

CEPAW became developed in Time Twine, Pulse MIG/MAG–Laser and Time Twin Pulse MIG/MAG–Laser processes, where two pulsed arcs, a
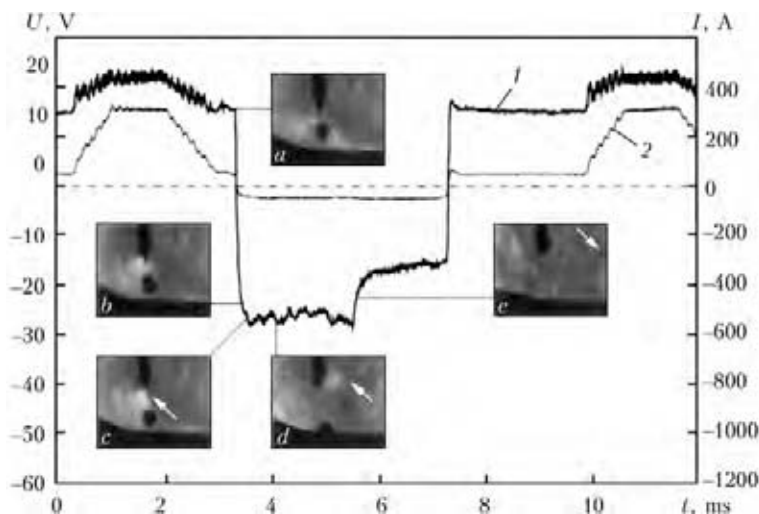
Figure 7. AC Pulsed MIG process [27]: *a–e* — cinegrams of electrode metal transfer; *1, 2* — current values of arc voltage and welding current (1.2 mm A5356 wire; acting values of welding current of 100 A; acting value of arc voltage of 16.8 V, reverse polarity of 20 %)

pulsed arc and laser and three pulsed arcs and laser are used [29–32].

Thus, CEPAW process has its advantages both in joining various class materials, and at various types of electrode metal transfer. Figure 8 gives the applications of CEPAW process with various types of electrode metal transfer.

CONCLUSIONS

1. Electric welding equipment for gas-shielded consumable electrode arc welding implements the main types of electrode metal transfer, and intermediate types of electrode metal transfer are being developed.

2. It is shown that the controllable pulsed-arc process is successfully applied in welding a wide range of metals, as well as in many combined technologies.

3. It is established that development of modern electric welding equipment implementing various types of electrode metal transfer, should be performed taking into account the controllable pulsed-arc welding process.

Figure 8. Applications of CEPAW process

1. Middeldorf, K., von Hofe, D. (2008) Trends in joining technology. *The Paton Welding J.*, **11**, 33–39.
2. Sato, K. (2008) Current power supplies for arc welding with low spattering. *Welding Technology*, **2**, 60–65.
3. (1978) *Welding in machine building*: Refer. book. Ed. by N.A. Olshansky. Vol. 1. Moscow: Mashinostroenie.
4. Potapievsky, A.G. (1974) *Consumable electrode shielded-gas welding*. Moscow: Mashinostroenie.
5. Lenivkin, V.A., Dyurgerov, N.G., Sagirov, Kh.N. (1989) *Technological properties of shielded-gas arc welding*. Moscow: Mashinostroenie.
6. Shejko, P.P., Zhernosekov, A.M., Shimanovsky, Yu.O. (2004) Consumable-electrode pulsed-arc welding with automatic stabilization of mode parameters. *The Paton Welding J.*, **1**, 7–10.
7. (2010) Criteri di scelta del gas di protezione per la saldatura a filo continuo con fili pieni. *Riv. Italiana della Saldatura*, **5**, 629–637.
8. Kusch, M. (2006) Metall-Inertgasschweissen von Aluminium mit gepulster Schutzgaszufuhr. *Schweissen und Schneiden*, **58(1)**, 19–22.
9. (2005) Automated pipeline welding: Welding abroad. *The Paton Welding J.*, **1**, 46–49.
10. Lebedev, V.A. (2010) Tendencies in development of mechanized welding with controlled transfer of electrode metal (Review). *Ibid.*, **10**, 37–44.
11. Voropaj, N.M. (1996) Parameters and technological possibilities of arc welding with pulsed feed of electrode and filler wire. *Avtomatich. Svarka*, **10**, 3–9.
12. Lankin, Yu.N. (2007) Automatic control of the MAG welding process with periodic short circuiting of arc gap (Review). *The Paton Welding J.*, **1**, 2–8.
13. Karasyov, M.V., Vyshemirsky, E.M., Bespalov, V.I. et al. (2004) Characteristics of modern units for mechanized GMA welding. *Ibid.*, **12**, 36–39.
14. Zyabkin, O.V., Kuskov, V.N., Potapov, D.A. et al. (2009) Influence of parameters of pulsed welding by STT method on heat generation and joint structure. *Zagot. Pr-va v Mashinostroenii*, **4**, 13–15.
15. Bondarenko, V.L. (2004) Arc welding with pulsed feed of electrode wire — CMT process proposed by Fronius. *Avtomatich. Svarka*, **12**, 55–58.
16. Himmelbauer, K. (2010) CMT process — the revolution in welding technologies. *Svarshchik v Rossii*, **3**, 28–32.
17. Hirota, Yu. (2010) New technologies of arc welding. *J. JWS*, 79(**6**), 15–39.
18. Technologies and guidelines EWM highspeed. *www*.ewm. ru/technologies/highspeed
19. Zhernosekov, A.M., Andreev, V.V. (2007) Pulsed metal arc welding. *The Paton Welding J.*, **10**, 40–43.
20. Pavshuk, V.M., Shejko, P.P. *Power supply for pulsed-arc welding*. USSR author's cert. 4696750/27. Int. Cl. B 23 K 9/09. Publ. 07.10.91.
21. Pavshuk, V.M. (1993) *Method and power supply for consumable electrode pulsed-arc welding with step-like pulse shape*: Syn. of Thesis for Cand. of Techn. Sci. Degree. Kiev.
22. Zhernosekov, A.M. (2006) *Systems of automatic stabilization of consumable electrode pulsed-arc welding process*: Syn. of Thesis for Cand. of Techn. Sci. Degree. Kiev.
23. Kamiyama, T. (2010) Development of arc welding machines. *Welding Technology*, 58(**2**), 46–57.
24. Shejko, P.P. (1996) Single-pass pulsed-arc welding of AMg6 alloy products by modulated current. *Avtomatich. Svarka*, **7**, 31–32.
25. Jaeschke, B., Vollrath, K. (2009) Speedpulse — eine produktivitaets- und effizensteigernde Weiterentwicklung des MSG-Impulsschweissens. *Schweissen und Schneiden*, 61(**9**), 548–553.
26. (2010) MT ADVANCE: specialist in welding of thin metal. *Avtomatich. Svarka*, **10**, 67–68.
27. Tong, H., Ueyama, T. (2004) Solutions to problems of tiny spatter and arc interruption in AC pulsed MIG arc welding. *Qart. J. JWS*, 22(**2**), 240–247.
28. Maxl, G., Posch, G. (2008) MAG — Wechselstromschweissen von hochfesten Feinkornbaustaehlen. *Schweiss & Prueftechnik*, **3**, 35–38.
29. Geke, S., Hegergard, J., Lundin, M. et al. (2002) Tandem MIG/MAG welding. *Svarochn. Proizvodstvo*, **4**, 30–35.
30. Staufer, H., Hackl, H. (2001) Laser-MIG process for automotive industry. *The Paton Welding J.*, **12**, 26–29.
31. Staufer, H., Ruehrnoebl, M. (2006) Fuer grosse Blechdicken und hohe Schweissgeschwindigkeiten: Laserhybrid- + Tandemschweissen. *Praktiker*, **10**, 300–302.
32. Kah, P., Salminen, A., Martikainen, J. (2010) Laser-arc hybrid welding processes (Review). *The Paton Welding J.*, **6**, 32–40.

CLADDING FLUX-CORED STRIPS (Review)

A.P. ZHUDRA and **A.P. VORONCHUK**

E.O. Paton Electric Welding Institute, NASU, Kiev, Ukraine

The history of development of a cladding electrode consumable in the form of flux-cored strip is presented. Various designs of the strips, compositions and application fields are considered. Equipment for manufacture of flux-cored strips and technological advantages of cladding using this consumable are described.

Flux-cored strip is now a well-known cladding consumable, which is extensively applied for manufacture and hard-facing of a wide range of parts in metallurgical industry, power engineering, mining, road construction and other industries. In contrast to flux-cored wire, the key advantages of the flux-cored strips are high deposition efficiency, possibility of alloying the deposited metal, and relative simplicity of manufacture.

The first to offer the flux-cored strip electrodes in the former USSR in 1959–1960 were O.A. Bakshi, E.F. Belousov and G.P. Klekovkin, associates of the Scientific Research Institute of Machine-Building Technology of the Chelyabinsk Sovnarkhoz (Council of National Economy) [1, 2]. The author's certificate [1] received by these specialists confirmed originality of this development not only for the USSR but also for the world welding industry. Initially, the flux-cored strips were manufactured from two strips, which were formed into a sheath directly by using the cladding device, the charge being made from the stalinite B powder. To prevent spilling of the core charge, the

Figure 1. Schematic of flux-cored strip according to the author's certificate [1] (*a*) and of the design of Chelyabinsk NPTIAM-MASh (*b*)

lower part of the sheath comprised corrugations, which formed separate cells (Figure 1, *a*).

Combining the electrode manufacture operation with subsequent cladding process made the design of the device much more complicated. Later on the flux-cored strip electrodes were manufactured separately by using the special equipment. The drawbacks of such flux-cored electrodes include high rigidity due to the presence of coarse cells, faulty sealing of locks, low compaction of the core charge, and non-uniform distribution of the sheath in width of the electrodes. Excessive rigidity of the flux-cored electrodes made it difficult to wind them into spools and feed to the arc zone during cladding. Faulty sealing of the locks did not allow a long-time storage of flux-cored electrodes and led to spilling of the core charge during transportation, loading into spools and cladding. This resulted in chemical heterogeneity of the deposited metal and decrease in its wear resistance.

Later on the Chelyabinsk Design Institute NPTIAM-MASh suggested a simpler design of the flux-cored strip (Figure 1, *b*). Transverse corrugations in this design imparted flexibility to the flux-cored strip, thus providing simplicity of its winding into spools. At the same time, the deep transverse grooves in the flux-cored strip sheath caused variations in its cross section, thus hampering the process of melting of the strip in the arc. Moreover, a serious drawback of this flux-cored strip was an insufficient density of the locks.

G.P. Klekovkin offered a flux-cored electrode for welding and cladding [3] which, physically, was made from one strip twisted into a spiral (Figure 2). Rigidity was ensured by using a shaped strip that formed a lock overlap joint along a spiral. To compact the lock material, a wick impregnated with ionising salts to stabilise the welding arc was put into its cavity. A powdered core material was located inside the spiral sheath.

Compaction of the powdered material was achieved by pressing the electrode. Twisted ribs of the sheath and recesses on its surface provided the uniform distribution of the core and the required longitudinal flexibility. Drawbacks of such flux-cored electrodes were complexity in manufacture and insufficient sealing of locks.

The stalinite B powder was used as a charge in the majority of the above designs of flux-cored strip electrodes, and cladding was performed by the submerged-arc
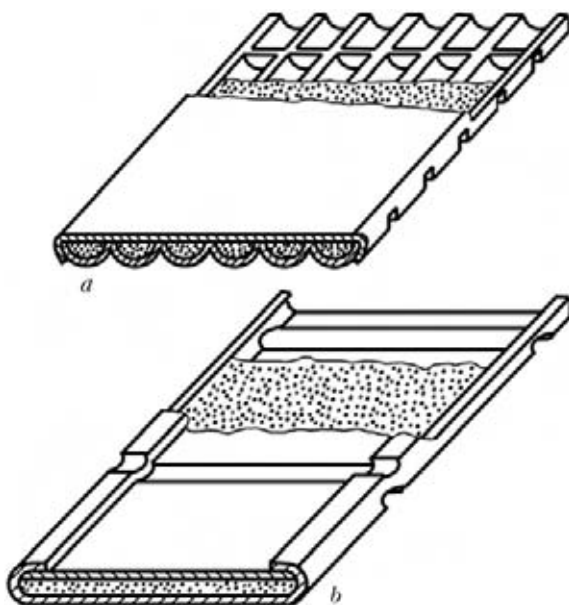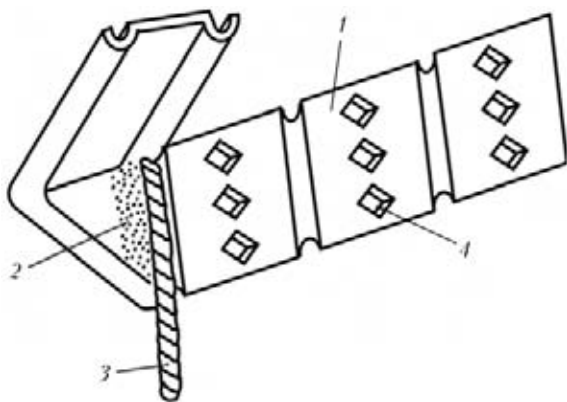
Figure 2. Schematic of Klekovkin's electrode: *1* — shaped strip; *2* — core material; *3* — wick; *4* — recess on the sheath surface

Figure 3. Schematic of double-lock flux-cored strip designed by the E.O. Paton Electric Welding Institute

method under a layer of flux AN-60. Owing to the efforts of VPTIstroidormash, at the initial stage the flux-cored strip electrodes found application for hard-facing of many parts of construction and road machines [3–7].

At the E.O. Paton Electric Welding Institute the work on development of cladding flux-cored strips was initiated in 1960 by Yu.A. Yuzvenko and V.P. Shimanovsky [8]. One of the variants of production of alkaline accumulator segments was used to manufacture the first samples of the flux-cored strips. In contrast to developments of the above authors who offered 30–50 mm wide strips [1–3, 5, 7], all developments of the E.O. Paton Electric Welding Institute were aimed at manufacture of strips of a small width (10–22 mm) designed to provide high fill factors, thus allowing solution to the alloying problems which can hardly be solved by using flux-cored wire.

Comparatively small width of the flux-cored strip allowed the more uniform distribution of the core materials across the section and the maximum possible prevention of their spilling. The required width of the deposited layer was achieved due to oscillations of the electrode. Advantages of such a strip were especially pronounced in decreasing chemical macroheterogeneity of the deposited layer.

Based on these developments, in 1965 the E.O. Paton Electric Welding Institute made the first such strip PL-AN101 [9] of the universal type, which was intended for open- and submerged-arc cladding. Then a wide commercial application of open-arc cladding by using the flux-cored strip was started in the USSR. Composition and design of flux-cored strip PL-AN101 were patented in eight countries of the world, e.g. Germany, France, Italy, etc. Design of this strip is shown in Figure 3.

Tight locks and fine-cell corrugations on the sheath provided good compaction of the flux-cored strip core, which resulted in substantial improvement of metal transfer in the arc and elimination of spilling of the charge materials into the weld pool. Several modifications of mills were developed to manufacture this design of the strip. The latest of these mills, i.e. OB 2240, is still in operation (Figure 4).
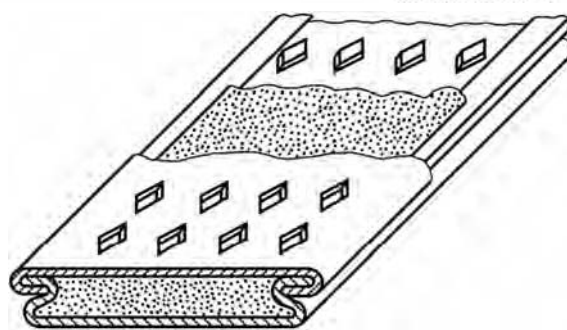
Mass production of flux-cored strips of this design on industrial scales was mastered by the Torez Plant for Surfacing Hard Alloys and Research and Production Association «Tulachermet». Drawbacks of this strip include non-uniform distribution of the sheath in its width. The welding current had the highest density in cladding at locations of the locks, where the maximal amount of the strip sheath was concentrated. This led to non-uniform melting of the sheath and formation of a protrusion in the central part of the pressed core, which, while periodically breaking off, got into the weld pool in the non-melted state.

The flux-cored strip with one overlap lock (Figure 5, *a*) was developed to provide a high fill factor, which is especially important for the case when materials with a low apparent density (carbides, chromium borides, etc.) are used as a core charge. This strip had a simple design, and was characterised by a simple manufacture technology and a high fill factor. In addition, location of the lock in the central part of cross section of the flux-core strip provided a more uniform melting of the core. Its drawbacks included leakage of the overlap lock, as a result of which the charge material of the core spilled out both during transportation and during cladding.

To eliminate the above drawbacks, in 1981 the E.O. Paton Electric Welding Institute offered a design of the flux-cored strip with a tight lock [10] (Figure 5, *b*). Replacement of the flat overlap lock by the tight one made it possible to compact densely the flux-cored strip core by rolling it in rolls and simultaneously make on the sheath the small hollows 0.6 mm deep and (2–4) × (2–4) mm in size, having a rhombic or square shape and arranged in large diagonals along the strip. Compaction provided removal of air from
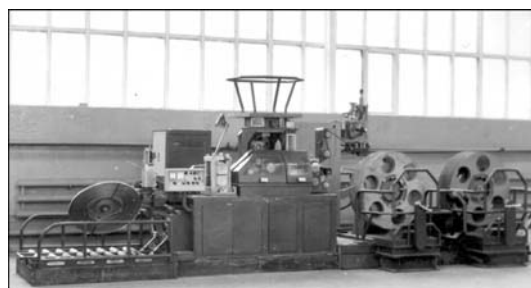
Figure 4. Mill OB 2240 for manufacture of double-lock flux-cored strip
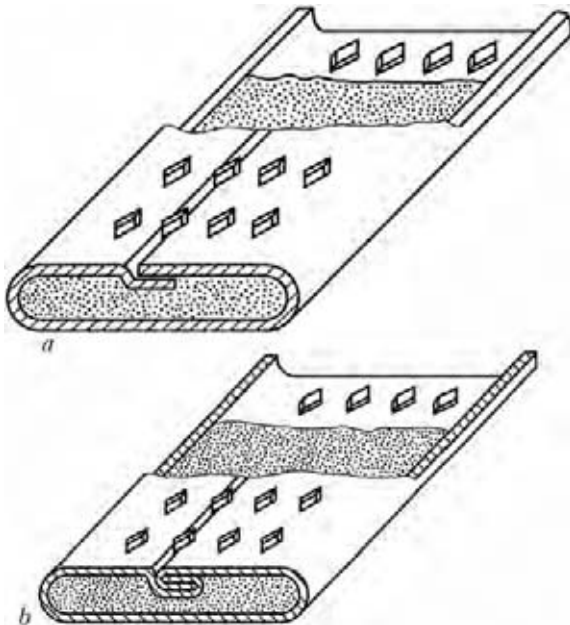
Figure 5. Schematic of design of single-lock flux-cored strip with overlap (*a*) and tight (*b*) lock

the core and prevented spilling of the core material. Small hollows on the sheath caused almost no deterioration in supply of current to the flux-cored strip sheath during cladding.

The tight lock was located in the central part of the flux-cored strip across its section. Hence, in cladding the current density per unit section of the flux-cored strip within the lock zone was higher than in its peripheral regions. This provided a more stable burning of the arc, improvement of metal transfer through the arc, uniform melting of the core, higher chemical homogeneity of the deposited metal and increase in its wear resistance.

Several modifications of the mill were developed to manufacture this design of the flux-cored strip. The latest modification was designated as OB 2324 (Figure 6). Mass production of this design of the flux-cored strips on industrial scales was arranged with participation of associates of the E.O. Paton Electric Welding Institute at Production Association «Dneprometiz» and «Tulachermet».

Figure 6. Mill OB 2324 for manufacture of single-lock flux-cored strip with tight lock
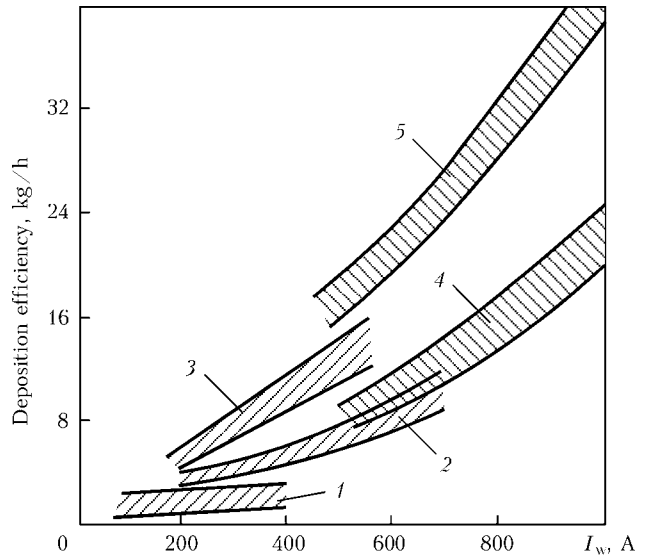
Figure 7. Deposition efficiency: *1* — stick electrodes: *2* — submerged-arc all-drawn wire; *3* — flux-cored wire; *4*, *5* — open-arc flux-core strip (one and two electrodes, respectively)

In 1985, associates of the E.O. Paton Electric Welding Institute worked out GOST 26467−85 «Cladding Flux-Cored Strip. General Technical Requirements», which is in force up to now. A short list of the developed and mass produced flux-cored strips is given in the Table.

At present two designs of the flux-cored strips are commercially manufactured — double- and single-lock strip with a tight lock, the latter being subdivided into two standard sizes — 16.5×4.0 and 10.0×3.0 mm.

Standard size of the flux-cored strip, parameters of cladding and strip design are chosen depending on the size of the surface to be hard-faced. Cladding can be performed in one, two or more layers. It can be done with separate beads and can be of the wide-layer type, with oscillation amplitude ranging from 50 to 400 mm. The cladding currents can be varied from 300 to 1200 A, arc voltage — from 25 to 38 V, and electrode movement speed — from 5 to 100 m/h. Twin- and multi-arc cladding is applied with the specially developed equipment to increase the deposition efficiency. Deposition of a wear-resistant layer 2 to 8 mm thick is provided in one pass with one-arc cladding. The deposition efficiency in one-arc cladding using the flux-cored strip amounts to 25−30 kg/h (Figure 7).

Consumption of the flux-cored strip per kilo of the deposited metal is 1.1−1.2 kg at the presence of volatile components and 1.20−1.35 kg at the presence of mineral components in the filling powder. The flux-cored strip is supplied in bundles with row-organised layout, 400−460 mm in inner diameter, up to 850 mm in outer diameter and 115−130 mm wide. Weight of one bundle is 80−150 kg. Figures 8 and 9 show the general view of the flux-cored strip and the bundle with a row-organised layout.

The commercial welding equipment is utilised for cladding with flux-cored strips. This equipment is ad-

Flux-cored strip for cladding

Flux-cored strip grade	Chemical composition of deposited metal, wt.%										
	C	Cr	Mn	Si	Ni	Nb	Mo	V	W	B	Ti
PL-AN-101	3.0	25	2.0	3.0	2.0	–	–	–	–	–	–
PL-AN-171	1.2	25	2.2	1.0	–	–	–	–	–	3.5	–
PL-AN-180	4.5	30	–	–	–	–	1.0	–	–	–	–
PL-AN-181	4.5	30	3.0	–	–	–	–	–	–	–	–
PL-AN-111	5.0	38	1.0	2.5	38.0	–	–	–	–	0.3	–
PL-AN-179	5.0	22	–	–	–	7.0	6.0	1.0	2.0	–	–
PL-AN-185	5.0	22	–	–	–	7.0	–	–	–	–	–
PL-AN-186	4.5	30	–	–	–	–	–	–	–	0.7	–
PL-AN-132-1	0.10	4	1.5	1.0	–	–	2.0	–	2.5	–	–
PL-AN-132-2	0.15	4	1.5	1.0	–	–	2.0	–	2.5	–	–
PL-AN-132-3	0.20	4	1.5	1.0	–	–	2.0	–	2.5	–	–
PL-AN-187	0.2	11	10.0	–	–	–	–	–	–	–	0.8
PL-AN-115	0.1	–	1.5	0.8	–	–	–	–	–	–	0.5
PL-AN-189	0.35	3	0.8	0.6	–	–	–	0.3	9.0	–	–
PL-AN-190	0.40	3	0.8	0.6	–	–	–	0.3	9.0	–	–
PL-AN-191	0.25	5	0.7	1.0	–	–	1.2	0.4	–	–	–
PL-AN-183	0.4	2	1.6	1.6	5.5	0.6	1.8	0.5	–	–	–
PL-AN-150	0.12	16	2.0	5.0	9.0	–	–	–	–	–	–
PL-AN-151	0.12	16	4.0	5.0	8.0	1.0	6.0	–	–	–	–

Tabl. (cont.)

Flux-cored strip grade	Hardness HRC	Application
PL-AN-101 PL-AN-171 PL-AN-180 PL-AN-181	50−56 54−59 58−62 58−60	Cladding of parts operating under abrasive wear conditions (bulldozer and grab knives, excavator ladle teeth, coke mill rolls, plough disks, protective surfaces of caps and bells, etc.)
PL-AN-111 PL-AN-179 PL-AN-185 PL-AN-186	50−58 58−62 56−60 57−62	Cladding of parts operating under intensive abrasive and gas-abrasive were conditions at normal and elevated temperatures (caps and bells of blast furnace charging equipment, chutes, hoppers, etc.)
PL-AN-132-1 PL-AN-132-2 PL-AN-132-3	18−28 28−34 35−45	Cladding of parts operating under contact load conditions at elevated temperatures (rollers of gravity roll carriers, rolls, etc.)
PL-AN-187	18−26	Cladding of parts operating under high contact load conditions (crane wheels, guides, etc.)
PL-AN-115	18−26	Cladding of large-size steel parts to restore their geometric dimensions (caps and bells of blast furnace charging devices, agglomachine carriages, etc.)
PL-AN-189 PL-AN-190 PL-AN-191	44−50 44−50 46−52	Cladding of metal hot rolling rolls
PL-AN-183	47−54	Cladding of metal hot cutting knives
PL-AN-150 PL-AN-151	27−34 38−50	Submerged-arc cladding of stop valve components operating at an environment temperature of up to 545 °C

ditionally fitted with special contact tubes and feeding rollers, which provide a reliable feed of the electrode material.

Flux-cored strips are most successfully applied for cladding of blast furnace charging devices [11−14], cap-free charging devices [12, 13], coal mill beaters [12, 13], bimetal wear-resistant plates [13, 15], road construction machines [16−18], metal hot cutting knives [13], stop valves at heat and nuclear power plants [19, 20] and many other parts in metallurgical industry, mining and power engineering.

No data on development of compositions and mass production of flux-cored strips to be used as electrode materials are available in foreign literature. However, promotion materials of an Argentine company contain data on a material in the form of a flux-cored strip used to add deoxidisers in steel casting.

Therefore, the world priority in development of the flux-cored strips as an electrode material belongs to the USSR. Development of the majority of compositions, arrangement of commercial manufacture and wide application of the flux-cored strips — all
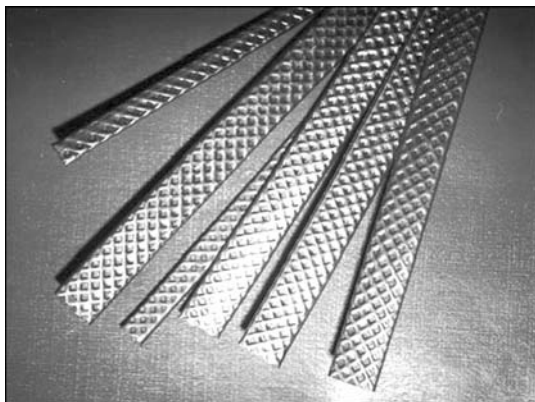
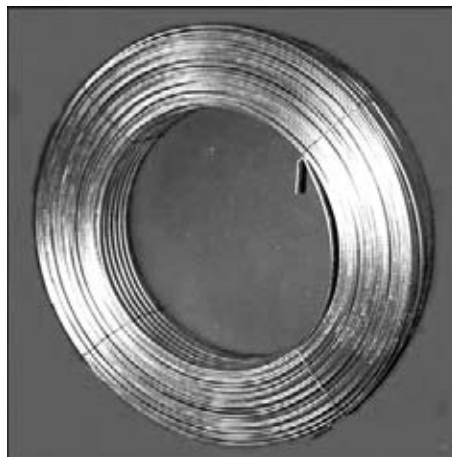**Figure 8.** General view of flux-cored strip

Figure 9. Flux-cored strip bundle

this is a merit of associates of the E.O. Paton Electric Welding Institute. Great contribution to development of flux-cored strip compositions and cladding technologies was made in different years by specialists of such institutions as TsNTI VNIIST (Scientific-and-Technical Information Centre of All-Russian Research Institute for Construction and Operation of Pipelines) (Moscow) [21, 22], National Technical University of Ukraine «Kiev Polytechnic Institute» [23−26], Priazovsky State Technical University, Open Joint Stock Company «Azovmash» (Mariupol, Ukraine) [27, 28], Dnepropetrovsk State University (Ukraine) and many others.

Before 1991 the USSR manufactured up to 1000 t of flux-cored strips a year. At present the flux-cored strips are manufactured in Ukraine by Open Joint Stock Company «Toreztverdosplav» (Torez) and Limited Liability Company «PLAN-T», and in Russia — by Limited Liability Company «Rosnamis» (Taganrog) and Research and Production Association «Polema» (Tula). Today the total output of the flux-cored strips of different grades is above 700 t a year. There is a stable trend to increase in production of these electrode materials, which is attributed to a growing demand in the industry for new types of products with increased wear resistance.

1. Klekovkin, G.P., Bakshi, O.A., Sumina, T.V. et al. *Flux-cored strip electrode*. USSR author's cert. 132271. Priority 30.01.1959.
2. Bakshi, O.A., Belousov, E.F., Klekovkin, G.P. et al. (1960) Wear-resistant cladding with flux-cored strip electrode. *Svarochn. Proizvodstvo*, **3**, 30−33.
3. Klekovkin, G.P. *Klekovkin's flux-cored electrode*. USSR author's cert. 143180. Publ. 1960.
4. Kortelev, G.A., Cherepakhin, A.V., Nikolaenko, M.R. et al. (1968) Wear-resistant flux-cored strip cladding of operating elements of earth-moving machines. *Stroit. i Dorozhn. Mashiny*, **7**, 35−37.
5. Kortelev, G.A. (1971) *Specifics of wear-resistant mechanised cladding with high-chromium cast iron of parts of road and construction machines and development of filler materials*: Syn. of Thesis for Cand. of Techn. Sci. Degree. Bryansk.
6. Nikolaenko, M.R. (1972) *Investigation and development of filler materials and technology for cladding of earth-moving machine parts*: Syn. of Thesis for Cand. of Techn. Sci. Degree. Bryansk.
7. Nikolaenko, M.R., Kortelev, G.A. (1972) *Strip electrode cladding of machine parts*. Series 5. Moscow: TsNIITEstrojmash.
8. Yuzvenko, Yu.A. (1960) Flux-cored electrode strip. *Avtomatich. Svarka*, **9**, 86−87.
9. Yuzvenko, Yu.A., Shimanovsky, V.P., Kopylets, I.P. (1967) Flux-cored strip PL-AN101. USSR author's cert. 200075. Publ. 1967.
10. Danilchenko, B.V., Shimanovsky, V.P., Kopylets, I.P. et al. *Flux-cored strip electrode for cladding of high-chromium alloys*. USSR author's cert. 1152159. Publ. 1984.
11. Shimanovsky, V.P., Voronchuk, A.P., Zvezdin, S.M. (1990) Materials and equipment for cladding of bells and cups of blast furnaces. In: *Equipment and consumables for surfacing*. Kiev: PWI.
12. Danilchenko, B.V., Shimanovsky, V.P., Voronchuk, A.P. et al. (1989) Cladding of rapidly wearing parts with self-shielding flux-cored strips. *Avtomatich. Svarka*, **5**, 38−41.
13. Zhudra, A.P., Voronchuk, A.P. (2010) Wear-resistant flux-cored wire cladding. *Svarshchik*, **6**, 6−10.
14. Zhudra, A.P., Voronchuk, A.P., Fomakin, A.A. et al. (2009) New equipment for hard-facing of charging device bells and cups. *The Paton Welding J.*, **9**, 44−46.
15. Zhudra, A.P., Voronchuk, A.P., Veliky, S.I. (2009) Equipment and consumables for hard-facing of lining plate elements. *Ibid.*, **6**, 44−46.
16. Kortelev, G.A., Nikolaenko, M.R., Litvinov, B.A. et al. (1973) Automatic wear-resistant cladding with flux-cored strip PL-AN 101 of loader bucket teeth. *Svarochn. Proizvodstvo*, **11**, 38−39.
17. Kortelev, G.A., Spektor, L.M., Nosov, I.M. et al. (1975) Automatic cladding of screw blades using flux-cored strip PL-AN-101. *Avtomatich. Svarka*, **2**, 49−50.
18. Kortelev, G.A., Zheravkov, V.P., Cherepakhin, A.A. (1972) Automatic cladding of bucket teeth of E-652 excavator using flux-cored strip PL-U30Kh30G3TYu. *Svarochn. Proizvodstvo*, **12**, 32−34.
19. Eremeev, V.B., Strelyany, Yu.Z., Frumin, I.I. (1978) Development of flux-cored wire and strip for cladding of pipe fittings. In: *Theoretical and technological principles of surfacing. Filler materials*. Kiev: PWI.
20. Eremeev, V.B. (1985) Mechanised cladding of worn-out fittings of thermoelectric power stations. In: *Surfacing. Experience and efficiency of application*. Kiev: PWI.
21. Nikolaenko, M.P., Grinberg, N.A. (1976) Heterogeneity of metal deposited with flux-cored strip electrode. In: *Technology and equipment of welding and surfacing operations*. Tula.
22. Nikolaenko, K.R., Kortelev, G.A., Grinberg, N.A. (1973) Effect of boron, vanadium and nickel on structure and properties of high-chromium cast irons deposited with flux-cored strip. *Svarochn. Proizvodstvo*, **4**, 32−34.
23. Patskevich, I.R. (1973) Experience of application and prospects for development of flux-cored strip cladding. In: *Proc. of All-Union Meeting on High-Efficient Processes of Surfacing and Filler Materials* (Kommunarsk). Kiev: PWI, 14−18.
24. Patskevich, I.R., Rykov, A.M. (1973) Static characteristics of arc in flux-cored strip cladding. *Svarochn. Proizvodstvo*, **2**, 9−11.
25. Patskevich, I.R., Rykov, A.M. (1972) Heat balance of arc in flux-cored strip cladding. *Ibid.*, **2**, 7−9.
26. Patskevich, I.R., Khejfets, L.A. (1971) About chemical heterogeneity of layer deposited with flux-cored strip in CO_2. *Avtomatich. Svarka*, **11**, 66−67.
27. Chigarev, V.V. (1994) Manufacture and application of flux-cored strips for cladding of wear-resistant alloys. *Ibid.*, **2**, 51−52.
28. Chigarev, V.V., Belik, A.G. (2011) Flux-cored strips for cladding. *Svarochn. Proizvodstvo*, **8**, 38−44.

COMPUTER SYSTEM FOR CALCULATION OF NORMS OF CONSUMPTION OF WELDING CONSUMABLES FOR MANUFACTURE AND REPAIR OF STEEL PIPELINES

G.A. IVANOV and **V.N. PRONCHEVA**

Institute of Welding and Protective Coatings, NASB, Minsk, Belarus

The paper describes the structure and main functions of a system for calculation of norms of the welding consumable consumption for welding of parts and assemblies of steel pipelines. The content of data and knowledge base of the system is given. Examples of forms with prepared source data and calculation results are given.

Large scope of works on construction and repair of the pipelines is performed in the Republic of Belarus each year and tendency to their increase can be noted. Variety of types of the pipelines (gas-, oil- and steam pipelines etc.), methods of welding being applied (gas-shielded consumable and noncomsumable electrode arc welding with filler metal, submerged arc welding, manual arc welding, gas welding), welded materials (steel, copper, cupronickel alloys etc.), welding consumables (coated and tungsten electrodes, metal solid and flux-cored wire), types of welded joints and equipment can characterize manufacture of the pipelines.

An improvement of welding methods and creation of new equipment as well as development of new technologies is necessary considering a constant increase of the pipeline length and application of large diameter pipelines from alloyed, corrosion-resistant and high-strength steels.

Significant scope of works on process preparation of welding-erection production is stipulated by large volume of welding operations in the pipeline construction.

Development of the technological regulations for welding of pipes is related with the necessity of making of the design solutions during selection of the method of welding, equipment, materials to be welded and consumables, the calculations for determination of norms of the welding consumable consumption, norms of the standard time and parameters of welding as well as performance of the large scope of routine operations connected with the preparation of process documentation.

Thus, the necessity of PC application for automation of a design of the technological regulations during manufacture of parts and assemblies of the pipelines is obvious for the purpose of reduction of consumable and labor outlay, improvement of quality of design solutions and process documentation as well as promotion of image of the designers.

The Institute of Welding and Protective Coatings of the NAS of the Republic of Belarus deals with the development of data-analytical and reference-information systems for PC. A system for calculation of norms of the welding consumable consumption for manufacture and repair of the steel pipelines was developed in scope of this subject. The system consists of a program complex, data (DB) and knowledge base (KB).

The program complex contains the design procedures for dialog preparation and entry of the source data, calculation of norms of the welding consumable consumption, determination of the weld lengths and formation of the output documentation.

A form, content and amount of the source data, controlled through the data being entered by the user, were developed and displayed for preparation and entry of the source data. This allows providing a confidence of the source data required by program for solving of a specific task and eliminating of the errors in data preparation. Numeric data, typing from the keyboard, are controlled by the maximum and minimum allowable values. An error message is displayed in the case of out of limits of the allowable values. An example of the system window with prepared source data is given in Figure 1. All fields for preparation of the source data can be divided into two types: data
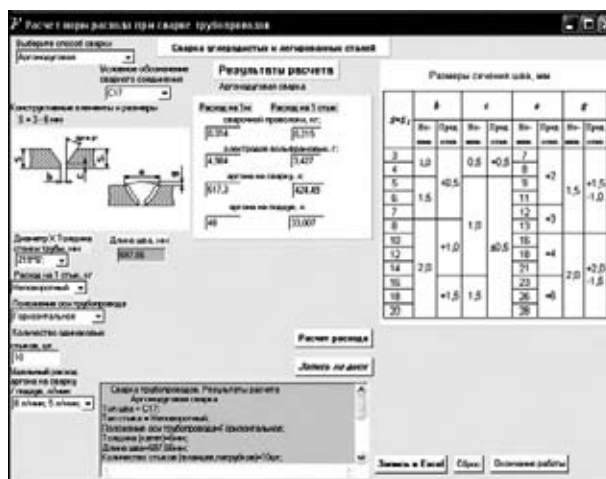

Figure 1. Main window of the system with prepared source data and calculation results
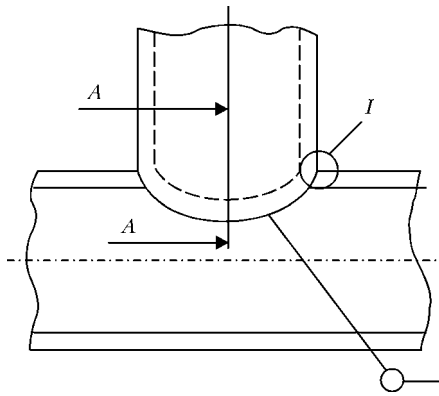
Figure 2. Scheme of pipe to pipe fillet joint (branch, fitting)

Figure 3. System window with prepared source data and calculation result

sampling from the lists, opened by a keystroke, and data typing form the keyboard. Content of information which should be entered and sampled, is described in the marks over the each field. The keys are designed for carrying out of the operations recorded on them.

The system alloys calculating of norms of the welding consumable consumption in manual arc, gas, argon-arc and combined methods of welding of parts and assemblies of the pipelines from carbon and low-alloyed steels. The welding method is selected by the user. Structural dimensions and reference designations correspond with GOST 16037–80.

The procedural materials and data, given in [1–6], were taken as a basis for development of an algorithm and program. Production norms of the welding consumable consumption for position butt joints of the pipes are given in from of the tables. The correction factors depending on method of welding and other conditions [1, 3–5] are used in the system for determination of norms of the welding consumable consumption for roll butt welding. Norms of the consumable consumption for welding-in of the branches positioned over the pipeline normal to its axis are indicated in the tables of standards. The correction factors, imbedded in the system, are used for correcting the norm of consumption at side or bottom position of the branch in the pipe and at angles different from normal one. Combined welding is used for performance of multilayer welds. At that a weld root (the first layer of the weld) is carried out by argon-arc welding, and manual arc welding with coated electrode is used for the rest ones. Pure consumption of the consumables, difficult to remove wastes and losses formed during welding operation performance, i.e. electrode stabs, rests of the wire in bundle, losses for burn-off, spattering and slag formation are considered in the production norms.

A program for determination of length of the welds during welding of tubular blanks at normal and acute angles was developed. It can be activated independently (including during operation in other systems) as well as automatically in particular system. Entry data and calculation results of this program are given in Figure 3.
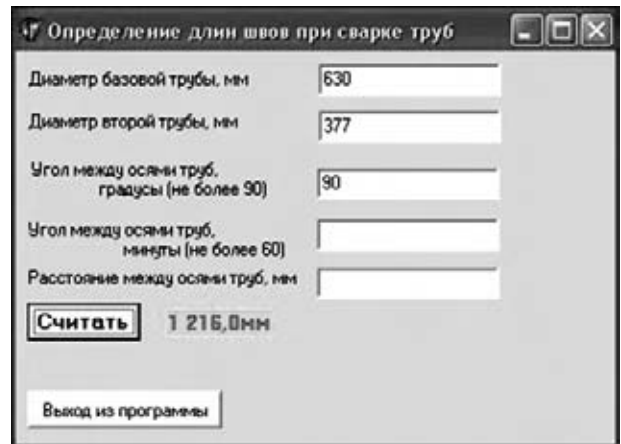
DB and KB of the system, having multilevel hierarchical structure, consist of number of files and contains:

• tables of reference data on norms of the consumable consumption per 1 m of the weld and per one butt joint (flange or branch), formed as separate files by methods of welding;

• drafts of structural elements of the prepared edges and welds;

• reference designations of the welded joints;

• tables of dimension characteristics of structural elements of the welded joints.

The following basic requirements, i.e. quick access to data, simple and open interface, possibility of data correcting without system correcting are provided in DB and KB operation.

The files divided on methods of welding compile the results of calculation and can be displayed or printed in Excel table format by the user request.

The system is designed for independent application at the enterprises involved in construction and repair of the pipelines as well as for it implementation as a component in a structure of corporate information systems of the enterprises.

Reduction of the labor costs for preparation of production and costs on materials due to more accurate and technically-grounded calculations is the result of efficiency of the system implementation.

1. Yuriev, V.P. (1972) *Reference book on normalization of materials and electric power for welding technique*. Moscow: Mashinostroenie.
2. (1971) *Reference book on welding*. Ed. by I.A. Akulov. Vol. 4. Moscow: Mashinostroenie.
3. Panashchenko, N.I., Kharchenko, P.F., Bejnish, A.M. et al. (1978) *Rating of electrode consumption for arc welding*. Kiev: Naukova Dumka.
4. (1962) *Rating of material consumption in welding and surfacing production*. Barnaul.
5. (1990) General production norms of material consumption in building. In: *Welding works*. 2nd ed. Moscow: Strojizdat.
6. (1997) Welding and welded materials. In: *Technology and equipment*. Vol. 2. Ed. by V.M. Yampolsky. Moscow: MGTU im. N.E. Baumana.

THERMAL SPRAYING OF PSEUDO-ALLOY COATINGS
(Review)

N.V. VIGILYANSKAYA, Yu.S. BORISOV and **I.A. DEMIANOV**
E.O. Paton Electric Welding Institute, NASU, Kiev, Ukraine

The paper presents the experience in development and application of thermal spray pseudo-alloy coatings, and describes the principle of their formation. Characteristics of the most extensively used pseudo-alloy coatings and the effectiveness of their practical application in different engineering fields are given.

Keywords: thermal spraying, electric arc spraying, composite coating, pseudo-alloy, pseudo-alloy coating, properties of coatings, practical application

Development and application of new high-performance materials and technologies for repair, improvement of reliability and extension of service life of different-purpose assemblies and parts are a pressing task in the field of production of protective coatings.

The composite coating is a heterophase coating formed in the process of its deposition, having a structure and properties typical of a composite material. Analysis of the process of thermal spraying, structure and physical-mechanical properties of the composite coatings reveals a number of advantages of such coatings and, in particular, their high strength, density, homogeneity and presence of phases with special properties [1].

Coatings with a pseudo-alloy structure are a separate type of composite coatings. They consist of materials that do not form solid solutions and compounds in the liquid and solid states (differing in melting temperatures and not fusing with each other). Owing to the absence of interaction between these materials in a wide range of concentrations and temperatures, the pseudo-alloy coatings combine the properties of each of their components. In the process of deposition of a multi-component coating particles of each of the deposited metals are preserved individually in a layer, although during metallising they were in the molten state. Such multi-component coatings are called the pseudo-alloy ones. Materials of the type of pseudo-alloys are characterised by a number of important properties, such as a combination of high values of melting and evaporation temperatures with mechanical strength, hardness, damping ability, wear resistance, self-lubrication ability under dry friction conditions, and a high level of electrical and thermal conductivity [2]. The required properties of pseudo-alloys are achieved by varying the ratio of their components. Properties of the pseudo-alloys strongly depend on the methods used to produce them: liquid- or solid-phase sintering, and impregnation.

At present the pseudo-alloys go in a wide range of compositions with different service properties. For example, the pseudo-alloys of the Ti–Mg (14–25 % Mg) system are characterised by good antifriction properties and corrosion resistance [3]. The pseudo-alloys of the Fe–Cu (15–25 % Cu) system feature a good ductility, strength and heat resistance. They are used to manufacture compressor blades, piston and sealing rings [3, 4]. Application of the pseudo-alloys of the Fe–Pb (10 % Pb, 2 % Sn, Fe — balance) system is attributed primarily to their good antifriction properties. They are used to manufacture sliding bearings [4]. The pseudo-alloys of the Fe–Mg (93 % Fe, 7 % Mg) system are used to manufacture consumable anodes for electrochemical protection of structural materials [3, 5]. The pseudo-alloys of the W–Cu, W–Ag, Mo–Cu, Mo–Ag and Ni–Ag systems are employed in electrical engineering as electrocontact materials and to manufacture plasmatron nozzles [6–10]. The pseudo-alloys of the Cu–Cr (35 % Cr) system are used to produce electric contacts for vacuum arc-extinguishing chambers [11].

Theoretical and experimental analyses showed the feasibility of preliminary calculation of physical properties of the composite materials (CM) and coatings, such as thermal expansion coefficient, thermal conductivity coefficient and elasticity modulus [12]. Based on the existing approaches to calculation of properties of CM, it is possible to make calculation-analytical estimation of the predictable properties of mechanical mixtures, where the thermal spray pseudo-alloy coatings belong to as to their structure. The latter consists of a mechanical homogeneous mixture of particles of the melt (splats) several micrometres thick and tens of micrometres in diameter, which were deformed at collision with the substrate surface. The Figure shows characteristic structure of the pseudo-alloy coating of the Cu–NiCr system.

The calculation method can be used to determine thermal conductivity coefficient λ_c [13], elasticity modulus E_c [11, 14] and thermal expansion coefficient α_c [11, 14] of the coatings:
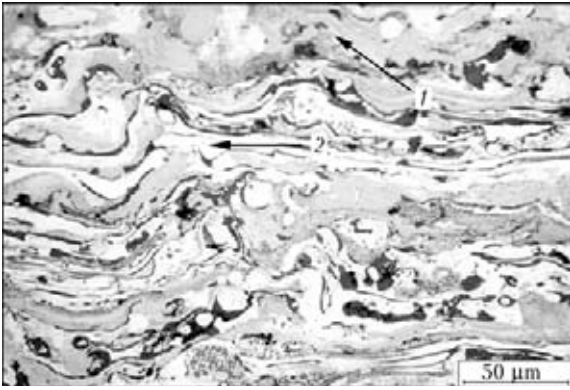
Microstructure of Cu−NiCr system pseudo-alloy coating: *1* − Cu; *2* − NiCr

$$\lambda_c = \lambda_1 m_1 + \lambda_2 m_2,$$
$$E_c = E_1 V_1 + E_2 V_2,$$
$$\alpha_c = [\alpha_1 E_1 (1 - V_2) + \alpha_2 E_2 V_2] / [E_1 (1 - V_2) + E_2 V_2],$$

where λ_1 and λ_2 are the thermal conductivities of the coating components; m_1 and m_2 are the weight contents of the coating components; E_1 and E_2 are the elasticity moduli of the coating components; V_1 and V_2 are the volume contents of the coating components; and α_1 and α_2 are the thermal expansion coefficients of the coating components.

Coatings with the pseudo-alloy structure can be produced by the methods of electric spark alloying [15], ion-plasma magnetron sputtering [16] and thermal spraying (plasma and flame spraying, and arc metallising). The electric arc metallising method received the widest acceptance for deposition of the pseudo-alloy coatings.

Up to now no reference and regulation literature specifying service properties and technology for deposition of the pseudo-alloy electric arc coatings is available. Therefore, the purpose of this study is to establish and substantiate, on the basis of analytical review, the efficiency of application of electric arc deposition of the pseudo-alloy coatings in manufacture and repair of parts.

Equipment and consumables for thermal spraying of pseudo-alloy coatings. The following types of units were used to deposit the pseudo-alloy coatings:

• plasma spraying units UPU-3, UPU-4, UMP-5 and UMP-6 [17] (using powder consumables), as well as plasmatron UShR-2 [18];

• gas metallising devices of the MGI-2, MGI-5 [17], MGI-1-57 and GIM-2 types with extension head UG-2 [19];

• twin-wire devices for electric arc spraying − stationary (machine tool) devices EM-6, EM-12, EM-15, MES-1, and portable (manual) devices EM-3, REM-3A, EM-9, EM-10 and EM-14 [20];

• three-wire electric arc metallisers UMA-1 [21], three-wire heads MTG and three-phase devices TM-2 [22].

The three-wire electric arc metallisers (with motor drive EM-6 and attached three-wire head MTG) allow separate regulation of wire feed speeds [23].

The following powders are used for thermal spraying of the pseudo-alloy coatings:

• mechanical mixtures of components (Al−Sn [18]) conglomerated on some binder (mechanical mixture of powders of conglomerated Al−Ni and molybdenum [24]);

• composite powders consisting of a base core surrounded by a cladding layer of the second component (Al−Cu, Pb−Cu, Mo−Ni, Ag−Ni [24], Al−Mo [25]), the cladding layer being applied either by chemical deposition or vacuum evaporation.

The pseudo-alloy coatings can also be deposited by plasma spraying of powders produced by mechanical alloying (Cu−Ta [26], Fe−Cu [27], Mo−Cu [28]).

The pseudo-alloy coatings can be deposited with flame metallisers by using polymetallic wires that consist of two or three metals arranged in layers, which are produced by wrapping a wire of one metal with a strip of the other metal, and then their combined drawing through a die (aluminium-lead or copper-lead one) [29].

When using the twin- and three-wire electric arc devices to produce the pseudo-alloy coatings, a device is loaded with dissimilar wires, the diameters and feed speeds of which are selected on a base of the required proportion of coating components. The pseudo-alloy coatings are formed from a mixture of particles of dissimilar metals [23, 29]. Consumables in the form of solid wires (steel, aluminium, brass, zinc, lead, tin-lead) or flux-cored wires with a metal sheath (sheath of steels Sv-08, Sv-08G2S, 30KhGSA, steels 70, U8, U10, 20Kh13, 40Kh13 and 65G) and different core components are used for electric arc spraying of the pseudo-alloy coatings.

The antifriction pseudo-alloy coatings are produced from steel, copper, lead with an addition of aluminium, brass and other metals. The pseudo-alloy coatings on a steel base with copper, brass and aluminium, as well as steel-molybdenum coatings are applied to increase wear resistance [29]. The Zn−Al system coatings are used mainly for corrosion protection [19]. The content of the second metallic component in such coatings may be varied from 5 to 50 wt.%.

The process of thermal spraying of pseudo-alloy coatings. Thermal spraying allows producing pseudo-alloy coatings from non-fusing metals with the required properties and a wide range of combinations of their components. This technology can provide the pseudo-alloy coatings by using the alloy-forming components. A short time of contact of particles of the components (milliseconds) prevents development of the interaction processes.

In combined spraying by the method of electric arc metallising of metals characterised by some mutual solubility or capable of entering into chemical interaction, structure of the pseudo-alloy coatings is characterised by the presence of different-concentration solid solutions or intermetallic phases. An example is a pseudo-alloy coating of the Al−Cu system [30]. In case of combined spraying of metals characterised by low mutual solubility, the oxidised particles of the initial metals are detected in structure of the pseudo-alloy coatings. Such coatings include Cu−Pb and Cu−steel.

High antifriction properties of the pseudo-alloy coatings are attributable to their specific structure. Characteristic features of the pseudo-alloy coatings are heterogeneity and microporosity. The heterogeneous structure and presence of developed roughness and porosity (8−12 vol.%) on the layer surface provide favourable conditions for preservation of oil film during the friction process even after termination of feeding of a lubricant.

Mechanical properties of the pseudo-alloy coatings are related to their structure and depend on the process parameters that change the quantity and form of location of oxides, as well as sizes and shapes of particles [31]. For instance, increasing the air pressure in electric arc spraying makes it possible to achieve a finer-grained structure of the layer, but causes considerable oxidation of a coating material. Also, the spraying distance has a strong effect on physical-mechanical properties of the coatings. With a 25 to 300 mm increase in the spraying distance the degree of oxidation of the spraying particles grows and the amount of oxides in the layer increases from 10 to 40 %. Moreover, the particles reach the substrate surface in a more cooled state, this causing a decrease in strength properties of the coatings (tensile and compressive strength − by 40 %, hardness − by 5−10 %) [31].

Physical-mechanical properties of the pseudo-alloy coatings can be improved by heat treatment, which is used for the pseudo-alloy coatings consisting entirely of refractory metals or containing them in the dominating amounts, as well as coatings of non-ferrous pseudo-alloys. The latter (MS25, M75 POS30) after heat treatment have improved running-in ability [19]. If dissimilar materials are used in the arc device as anode and cathode, the question arises of analysis of the character of formation of a spraying material jet in simultaneous spraying of two wires (whether they can interact between each other during the spraying process). Study [32] presents analysis of the particles produced by simultaneous spraying of steel and copper wires by using the electric arc device. Copper and iron are almost insoluble, and this may cause difficulties with formation of solid solution between them. In addition, at the initial stage of melting and detachment of a drop from the tips of the two wires they have a low possibility of contact because of the effect of a spraying gas flow. Meanwhile, after spraying and in flight the particles may enter into contact with each other. However, as shown by analysis, contact interaction and solubility of the two materials are insignificant (an iron particle contains 1.27 wt.% Cu, and a copper particle contains 1.9 wt.% Fe).

The technology for deposition of the pseudo-alloy coatings has some drawbacks related to violation of stability of the electric arc metallising process because of different melting rates of wires with different compositions. To eliminate them, it is necessary to work out special measures (using wires of different diameters or feeding them with different speeds, removal of oxide film from the wires), this making the technological process more complicated and limiting the possibility of regulation of composition of the coatings.

Spraying parameters, structure and properties of thermal spray pseudo-alloy coatings. *Antifriction pseudo-alloy coatings.* The pseudo-alloy coatings produced by electric arc spraying and used as antifriction materials in sliding friction units have a number of advantages. Similar to cermet materials, their structure consists of particles of metals, oxides, nitrides, pores etc. The pseudo-alloy coatings can be well and quickly run-in and exhibit a lower susceptibility to scores, compared to other antifriction coatings [33].

Compositions of the most extensively used antifriction pseudo-alloy coatings and some data characterising their properties [29] are given in Table 1.

Parameters of spraying of the pseudo-alloy coatings using electric arc devices EM-3A are given in Table 2 [29].

Parameters given in Table 3 are recommended for spraying of the pseudo-alloy coatings using electric arc device EM-6 with three-wire head MTG [23].

Table 4 gives parameters for spraying of the pseudo-alloy coatings by the flame method [29].

Table 5 gives values of physical-mechanical properties of the pseudo-alloy coatings (under liquid friction conditions) produced by electric arc metallising using device EM-3A [19].

The Cu−Pb system pseudo-alloy coatings deposited by using the three-wire metalliser have characteristic laminated structure [30]. Peculiarity of structure of these pseudo-alloy coatings is their porosity. Specific structure and character of adhesion between the particles of the Cu−Pb system coatings are attributable to relatively low values of their physical-mechanical properties, which can be increased by annealing to sintering in a reducing environment. The concentration of absorbed oxygen and porosity of the coatings reach minimal values, and laminated structure fully vanishes in 3 h at an annealing temperature of 900−940 °C in the 10−15 % mixture of charcoal and aluminium oxide. This change of structure of the Cu−Pb system pseudo-alloy coatings leads to a considerable improvement of their wear resistance.

Independently of the surface preparation method, annealing provides a substantial decrease in strength of adhesion of the pseudo-alloy coating to the substrate. In case of deposition of the Cu−Pb system coating on the steel substrate prepared by cutting a ragged thread, the adhesion strength after annealing decreased to 3.8−4.6 MPa, compared to 10−15 MPa before annealing, because of formation of the intermediate film of the copper and iron oxide mixture, i.e. Cu_2O, FeO and Fe_3O_4. This led to the necessity to exclude direct chemical interaction between the pseudo-alloy coating components and steel by depositing a protective sub-layer of tin, brass, nickel or copper. Appli-

Table 1. Antifriction pseudo-alloy coatings and their properties

Pseudo-alloy coating	Composition, %	Brinell hardness under 250 kg load	Oil absorbability, %	Running-in compared to babbit metal B83, %	Ultimate load·10^{-4}, N/m^2, at sliding speed, m/s	
					1	4
Al−steel (AZh50)	Al 48−50 Fe 50−52	37−44	10−14	58	1030	1079
Cu−steel (MZh50)	Cu 45−50 Fe 50−55		−	64	883	1128
Cu−steel (MZh75)	Cu 25−30 Fe 70−75	95−107	3.0−3.2	80	668	785
Brass−steel (LZh75)	Cu 17−20 Zn 8−10 Fe 70−75	95−107	2.5−3.0	42	490	834
Cu−Pb (MS25)	Pb 25−30 Cu 70−75	35−37	−	47	1030	1373
Same after heat treatment	Pb 25−30 Cu 70−75	24−27	−	75	1962	2158
Cu−Sn−Pb (M75, POS30)	Sn 2−3 Pb 6−7 Cu 90−91	25−28	−	80	1570	1619
Al−Pb (AS50)	Al 48−50 Pb 50−52	33−34	5.2	—	1760	1962

Table 2. Parameters of spraying of pseudo-alloy coatings by using electric arc devices EM-3A

Pseudo-alloy coating	Compressed air pressure·10^{-4}, Pa	Electrode voltage, V	Productivity of device, kg/h	Distance from nozzle to workpiece surface, mm
Al−steel (AZh50)	49−59	20−40	2.0−2.4	100−125
Cu−steel (MZh75)	59−69	30−40	4.0−8.0	125−150
Brass−steel (LZh75)	49−59	30−40	4.0−8.0	125−150
Al−Pb (AS50)	49−59	20−30	2.0−2.4	75−100

cation of the copper sub-layer allowed the adhesion strength of the Cu−Pb system coating after annealing to be increased 3 to 4 times (Table 6) [30].

It was found that the annealed pseudo-alloy coating with a 25−30 % Pb content is optimal in a combination of physical-mechanical and antifriction properties, adhesion strength, wear resistance and compo-

Table 3. Parameters of spraying of pseudo-alloy coatings by using three-wire device (2 mm wire diameter, 20−40 V voltage)

Coating material	Content of element, wt.%	Wire feed speed, m/min	Current in each phase, A	Productivity of device, kg/h
Steel Copper	75	1.0−2.0	50−125	4.0−8.0
	25	0.6−1.2	75−150	
Steel Brass	75	1.0−2.0	75−150	4.0−8.0
	25	0.6−1.2	60−110	
Aluminium Lead	50	1.0−2.0	40−90	2.0−4.0
	50	0.5−1.0	15−30	
Aluminium Steel	30	1.0−1.2	90−110	3.0−3.6
	70	1.3−1.6	40−60	
Aluminium Steel	50	1.0−1.2	90−110	2.0−2.4
	50	0.70−0.85	50−80	

sition [30]. Structure of the pseudo-alloy coatings is a mixture of lamellae of the steel and copper particles with oxides and pores located along their boundaries. The reason for using the Cu−steel system pseudo-alloy coatings as a bearing material is heterogeneity of their structure and possibility of producing them from inexpensive metals. It was shown that the Cu−steel system pseudo-alloy coatings are characterised by a higher wear resistance than steel coatings (see Table 5). The Cu−steel pseudo-alloy coatings containing 10−30 % Cu can be easily run-in, and can operate under conditions of substantial loads, low temperatures and low friction coefficient. A drawback of the Cu−steel system pseudo-alloy coatings is that they are hard to machine, and scrape in particular, because of the oxide and nitride inclusions characterised by an

Table 4. Parameters of flame spraying of pseudo-alloy coatings (1.5 mm wire diameter)

Pseudo-alloy coating	Productivity of device MGI-1-57, kg/h	Pressure, Pa	
		Oxygen	Fuel gas
Cu−Pb (MS25)	0.50−0.60	$(2.5−5.0)·10^5$	$(0.35−0.75)·10^4$
Al−Pb (AS50)	0.45−0.90	$(2.5−5.0)·10^5$	$(0.35−0.75)·10^4$

Table 5. Physical-mechanical properties of pseudo-alloy coatings under liquid friction conditions

Pseudo-alloy coating	Friction coefficient, MPa, at $v = 1-4$ m/s for specific pressure				Running-in ability[*]	Brinell hardness at $P = 250$ kg, $\delta = 5$ mm	Oil absorbability, %
	50	100	150	200			
Al−steel (AZh50)	0.0049−0.0061	0.0045−0.0053	−	−	0.58	37−44	10−14
Cu−steel (MZh50)	0.0056−0.0063	0.0035−0.0036	−	−	0.64	−	−
Cu−Pb (MS25)	0.0044	0.0037−0.0042	−	−	0.47	35−37	−
Cu−Pb (MS25) (heat treatment)	0.0039−0.0045	0.0033	0.0030−0.0033	0.0032−0.0037	0.75	24−27	−
Cu−Sn−Pb (M75, POS30) (heat treatment)	0.0039−0.0047	0.0033−0.0035	0.0028−0.0041	−	0.80	25−28	−
Al−Pb (AS50)	−	−	−	0.0041	−	33−34	5.2
Cu−steel (MZh75)	0.0056−0.0061	−	−	−	0.80	95−107	3.0−3.2
Brass−steel (LZh75)	0.0065−0.0072	−	−	−	0.42	95−107	2.5−3.0
Steel (Zh100)	0.0070−0.0133	−	−	−	0.73	107	1.8−2.0

[*]Running-in ability of babbit metal of the B83 grade was assumed to be equal to 1.

increased hardness. It was suggested that to improve properties of the Cu−steel coatings they should be subjected to heat treatment (annealing and normalising), which leads to a change in shape of the oxide particles and decrease in hardness of the coatings from 1850 to 125 MPa [30].

The Cu−Al system pseudo-alloy coatings produced by flame spraying differ greatly in their structure and oxide content from those produced by the electric arc metallising method, as the latter causes overheating of the initial metal particles. In flame spraying the temperature of the molten particles corresponds to the liquidus curve. Because of this and owing to a substantial concentration of the combustion products in the gas flow, the melt is not much subjected to intensive oxygen saturation [30].

Wear-resistant pseudo-alloy coatings. The mechanism of formation and structural peculiarities of the steel 65G−Al system electric-arc coatings were investigated in study [34]. In simultaneous spraying of electrode wires of steel 65G and aluminium, all the intermediate phases forming in interaction of iron with aluminium both in the solid and molten states were fixed in structure of the products. The optimal combination of properties (moderate microhardness and sufficient ductility) determined by the corresponding composition of intermetallics was noted in the coatings with the 10 % Al content.

Spraying of the steel-aluminium pseudo-alloy coatings with a content of steel in the spraying material equal to 50−65 wt.%, and their subsequent pressure treatment involving compression provide the optimal structure of the coatings consisting of a hard reinforcement (hard particles of intermetallics formed in spraying of a coating) and a soft matrix (aluminium, steel), as well as plastic deformation of the soft component achieved during compression as a result of separation of oxide films from its particles. The

stresses leading to separation of the oxide films from the surface of the particles increase with growth of the content of steel in the pseudo-alloy layer. Separation of the oxide films leads to increase in cohesion strength of a coating, thus resulting in a considerable increase in its wear resistance and, hence, extension of service life of the coated parts [35].

The method is available for production of composite electric arc coatings from two dissimilar electrode materials, one of which being a low-carbon mild steel with a hardness not in excess of 1500 MPa. Flux-cored wire of the Fe−Cr−B−C alloying system is used as a second wire [36]. This method is employed to produce coatings based on a combination of commercial flux-cored wires of the Fe−Cr−B−C system (PP-AN-307) and all-drawn wires Sv-08 for repair of machine parts, whose friction surfaces operate under boundary friction and abrasive wear conditions. Increased wear resistance is attributed to the presence in a coating of a large amount of oxygen, iron and boron oxides, which provide a low level of the friction coefficient, whereas the presence of borides Fe_2B in the coating favours its high wear resistance. It was established that under the abrasive wear conditions using a fixed abrasive the value of wear resistance of the composite PP-AN-307 + Sv-08 coatings is 2.1 times higher than that of the similar coatings of flux-cored wire AN-307, and 1.4 times higher than that of steel ShKh-15 [37].

Corrosion-resistant pseudo-alloy coatings. Protection from water and atmospheric-water corrosion can be provided by using the Zn−Al (1:1) system pseudo-alloy coatings. Wetting parts with the Zn−Al coatings by water causes intensive oxidation of zinc, while oxides plug up the coating pores, thus preventing the access of water to the base metal [19].

Study [38] reports investigations of corrosion properties of the Zn−Al system coatings produced by the electric arc method with simultaneous zinc and alu-

Table 6. Adhesion strength of Cu−Pb system coating deposited on copper-plated low-carbon steel, MPa

Lead content of coating, wt.%	Before annealing	After annealing
0	13.0	35.0
10	11.2	34.0
30	7.8	32.0
50	6.2	17.5

minium wire spraying, as well as spraying of the zinc and flux-cored wires Al−5 wt.% Mg. The 3.5 % solution of sodium chloride was used for the tests. As shown by the investigations, the Zn−Al pseudo-alloy coatings have a 3 times higher corrosion resistance than the zinc or aluminium wire coatings, while the Al−Mg−Zn system pseudo-alloy coatings (73 % Zn−25.6 % Al−1.4 % Mg and 86 % Zn−13.3 % Al−0.7 % Mg) have a 1.25 times higher corrosion resistance than the Zn−Al system pseudo-alloy coatings.

Experience in practical application of thermal spray pseudo-alloy coatings. Antifriction pseudo-alloy coatings feature a good and quick running-in ability and exhibit a lower susceptibility to scores compared to other antifriction coatings. The heat-treated Al−steel, Cu−steel, Cu−Pb, Cu−Sn−Pb and Al−Pb system pseudo-alloy coatings can be applied instead of tin and tin-free brasses and babbit metals over the acceptable ranges of loads and speeds under static loads for non-split bushings, reducing gears, transmissions, cranes, machine tool equipment, metal-cutting machine tools, ventilators, smoke exhausters, compressors and centrifugal pumps operating in pair with quenched and non-quenched necks [19].

Application of the Cu−Pb coatings as an antifriction material is efficient for the internal surfaces of steel bushings [30].

The Cu−Al coating with the 20 wt.% Cu content is recommended for sliding bearings operating in assemblies of metal-cutting equipment and hoisting devices [30].

Study [39] presents the investigation results on development of wear-resistant coatings for strengthening and repair of hubs of guide vanes of centrifugal pumps of the ETsN type. The 20Kh13 + AMg coating composition produced by spraying of the 1.6 mm diameter wires at the same feed speed was tried out as one of the variants of the coatings.

Thermal conductivity of these coatings is markedly higher than that of steel 12Kh13, which should affect the calorific intensity at the point of contact of the interacting surfaces. Good results on all of the investigated parameters were also exhibited by the 12Kh13 + 08G2S coating produced from the 1.6 and 1.2−1.4 mm diameter wires. It has a ferritic-pearlitic and martensitic structure with a small amount of carbides, features sufficient density (porosity − 6−7 %), and consists of a layer of structural components uni-

formly distributed in the bulk. The coating can be easily machined by cutting even at a speed of up to 6 m/s (600 rpm). The content of chromium in such coatings decreases to some extent and is equal to about 8 %. Nevertheless, they are characterised by satisfactory corrosion resistance and comparatively high wear resistance [39].

The steel−Al pseudo-alloy coatings are sprayed on the surfaces of pistons by the electric arc method to increase their wear resistance. To improve quality of a coating, prior to deposition of the pseudo-alloy layer an aluminium sub-layer is sprayed on it, which can be easily deformed under the effect of shrinkage stresses induced in the steel-aluminium pseudo-alloy applied to it, thus preventing cracking and favouring increase in the coating to substrate adhesion strength [40].

Study [41] describes the electric arc coatings for piston compression rings of marine medium-reverse engines. These coatings consist of the steel−bronze (60S2-Br.KMts) pseudo-alloy with high tribotechnical and adhesion properties. It was established based on the results of comparative tribotechnical tests that in operation of the 60S2-Br.KMts-3-1 pseudo-alloy coating in pair with the cylinder bushing material (SCh 25) the consumption of power for overcoming the friction forces decreases to 20 %. Moreover, growth of wear resistance of the piston ring material (more than 5 times) and cylinder bushing (3 times) is fixed, this providing extension of the inter-repair period without disassembling. A substantial increase (by 50 % for score load) in score resistance of the tribo-coupling is noted.

In study [42] the steel−Mo pseudo-alloy coatings were deposited by the twin-wire metallising method with an independent feed of the molybdenum and steel wires on piston rings of a cylinder diesel locomotive. The rings with the coatings were removed and investigated after 4000 h of operation. Investigation of the degree of wear after operation showed that in the case of coating the rings with electrolytic chromium the wear was higher compared to the pseudo-alloy coating. Examinations of the wear surface indicated that wear was mostly of the abrasive type. Increase in hardness compared to the initial state was noted for the molybdenum component of the layer in all the rings after operation. Also, increase in hardness for the steel particles in a range of HV 5000−6000 MPa compared to the initial state, as well as disappearance of the particles with hardness of HV 3000−4000 MPa were fixed. The offered technology for thermal spraying of coatings provides extension of service life of the piston rings and other parts operating under wear conditions, and can be employed to improve reliability and durability of parts experiencing substantial wear during operation.

CONCLUSIONS

1. The most common method for production of pseudo-alloy coatings is electric arc spraying, as it is charac-

terised by high productivity and practicability. Thickness of the deposited layer can be varied from 50–100 μm to 3–6 mm or more. Composition of the coatings is regulated by changing diameters of the wires and their feed speeds.

2. The data presented on practical application of the pseudo-alloy coatings indicate that the metallised pseudo-alloy coatings are efficient as antifriction, wear- and corrosion-resistant materials.

3. Antifriction pseudo-alloy coatings are applied in manufacture of sliding bearings instead of bronzes and babbit metals to improve performance of parts under the abrasive wear conditions both in primary strengthening and in repair of parts. The Zn–Al pseudo-alloy coatings are used for corrosion protection of pipelines, tanks, vessels, metal structures of feed-processing shops of cattle-breeding complexes and agrochemical equipment.

1. Kulik, A.Ya., Borisov, Yu.S., Mnukhin, A.S. et al. (1985) *Thermal spraying of composite powders*. Leningrad: Mashinostroenie.
2. (1977) *Encyclopedia of inorganic materials*. Kiev: Ukr. Sov. Encyclop., Vol. 2.
3. Karpinos, D.M., Tuchinsky, L.I., Sapozhnikova, A.B. et al. (1985) *Composite materials in engineering*. Kiev: Tekhnika.
4. Andreeva, A.V. (2001) *Principles of physical chemistry and technology of composites*: Manual for higher education institutions. Moscow: IPRZhR.
5. Shahparast, F., Davies, B.L. (1978) A study of the potential of sintered iron–lead–tin alloys as bearing materials. *Wear*, **1**, 145–153.
6. (1981) *Sintered materials for electrical engineering and electronics*. Ed. by G.G. Gnesin. Moscow: Metallurgiya.
7. Rakovsky, V.S. (1978) *Sintered materials in engineering*. Moscow: Metallurgiya.
8. Skorokhod, V.V., Solonin, S.M., Chernyshov, L.I. (1978) High-porosity tungsten-copper materials produced by liquid phase sintering. Rep. 1. *Poroshk. Metallurgiya*, **2**, 17–21.
9. Skorokhod, V.V., Solonin, S.M., Chernyshov, L.I. (1978) High-porosity tungsten-copper materials produced by liquid phase sintering. Rep. 2. *Ibid.*, **10**, 89–92.
10. Tikhy, G.A., Kachalin, N.I., Belova, V.P. (2007) Study of Mo–Cu pseudo-alloy produced from mechanically activated charge. *Metalloved. i Termich. Obrab. Metallov*, **9**, 25–29.
11. Pimenova, N.V. (2009) *Production and investigation of properties of copper based composites*: Syn. of Thesis for Cand. of Techn. Sci. Degree. Perm.
12. Karpinos, D.M. (1985) *Composites*: Refer. book. Kiev: Naukova Dumka.
13. Dulnev, G.N., Zarichnyak, Yu.P. (1974) *Thermal conductivity of mixtures and composites*. Moscow: Energiya.
14. Misnar, A. (1968) *Thermal conductivity of solids, fluids, gases and their compositions*. Moscow: Mir.
15. Galinov, I.V. (1993) Investigation of the composition of Ag, Ni and Ag–Ni pseudoalloy coatings applied by electrospark alloying on a Cu substrate. *Surface and Coatings Technology*, **56**(**2**), 131–135.
16. Technologies for deposition of coatings. *www*.inacotec.com/technology
17. Zalyaeva, G.O. (2007) *Diagnostics, repair, assembly and maintenance of equipment*: Manual. Petropavlovsk-Kamchatsky: KamchatGTU.
18. Versatile plasmatron UShR-2 for spraying of coatings. *www*.plasmacentre.ru/index.php
19. Shashkov, A.N. (1960) *Antifriction pseudo-alloys*. Issue 21. Moscow: Mashgiz.
20. *www*.ai08.org/index.php/list/Технический+словарь+Том+I/3,Э.xhtml
21. Tylkin, M.A. (1981) *Reference book of repair service specialist in heat treatment*. Moscow: Metallurgiya.
22. *www*.ai08.org/index.php/index/Технический+словарь+Том+I/.xhtml
23. Kats, N.V., Antoshin, E.V., Vadivasov, D.G. et al. (1966) *Metallising by spraying*. Moscow: Mashinostroenie.
24. Borisov, Yu.S., Kharlamov, Yu.A., Sidorenko, S.L. et al. (1987) *Thermal spray coatings from powder materials*: Refer. book. Kiev: Naukova Dumka.
25. Hasui, A., Morigaki, O. (1985) *Surfacing and spraying*. Moscow: Mashinostroenie.
26. Venugopal, T., Prasad Rao, K., Murty, B.S. (2007) Mechanical properties of Cu–Ta nanocomposites prepared by high-energy ball milling. *Acta Mater.*, **55**(**13**), 4439–4445.
27. Wille, C.G., Tala'at Al-Kassab, Kirchheim, R. (2011) Time evolution of morphology in mechanically alloyed Fe–Cu. *Ultramicroscopy*, **111**(**6**), 730–737.
28. Sun, A., Wang, D., Wu, Zh. et al. (2011) Mechanochemical synthesis of Mo–Cu nanocomposite powders. *J. Alloys and Compounds*, **509**(**5**), 74–77.
29. Kats, N.V. (1968) *Restoration of textile machine parts by metallising*. Moscow: Lyog. Industriya.
30. Krasnichenko, L.V., Smolyaninov, A.I., Podkovich, E.G. et al. (1966) Complex metallised pseudo-alloys as bearing materials. In: *Application of new materials in agricultural machine-building*: Coll. Rostov-na-Donu.
31. Krasnichenko, L.V. (1958) *Modern technology for metallising by spraying*. Moscow: Trudrezervizdat.
32. Liao, H.L., Zhu, Y.L., Bolot, R. et al. (2005) Size distribution of particles from individual wires and the effects of nozzle geometry in twin wire arc spraying. *Surface and Coatings Technology*, **200**(**7**), 2123–2130.
33. (1991) *Application of new materials in agricultural machine-building*: Coll. Ed by V.V. Rubanov. Rostov-na-Donu: RISKhM.
34. Borisova, A.L., Gubenko, B.G., Kostin, V.A. et al. (1990) Peculiarities of formation and structure of electrometallised coatings of steel-aluminium system. *Avtomatich. Svarka*, **8**, 41–44.
35. Titlyanov, A.E., Radyuk, A.G., Pedos, S.I. *Method for production of thermal spray coatings*. Pat. 2063470 RF. Int. Cl. C 23 C4/18, C23 C4/04. Publ. 10.07.1996.
36. *Method for production of composite arc coatings*. Pat. 19967 Ukraine. Int. Cl. C 23 C 4/00. Publ. 15.01.2007.
37. Markovich, S.I. (2007) *Increase in wear resistance of machine parts by arc spraying of composite coatings using different wires*: Syn. of Thesis for Cand. of Techn. Sci. Degree. Kyiv.
38. Lester, T., Kingerley, D.J., Harris, S.J. et al. (1998) Thermally sprayed composite coatings for enhanced corrosion protection of steel structures. In: *Proc. of 15th ITSC* (Nice, France, 25–29 May), Vol. 1, 49–55.
39. Isakaev, E.Kh., Gusev, V.M., Mordynsky, V.B. (2008) Extension of service life of oil-field equipment parts with thermally sprayed coatings. *Tekhnologiya Mashinostroeniya*, **12**, 18–22.
40. Ponomaryov, A.I., Makaeva, Z.A., Komlyukov, N.V. et al. *Method for increasing wear resistance of pistons*. USSR author's cert. 291994. Int. Cl. C 23 C 7/00. Publ. 06.01.71.
41. Efremov, S.Yu. (2005) *Extension of service life of piston compression rings in manufacture of spare parts for ship repair*: Syn. of Thesis for Cand. of Techn. Sci. Degree. Novgorod.
42. Pyatak, A.I., Lyubchenko, A.P., Glushkova, D.B. et al. (2010) Nondestructive method for testing of piston rings after running-in and operation. *Mir Tekhniki i Tekhnologij*, **1**, 126–128.

INFLUENCE OF SURFACTANTS ON PHASE FORMATION DURING PRODUCTION OF Al−Cu−Fe SYSTEM POWDERS FOR THERMAL COATINGS BY THE METHOD OF MECHANOCHEMICAL SYNTHESIS

A.N. BURLACHENKO and **Yu.S. BORISOV**

E.O. Paton Electric Welding Institute, NASU, Kiev, Ukraine

Influence of the quantity and methods of adding surfactants on phase formation during mechanochemical synthesis of composite powder of $Al_{70}Cu_{20}Fe_{10}$ system was studied. It is established that surfactant application allows avoiding sticking of charge compounds to the drum wall and intensifies the process of new phase formation.

K e y w o r d s : *thermal coatings, powders, mechanochemical synthesis, surfactants, sticking, phase composition, quasicrystalline phase*

One of the urgent trends in thermal spraying (TS) is development of the technology of deposition of coatings with special structure types (nanocrystalline, nanocomposite, quasicrystalline) [1−4]. One of the stages of development of such technologies is application of powders of a new type ensuring under TS conditions formation of coatings with specified structure type. Among the methods of producing such powders, widely applied are those of mechanical alloying and mechanochemical synthesis (MCS), which are based on phenomena of repeated processes of cold welding and crushing of particles of obtained material

components during their processing in high energy ball mills (attritor, planetary mill). Examples of mechanical alloying application are producing powders, for instance, of FeCr−TiCN system to form nanocomposite coatings [5], and of MCS application − producing powders, for instance, of Al−Cu−Fe system to form coatings of a quasicrystalline structure [5−7]. However, in case of processing during MCS a mixture of powders of Al−Cu−Fe system, containing ductile metals (aluminium, copper, iron), a phenomenon of charge particle sticking to the drum wall and planetary mill crushers is observed. As a result, part of the powder is eliminated from MCS process, thus lowering both process efficiency and its effectiveness. To eliminate the phenomenon of sticking and intensify phase formation process, additives of surfactants (SA) to the powder mixture are used. Here, SA amount and method of their addition to the charge should not only prevent charge sticking to the drum wall and crushers, but also ensure the equilibrium of the multiple process of welding and crushing of the formed composite conglomerate, which exactly results in new phase formation.

This work gives the results of investigation of SA influence on phase composition and structure of par-

Table 1. SA characteristics

SA	T_m, °C	T_b, °C	σ, mN/m	γ, g/cm³
Oleic acid $CH_3(CH_2)_7CH = = CH(CH_2)_7COOH$	13.40	228.0	32.8	0.895
Ethyl alcohol C_2H_5OH	−114.65	78.3	22.8	0.789

Table 2. Modes of SA addition during MCS (5 h duration)

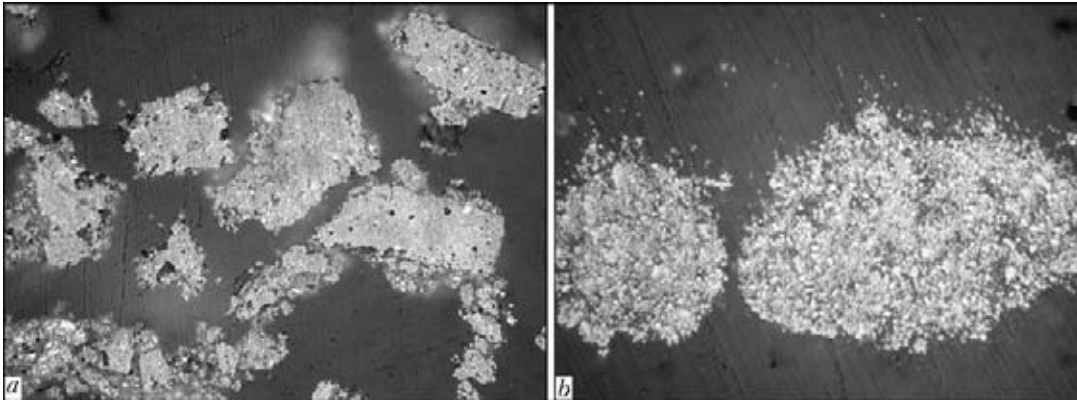| No.	SA	Method of SA addition	SA amount, wt.%	Product phase composition
1	–	–	–	AP, β, θ, ω, ψ
2	Oleic acid	Once	1	Same
3		Same	5	23 % AP + 77 % (44 % ψ-phase + 56 % β-phase)
4		Periodically, by 1 wt.% every hour of processing	5	27 % AP + 73 % (68 % ψ-phase + 32 % β-phase)
5	Ethyl alcohol	Once	1	AP, β, θ, ψ, ω
6		Same	5	18 % AP + 82 % (41 % ψ-phase + 59 % β-phase)
7		Periodically, by 1 wt.% every hour of processing	5	22 % AP + 78 % (60 % ψ-phase + 40 % β-phase)

Figure 1. Microstructures (×1000) of powder particles of Al−Cu−Fe system produced in MCS processes without (*a*) and with (*b*) SA (oleic acid; periodical addition by 2 wt.% every hour of treatment)

ticles during MCS of powder mixture of Al−Cu−Fe system, close by its composition to the region of existence of quasicrystalline ψ-phase.

Experimental procedure. To study SA influence on phase formation at MCS of powders of Al−Cu−Fe system, corresponding by their composition to $Al_{70}Cu_{20}Fe_{10}$ (at addition of extra iron as a result of crushing, it approaches $Al_{63}Cu_{25}Fe_{12}$ of a quasicrystalline structure), initial powders of PA-4 aluminium (40−60 μm), PMS-1 copper (20−40 μm) and PZhR

iron (100−160 μm) were used. MCS process was conducted in Activator 2-SL planetary mill at drum rotation speed v_{dr} = 1500 rpm, and ratio of spheres weight to charge weight of 10:1 for 5 h. Used as SA were oleic acid and ethyl alcohol (Table 1) in the amount from 1 up to 5 wt.% with different methods of SA addition (Table 2).

MCS process was periodically interrupted (every hour of processing), processed charge was removed, and in case of its sticking to the drum wall, it was
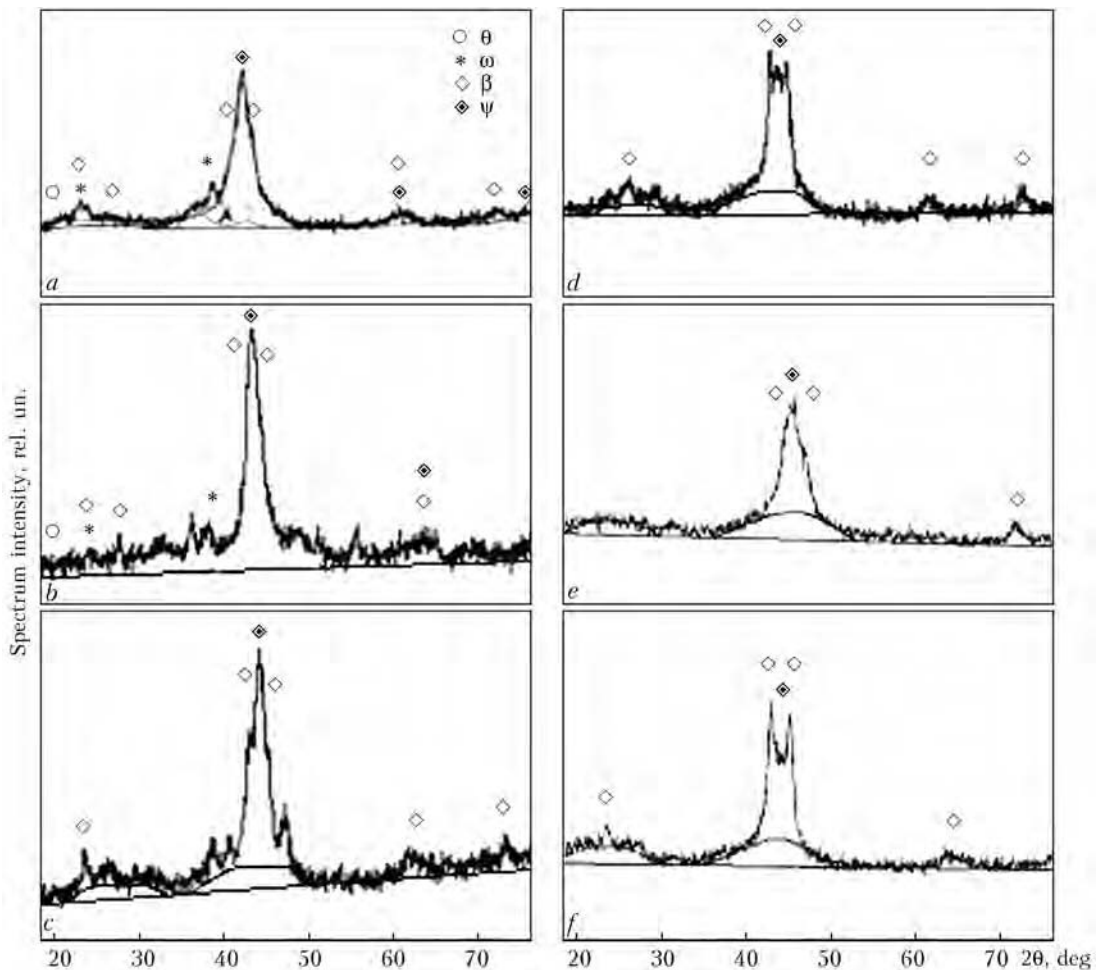

Figure 2. Roentgenograms of powders of Al−Cu−Fe system obtained by MCS at v_{dr} = 1500 rpm for 5 h without SA (*a*) and at different SA addition methods: once by 1 (*b*) and 5 (*c*, *e*) wt.%; periodically by 1 wt.% every hour of MCS (*d*, *f*) with oleic acid (*b*, *e*, *f*) and ethyl alcohol (*c*, *d*)

knocked off and crushed in a ceramic mortar, poured into the drum, and MCS process was carried on. Temperature measurement inside the drum was conducted with UT-70V multimeter. Synthesized powders were studied using metallography (Neophot-32 optical microscope with digital photography attachment) and X-ray structural phase analysis (DRON-UM1 diffractometer with monochromatic CuK_α-radiation).

Experimental results. Temperature measurement inside the drum directly after MCS showed that in all the modes of SA addition, it practically did not change, and was equal to 70–75 °C.

During treatment of initial powders without SA application, continuous sticking of up to 5–10 mm layer to drum wall is observed. Here, a multiphase system forms in the end product (Table 2, No.1; Figure 1, a; Figure 2, a).

After operation for 1 h with addition of SA in the amount of 1 wt.%, no sticking is observed, particles are of a round shape with average size of about 1 mm. Further continuation of the process leads to sticking, and, as a consequence, to producing the end product similar to the one produced without SA application (Table 2, Nos. 2, 5; Figure 2, b).

Periodical addition of 1 wt.% of SA every hour of MCS in the total amount of 5 wt.% (Table 2, Nos. 4, 7) leads to absence of sticking during the entire synthesis process, powder particles have a shape close to the round one with finely-dispersed structure (Figure 1, b) and phase composition, consisting of amorphous (AP), quasicrystalline ψ- and crystalline β-phases (Table 2, Nos. 4, 7; Figure 2, d, f).

One-time addition of 5 wt.% of SA (Table 2, Nos. 3, 6) leads to absence of sticking in the first 3 h of mechanical processing, the powder being loose, and in some places small local heating of MCS products up to 200–250 °C occurs at charge unloading from the drum. MCS continuation leads to sticking of a thin layer of about 2–3 mm to the drum wall after 1 h, and after 2 h — to sticking of a layer of up to 5–10 mm thickness to the drum wall. Final product of synthesis, similar to periodical addition of SA, consists of AP, quasicrystalline ψ- and crystalline β-phases (Table 2, Nos. 3, 6; Figure 2, c, e).

Thus, it is established that SA application in production of Al–Cu–Fe system powders for TS by MCS method promotes an intensification of the process of new phase synthesis and formation of spherical particles of 20–40 μm size. An optimum mode of SA addition, preventing sticking of processed material during the entire time of MCS (5 h) at processing of a mixture of Al–Cu–Fe system, is a regular periodical (every hour) addition of SA in the amount of 1 wt.%. In this case, maximum content of quasicrystalline ψ-phase of 68 wt.% in MCS product was achieved. No essential difference between the influence of oleic acid and ethyl alcohol on the process of new phase synthesis at MCS in a mixture of Al–Cu–Fe system was found.

1. Tjong, S.C., Chen, H. (2004) Nanocrystalline materials and coatings. *Materials Sci. and Eng.*, **1/2**, 1–88.
2. Ragulya, A.V., Skorokhod, V.V. (2007) *Consolidated nanostructured materials*. Kiev: Naukova Dumka.
3. Moya, J.S., Lopez-Esteban, S., Pecharroman, C. (2007) The challenge of ceramic-metal microcomposites and nanocomposites. *Progress in Material Sci.*, **52**, 1017–1090.
4. (2005) Thermal spray coatings having quasi-crystalline phase, properties and applications (Review). *Fizyka i Khimiya Tv. Tila*, 6(**1**), 124–136.
5. Borisov, Yu.S., Borisova, A.L., Adeeva, L.I. et al. (2010) Producing of powders for thermally sprayed coatings by methods of mechanical alloying and nanomechanical synthesis. *Svarochn. Proizvodstvo*, **12**, 18–22.
6. Borisova, A.L., Borisov, Yu.S., Adeeva, L.I. et al. (2008) Effect of parameters of mechanochemical synthesis on structure, phase composition and properties of thermal spraying of Al–Cu–Fe system powders containing quasicrystalline phase. *The Paton Welding J.*, **9**, 14–21.
7. Borisova, A.L., Adeeva, L.I., Tunik, A.Yu. et al. (2009) Investigation of thermal spraying of Al–Cu–Fe–Ti–Cr–Si system powders produced by mechanochemical synthesis with subsequent annealing. *Poroshk. Metallurgiya*, **9/10**, 31–40.

THESIS FOR A SCIENTIFIC DEGREE

E.O. Paton Electric Welding Institute of the NAS of Ukraine

B.V. Knysh (PWI of NASU) defended on November 23, 2011 the Doctor's thesis on the subject «Improvement of cyclic fatigue life of welded joints at the stages of damage accumulation and fatigue crack development».

The thesis is devoted to scientific substantiation of application of high-frequency mechanical peening (HFMP) for improvement of cyclic fatigue life of welded joints in operating metal structures at the stage of fatigue damage accumulation and investigation of various design-technological methods of retardation of developing fatigue cracks, including repair welding.

The author developed and protected by patents of Ukraine and USA an ultrasonic system USP-300 of 300 W power with piezoelectric transducer for strengthening treatment of welded joints. It is shown that HFMP of the fusion zone by USP-300 system lowers the stress concentration factor by 15 %, and residual compressive stresses of up to $-0.9\sigma_y$ are introduced on the metal surface in the processing zone instead of residual tensile welding stresses of about 0.9 of material yield point. Here, a submicrocrystalline structure forms in the thin surface layer (up to 30 μm), which consists of dispersed subgrains with high angles of disorientation, elongated in the direction of processing tool motion.

Proceeding from fatigue curves derived when testing samples of welded joints with low residual stresses, a procedure was developed of plotting design fatigue curves for the welded element of the operating metal structure, allowing for the characteristics of the alternating loading cycle, stress concentration factor of the joint, set level of residual welding stresses and mechanical properties of the metal. PC software was developed, which realizes the proposed sequence of determination of design fatigue curves for welded joints of operating metal structures. It was established for the first time that under the conditions of regular loading the effectiveness of strengthening by HFMP technology of welded joints with accumulated fatigue damage depends on the level and duration of the impact of applied loading. It is shown that the residual fatigue life of highly loaded tee welded joints of low-alloyed steels after HFMP strengthening at 70 % of accumulated damage is not inferior to that of the joints strengthened in as-welded condition. Reduction of used operating life of such joints from 70 to 10 % of their fatigue life increases the effectiveness of joint strengthening up to 3.5 times compared to strengthening in as-welded condition.

It is established that the regularities of development of fatigue cracks in non-uniform fields of tensile and compressive RWS, the rates of which correspond to mean-amplitude section of FFD, are described by Paris equation with parameters invariant relative to the loading cycle characteristics. Three parameter relations for the rate of growth of surface and through-thickness fatigue cracks in structural steels were proposed and experimentally substantiated, which alongside SIF range contain the coefficient of stress cycle asymmetry in the explicit form. A method for calculation of cyclic fatigue life of steel structure elements damaged by a fatigue crack at its propagation in a non-uniform field of residual tensile stresses was proposed.

More effective structural and technological methods of crack retardation were proposed: hole drilling around the crack tips with mounting of high-strength bolts with 20 tf tension in them; local heating up to the temperature of 300−350 °C at 30 mm distance from the crack tip; local explosion treatment by cylindrical charges of 5.5 mm diameter located in holes of 6 mm diameter at 1 mm distance behind the crack front. These methods extend the cyclic fatigue life of structural elements by 10 to 20 times. Proceeding from fracture mechanics approaches, a method was developed for calculation of cyclic life of structural elements, containing propagating fatigue cracks at their retardation by artificially induced field of residual compressive stresses.

SUBSCRIPTION
FOR «THE PATON WELDING JOURNAL»

If You are interested in making subscription directly via Editorial Board, fill, please, the coupon and send application by fax or e-mail.

The cost of annual subscription via Editorial Board is $324.

Telephones and faxes of Editorial Board of «The Paton Welding Journal»:

Tel.: (38044) 200 82 77, 200 81 45

Fax: (38044) 200 82 77, 200 81 45.

«The Paton Welding Journal» can be also subscribed worldwide from catalogues of subscription agency EBSO.

SUBSCRIPTION COUPON

Address for journal delivery _____

Term of subscription since _____ 20 ____ till _____ 20 ____

Name, initials _____

Affiliation _____

Position _____

Tel., Fax, E-mail _____

Subscription to the electronic version of «The Paton Welding Journal» can be done at site: *www: rucont.ru*

РУКОНТ
национальный цифровой ресурс

We offer for the subscription all issues of the Journal in pdf format, starting from 2009. You can subscribe to individual issues or to the entire archive including all issues over a period of 2009–2011. The subscription is available for natural persons and legal entities.

ADVERTISEMENT
IN «THE PATON WELDING JOURNAL»